Università
Ca'Foscari
Venezia

PhD in

Science and Management of Climate Change
Graduate School of Global Change Science and Policy

Cycle XXVI
Academic Year 2014-2015

Climate Variability in West Africa during the Monsoon Season: the Impact of Sea Surface Temperatures and Anthropogenic Sulfate Aerosols in the CMCC Global Climate Model.

PhD Thesis
Discussed on December 5th, 2014, by

Claudine WENHAJI NDOMENI
Matricule: **955881**

PhD Coordinator:	**Pr. Carlo Barbante**	**Ca/Foscari University, Venice**
PhD Tutor:	**Dr. Silvio Gualdi**	**CMCC, Bologna, Italy**
PhD Co-Tutors:	**Dr. Stefano Materia**	**CMCC, Bologna, Italy**
	Dr. Alessandra Giannini	**IRI, Columbia University, USA**

To my mother,
my princess, Esther,
and a person i will miss forever, my father.

Acknowledgements

In the first place, I would like to express my gratitude to my tutor Dr. Silvio Gualdi for providing numerous advices and support, for his human and professional qualities.

I am particularly thankful to my co-tutor Dr. Stefano Materia, from whom I have learned a lot: your scientific guidance, your patience, passion, energy and thoughts have encouraged me to complete and consolidate the present work. Overall, you cared not only about the personal scientific skills I have developed during these years but more, about what I should always bear in mind for my futur career. I really appreciate and be sure, i will always keep your advices.

My special thanks go to Dr. Lisa Goddard for providing hospitality and scientific support at IRI during my reasearch period abroad. Indeed, I am indebted with Dr. Alessandra Giannini who has given me all as my mentor: you are a model example for me. I was astonished not only by your incredible scientific skills, but what marked me the most is the humility and the social aspects that characterize your person. You are definitely a source of inspiration for me.

I would also like to thank the two reviewers of this work, Dr. Neil Ward and Dr. Joseph Mutemi, for their availability, their valuable and constructive revisions and recommendations during the crucial drafting phase of the dissertation. Your comments and remarks have pretty much improved the quality of this thesis.

I acknowledge CMCC, particularly Dr. Antonio Navarra, for allowing me the working space and the Ca'Foscari University of Venice for the financial support throughout these years. Part of this thesis has been as well financed within CLIMAFRICA project to which I am definitely grateful.

This research would have not been possible without the overall support from my colleagues and friends in Bologna. Not to forget the morale boost I received from all of them throughout these last years. A special thank is due to Dr. Chiara Cagnazzo, for her support during the first steps of this Ph.D. career. An enormous thank to Beppe Fogli and Andrea Borelli, for their computational assistance with softwares and servers.

These years have been a difficult journey made of ups and downs, which would have been difficult to overcome alone. My gratitude goes to Flora and Guido Fioretti and to family Youatou for the assistance, encouragement and support during the very crucial stage of

this PhD.

Last, but not least, I would like to thank my mother for her inconditional love, for values tranfert. Everything starts from her: she is my first lecturer. I do not forget my family, brothers and sisters, my friends all over the world, my lecturers and colleagues at ICTP and in Cameroon. Thanks to you all. Finally, I simply thank God for His infinite mercy.

Abstract

West Africa (WA), particularly the Sahel region, has experienced a long-term drought during the last three decades of the 20th century. This episode has had dramatic consequences on economical and societal needs of a population that mainly substains on rain-fed agriculture. State of the art global climate models (GCMs) poorly simulate the West-African climate and the long Sahel drought.

In this regard, this thesis aims to improve the understanding of the WA climate, through an analysis of precipitation variability at the interannual to decadal time scale.

The ability of one of the state-of-the-art sophisticated GCMs (the Centro Euro-Mediterraneo sui cambiamenti climatici - CMCC) was tested to reproduce the main features of the West African Monsoon (WAM) system. A set of experiments was performed to understand the role of sea surface temperatures (SSTs), which have long been proposed as the main drivers of interannual variability, and anthropogenic sulfate aerosol (ASA) loadings, that only very recently have been suggested as possible players for decadal variability. To this aim, the GCM was run in fully coupled mode as well as in AMIP mode, in which SSTs are prescribed. Besides, experiments with varying and climatological aerosols were carried out.

In agreement with the well documented results, the atmospheric model used in this work, forced at the bottom boundaries with prescribed observed SSTs and Sea ice, is able to reproduce the long-term drought that governed the Sahel region during 1970s-1980s. Interestingly, CMCC model, set in the coupled atmosphere-ocean configuration, is also able to reproduce the low frequency variability for Sahel precipitation even when it does not run with observed SSTs, thanks to the forcing imparted by varying aerosols. Furthermore, the performance of AMIPlike run makes this work unique as the model's skills are revealed to be improved when it is used in uncoupled mode, strengthening the importance of the common AMIP run.

Two main physical mechanisms are proposed to explain the role that SSTs and ASAs have played in shaping the past Sahel drought:

1. Warmer-than-average low-latitude SSTs around Africa favors deep convection over the ocean and an anomalous heating spread through an unstable atmosphere is established. The higher-level warm temperature anomalies then extend over Africa where subsidence occurs and engenders widespread drought over Sahel;

2. Higher loadings of past historical ASAs in the northern hemisphere than in the southern, has induced, via their direct and indirect effects, a hemispheric asymmetry of SSTs which has affected the Atlantic multidecadal oscillation (AMO), and in turn, has affected tropical rainfall, especially rainfall over West Africa.

We suggest that the strong relationship of the Low Frequency variability of the Sahel rainfall, to ASAs radiative forcing as revealed in this work, should be considered as an important element for future global warming debate.

Keywords: West African Climate. Decadal Variability . Interannual Variability . Sea Surface Temperatures . Anthropogenic Sulfate Aerosols. AMIP simulations . Coupled Models . GCMs . Model performance .

Sommario

L'Africa Occidentale, e in particolare la regione del Sahel, ha vissuto un grave periodo di siccità nel corso degli ultimi tre decenni del ventesimo secolo. Questo ha avuto drammatiche conseguenze sulle esigenze economiche e sociali di una popolazione che trova sostentamento dall'agricoltura. Gli attuali modelli climatici globali (GCM) hanno ancora difficoltà a simulare il clima della regione.

A questo proposito, questa tesi mira a migliorare la comprensione del clima africano, attraverso l'analisi della variabilità interannuale e decennale scala delle precipitazioni.

L'abilità di un sofisticato GCM (il modello del Centro Euro-Mediterraneo sui cambiamenti climatici - CMCC) è stata testata per riprodurre le caratteristiche principali del monsone africano (WAM). È stata realizzata una serie di esperimenti per capire il ruolo delle temperature superficiali oceaniche (SST), a lungo proposte come fattore principale di variabilità interannuale, e delle emissioni di aerosol di origine antropica solfato (ASA), che solo di recente si sono scoperti avere un ruolo nella variabilità decadale. A tale scopo, il GCM è stato utilizzato sia in modo accoppiato, in modalità AMIP, ossia con SST variabili e climatologici.

Il modello forzato da SST osservate è in grado di riprodurre la siccità a lungo termine che ha flagellato la regione del Sahel durante 1970s-1980s. È interessante notare che il CMCC-GCM, nella configuration atmosfera-oceano accoppiato, è anche in grado di riprodurre la variabilità delle precipitazioni a bassa frequenza anche senza SST osservate, grazie al forzante impartito dagli aerosol.

Questa tesi propone due meccanismi fisici per spiegare il ruolo che le SST e gli ASA hanno giocato nella recente siccità del Sahel:

1. SST più calde della media nelle zone equatoriale intorno all'Africa favoriscono convezione profonda sul mare, con le anomalie di temperatura che si estendono sull'Africa, dove si verifica subsidenza generando siccità diffusa nel Sahel;

2. Gli alti livelli di ASA nell'emisfero nord hanno indotto, attraverso effetti diretti e indiretti, un'asimmetria emisferica di SST che ha colpito l'Oscillazione Atlantica Multidecadale (AMO), che, a sua volta, ha influenzato le precipitazioni tropicale, in particolare sull'Africa occidentale.

Il forte legame della variabilità a bassa frequenza delle precipitazioni Sahel con il forzante radiativo degli ASA, dovrebbe essere considerato un elemento importante per il futuro dibattito sul riscaldamento globale.

Parole chiave: Clima dell'Africa occidentale. Variabilità decadale. Variabilità interannuale. Temperature superficiali oceaniche. Aerosol di origine Antropica Solfato. Simulazioni AMIP . Modelli Accoppiato . GCM . Prestazioni del modello.

Contents

List of Figures

List of Tables

Chapter 1

Introduction

1.1 Background: The West Africa Climate

West Africa (WA) has been identified as one of the world hot spot regions for climate change ([73] Solomon 2007; [39] Koster et al.2004): a region significantly under threat from humans due to climate change.

The climate of the region is dominated by the so-called large-scale monsoon circulation, which is of a major social importance to local populations whose economy primarily relies on rainfed agriculture. As in all monsoon systems, the circulation is forced and maintained by thermodynamic contrasts between the land (i.e, the Sahara) and the ocean (i.e, equatorial Atlantic). As shown in Figure 1.1, Rainfall is associated with a band of prevelantly convective precipitation called the Intertropical Convergence Zone or ITCZ, traversing twice the equatorial regions during the year. During summer, the ITCZ is marked by the convergence, at the lower levels of the atmosphere, of the dry north-easterly Harmattan winds originating from the Sahara and the southwest monsoon flow that brings moist air from the Atlantic ocean into land ([31] Hourdin et al.2010).

The main tropical circulation features associated with the West African monsoon (WAM) (Figure 1.1 and Figure 1.2) are the upper-level Tropical Easterly Jet (TEJ), the mid-level African Easterly Jet (AEJ) and low-level equatorial westerlies associated with the southwest monsoon flow. The TEJ develops as a response to the intense north-south temperature gradient between the Himalaya plateau and the Indian ocean. Its core lies in the Asian sector at around 200 mb and appears to play a role in the development of the rainbelt over West Africa ([53] Nicholson 2013; [54] Nicholson et al.2001). The AEJ, a mid-tropospheric core of strong zonal winds (600-700 mb) is thermally induced by the contrast between the hot Sahara and the Atlantic ocean and maintained by the juxtaposition of moist convection to the South and dry convection to the North ([53] Nicholson 2013). The disturbances around this zonal circulation, the so-called African

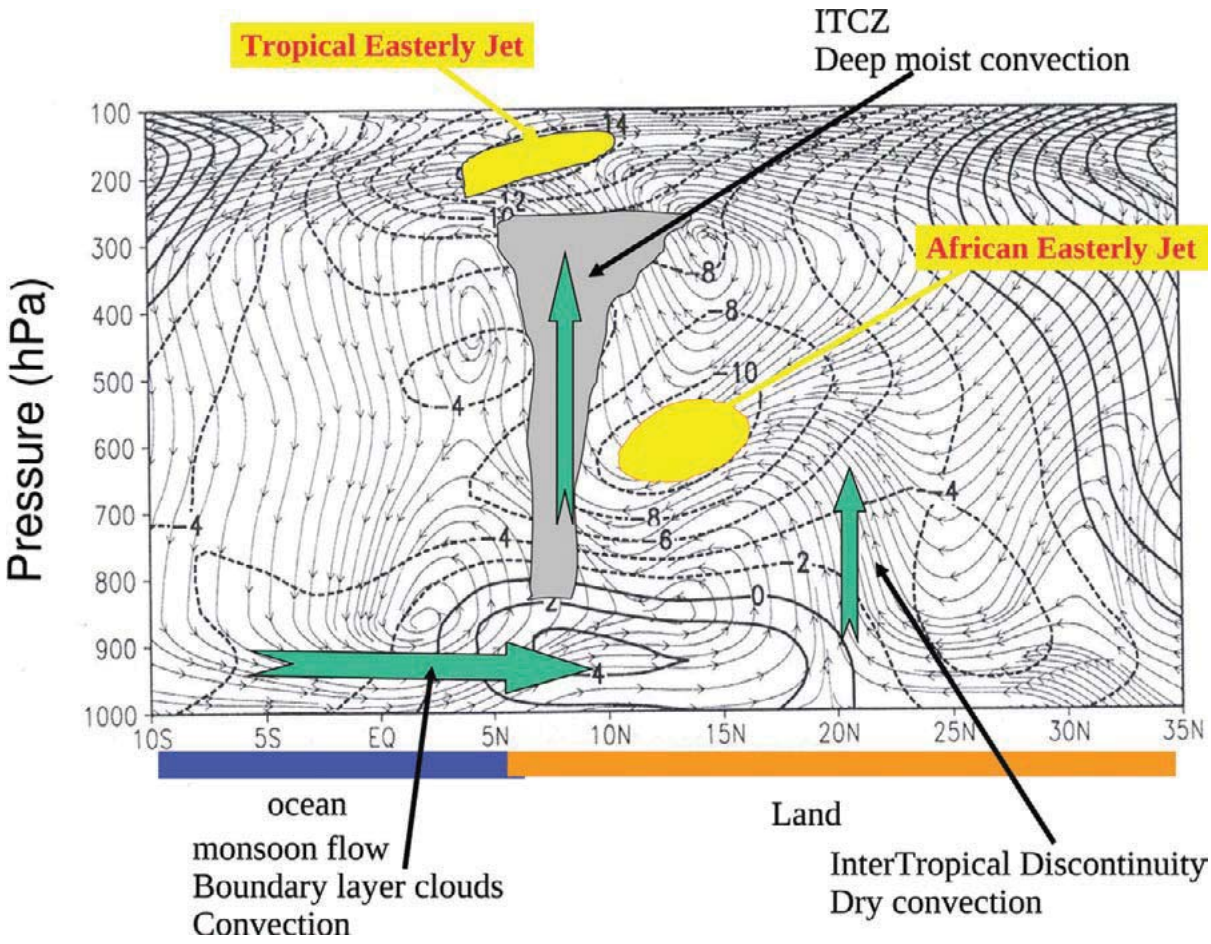

Figure 1.1: *Mean Meridional Circulation (stream lines) and associated mean Zonal winds (m/s in contours) over West Africa during the summer season [from Hourdin et al. (2010)].*

Easterly Waves (AEWs) have been identified to be the key driver of convection and rainfall patterns ([22] Diedhiou et al.1998).

During the last century, the climate of WA has experienced a strong rainfall variab-

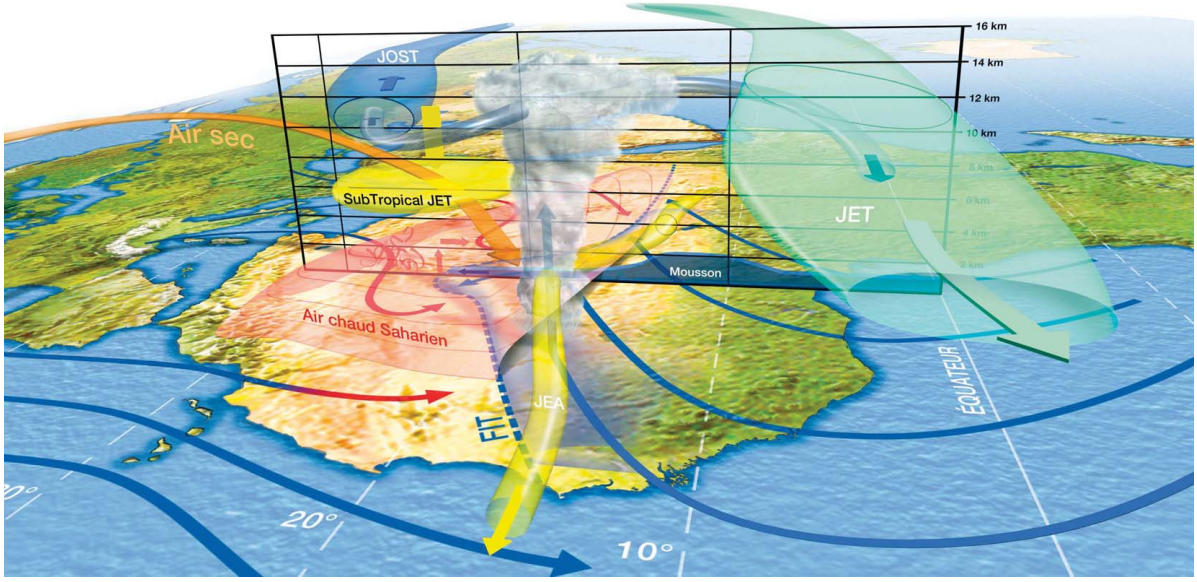

Figure 1.2: *Three-dimensional schematic view of the WAM. FIT stands for ITD, intertropical discontinuity; Air chaud Saharien for warm Saherian Air, JET for TEJ, tropical easterly jet; STJ, subtropical westerly jet; JEA for AEJ, African easterly jet. The oscillation of the AEJ yellow tube figures an African easterly wave [from [41], Lafore et al.2010].*

ility. Specifically, the Sahel, the semi-arid transition zone between the Sahara desert and the humid tropical rainforest, has been characterized by a pronounced multi-decadal rainfall trend contrasting a wet (1950s-1960s) and a dry (1970s-1980s) period followed by a partial recovery over the last decade of the twentieth century ([27] Giannini etal.2003).

The efforts of the scientific communities to explain the rainfall variability over WA progressed along two main directions:

1. The first point of view emphasizes feedbacks between land surface properties (soil moisture, vegetation and albedo) and atmospheric circulation ([57] Otterman 1974, [12] Charney 1975 and [13] Charney et al.1977). The so-called Charney's hypothesis, which highlights the vegetation cover effects, states that an increase in surface albedo due to human-induced change in vegetation cover could cause a decrease in precipitation that in turn, would lead to a decrease in vegetation cover and thus to a further enhancement of the albedo. Very recently, [39] Koster et al.2004, has identified the Sahel region to be one of the world regions with the strongest coupling between soil moisture and precipitation.

2. The second point of view emphasizes the alternative hypothesis of the role of global tropical sea surface temperatures (SSTs) conditions upon the twentieth century rainfall variability over the Sahel, ([42] Lamb 1978a, [43] Lamb et al.1978b, [25] Folland et al.1986, [59] Palmer 1986, [64] Rowell et al.1995, [34] Janicot et al.1996 and [26] Fontaine et al.1998). This alternative mechanism has been recently confirmed in atmospheric global circulation models (GCMs) which are able to reproduce the spatio-temporal variability of observed Sahel rainfall when only forced by observed SST time evolution ([27] Giannini et al.2003, [9] Caminade and Terray 2010). The decrease of the historical Sahel rainfall has been related to an interhemispheric pattern of global SST anomalies with warmer temperatures in the northern hemisphere and cooler in the south. The arguments for this mechanism are related to the concept of thermodynamic contrast between land and ocean ([18] Chou et al.2001), as well as the classical description of the zonally symmetric or Hadley circulation ([45] Lindzen et al.1988) whose concepts are related to equatorial wave dynamics ([48] Matsuno 1966, [29] Gill 1980).

To further investigate the impact of SSTs on west Africa rainfall, few authors have focused on the impact of different ocean basins on the West African rainfall. Positive Mediterranean SST anomalies have been related to positive Sahel rainfall anomalies through an increase of evaporation and southward moisture advection ([62] Rodriguez-Fonseca et al.2010). The role of tropical Atlantic SSTs has been highlighted by works by [80] Ward et al.1998, pointing out an anomalous West African dipole rainfall response while [27] Giannini et al.2003, [28] Giannini et al.2005; [71] Rowell 2003, [35] Janicot et al.2001, [34] Janicot et al.1996, [80] Ward et al.1998, related a decrease of rainfall over Sahel to the tropical Pacific during strong positive El Nino Southern Oscillation (ENSO) phase years.

Additionnally to the above studies, few works have highlighted the role of anthropogenic sulfate aerosols, ASAs, which indeed seem to be of great importance in shaping the climate of WA. In fact, [10] Chang et al.2011 have found that, there was a pronounced secular trend in the tropical Atlantic interhemispheric SSTs gradient over the twentieth century, with the tropical South Atlantic warming faster than the tropical North Atlantic due to the increase of ASA loadings recorded in the northern hemisphere over Europe and America until early 1970s-1980s ([72] Smith et al.2001). This change in the tropical Atlantic circulation may have in turn altered rainfall climate over the tropical Atlantic sector including drought over WA.

In the framework of the African Monsoon Multidisciplinary Analyses (AMMA) project, [31] Hourdin et al.2010, it has been of agreement that among the discrepancies between current climate models in representating the cumulative rainfall over the Sahel, the parametrized convection plays a major role in reproducing for instance the right location of the AEJ which affects rainfall intensity (a larger rainfall over Sahel is generally associated with an AEJ location father north). They showed that both the ascent of the mean meridional circulation (MMC) in the region of the ITCZ penetrates much higher in the Emmanuel scheme case ([23] Emmanuel 1993) compared to the ([75] Tiedtke 1989) scheme. The AEJ was well represented in the Emmanuel case than the Tiedtke case as

well.

Before applying a GCM to climate variability or climate change studies for a given region, the accuracy/performance of the model to successfully reproduce the observed main features, characteristics of the climate of the region should be assessed, in order to establish its strengths and weaknesses. This can be best achieved, in the case of Sahel region, using observed dataset as boundary conditions as suggested in the Atmospheric Model Intercomparison Project (AMIP), which methodology consists to carry out simulations with the atmospheric part of the GCM forced at lower boundaries by observed SSTs and Sea ice. At the state of the art, atmospheric models only when forced with observed SSTs, as reported in the last IPCC report ([73] Solomon et al.2007) are able to well reproduce the main African climate features. Coupled atmosphere-ocean models ([21] Cook et al.2006) poorly simulate the West-African climate, [31] Hourdin et al.2010). Nevertheless, most of them tend to capture the mean seasonal migration of rainfall over the area and its intraseasonal variability associated with the mean horizontal wind.

1.2 Objectives of the thesis

This work includes two main objectives which aim to improve the understanding of the WA climate:

1. The first objective is to disentangle the sources of WA rainfall variability at interannual and decadal time scales. Particular attention is given to the role of SSTs and Anthropogenic Sulfate Aerosols (ASAs) on Sahel rainfall variations in terms of physical mechanisms, including recognizing the possible role of ASAs by influencing the key SST patterns that subsequently drive Sahel variations.
2. The second one investigates the main features of WAM climatology and variability as reproduced by one of the state-of-the-art sophisticated GCM. This is reached carrying out different model experiments in coupled and uncoupled configurations representing the past historical simulations performed within the CMIP5 (Coupled Model Intercomparison Project, Phase 5) project.

1.3 Structure of the thesis

This thesis is sectionned as follows:

1. The first chapter is dedicated to the description of the model used, the designed experimental set-up and the description of the observational/reanalysis datasets that

are used for comparison.

2. The second chapter resumes the scientific methodology followed to reach the results. Here the reason of the choice of some particular analysis technique is given.

3. The results are presented from the third chapter with focus on the validation of CMCC model in terms of mean West African climate climatology, Annual and Seosonal rainfall evolution. More precisely, the capability of the model to reproduce the mean features that characterize the climate of WA in terms of rainfall and the associated dynamical structures is assessed.

4. The fourth chapter is dedicated to the variability of the WA rainfall at both the interannual and the interdecadal time scales explained by SSTs forcing and the associated mechanisms.

5. In the fifth chapter, a particular regard is given to the role of the ASAs in shaping the low-frequency Sahel rainfall variability and the mechanisms that are involved.

6. This thesis ends with a summary of the results found in this work and opens a discussion/outlook to particular perspectives.

Chapter 2

Model description, Data and Experimental set-up

In this chapter, we present a detailed description of the model used in this work as well as the experimental set-up. The observational datasets that are used for comparison are also described. The chapter ends with the description of the analysis metrics and techniches we use to reach our results.

2.1 The CMCC Model description and Set-up of the experiments

2.1.1 Model description

The general circulation model used is the Centro Euro-Mediterraneo sui Cambiamenti Climatici, CMCC. The model consists of two main components that communicate through a coupler:

1. The atmospheric component is formed by the fifth generation of ECHAM developed at the Max Planck Institute for Meteorology in Hamburg ([69] Roeckner et al.2003; [70] Roeckner et al.2006). It has a horizontal resolution at T63 triangular truncation, corresponding to a grid of about 1.875° in longitude and in latitude. The shortwave radiation scheme covers the 185-4000 nm spectral interval with a spectral resolution of 6 bands separating the UV and visible ozone absorption ([7] Cagnazzo et al.2007). This version of ECHAM5 includes a well-resolved stratosphere (95 sigma pressure levels in the vertical with the top at 80km - 0.01hPa): stratospheric planetary wave-mean flow interaction is explicitly resolved and the effects of both orographic and non-orographic gravity waves on the stratospheric and mesospheric large-scale flows are parameterized ([47] Manzini et al 2006; [11] Charlton et al.2007; [8] Cagnazzo and Manzini 2009). The parametrization of convection is based on the mass flux concept ([75] Tiedtke 1989), modified following [55] Nordeng (1994).

2. The ocean - sea ice component is OPA-LIM, 31 depth levels with 10 in the upper 100 m and a horizontal resolution of 2° in longitude and in latitude with an increase of the meridional resolution to 0.5° around the equator ([46] Madec et al., 1999; [76] Timmermann et al.2005). The physical and technical coupling interface is described by [24] Fogli et al.2009.

The communication between the atmospheric and the ocean components is carried out with the Ocean Atmosphere Sea Ice Soil version 3 (OASIS3) coupler2 ([81] Valcke et al.2006). Every day (coupling frequency), heat, mass, and momentum fluxes are computed and provided to the ocean by the atmospheric model. SSTs and sea surface velocities are provided to the atmospheric model by both ocean models. The global ocean model also provides sea ice cover and thickness to the atmospheric model. The relatively high coupling frequency adopted allows an improved representation of the interactions occurring at the air-sea interface. No flux corrections are applied to the coupled model.

2.1.2 Experimental set-up

In this work, we perform two set of model runs representing the past historical simulations. There are realized in coupled or uncoupled mode configuration: atmosphere and ocean interacting or not.

In the first set of three model runs, ASAs vary at monthly time resolution from year to year:

1. **AOCOUP run:** in this experiment, the atmospheric model (ECHAM5) is coupled to the above described OPA-LIM ocean model via the coupler OASIS3. This simulation aims to reproduce the observed climate of the region of interest and its variability. Furthermore, it provides a test-bed to evaluate the role of air-sea feedbacks on the WA climate and variability.

2. **AMIP run:** the atmospheric model ECHAM5 is forced at the bottom boundaries with observed Hadley Centre SSTs and Sea Ice dataset ([61] Rayner et al.2003). This simulation helps to assess the capability of the atmospheric model to reproduce the observed variability of the WA climate, when forced by observed SSTs. Furthermore, it helps to explore the mechanisms that link the WA variability to the oceanic SSTs variations.

3. **AMIPlike run:** in this simulation, the atmospheric model ECHAM5 is forced with prescribed SSTs and sea ice (as in the AMIP experiment), obtained from the above described AOCOUP coupled simulation . This experiment, in combination with the AOCOUP run allows to explore the role of the air-sea feedbacks, whereas its comparison with AMIP allows to understand the role of the different SST forcings on the WA climate variability.

In the second set of two model runs, ASAs are set to climatology, which is the yearly monthly average over 55 years, from 1950 to 2004. There are hence kept constant from one year to another, and vary from one month to another month within the same year.

4. **AMIP-Aero run:** Same as AMIP run with prescribed climatological ASAs and prescribed varying SSTs and Sea ice from the observed Hadley dataset.

5. **AMIPlike-Aero run:** Same as AMIPlike run with prescribed climatological ASAs and prescribed varying SSTs and Sea ice from AOCOUP.

AMIP-Aero and AMIPlike-Aero, compared to AMIP and AMIPlike, aim to assess the role that ASAs might play in shaping the climate of WA.

All Simulations are Historical

Simulation	Time period	SSTs and Sea Ice	Aerosols
AOCOUP	1850-2005	Coupled Ocean-Atmosphere	Vary
AMIP	1950-2007	Hadley	Vary
AMIPlike	1950-2004	AOCOUP	Vary
AMIP-Aero	1950-2004	Hadley	Climatology
AMIPlike-Aero	1950-2004	AOCOUP	Climatology

Table 2.1: *Summary of the model runs performed in this thesis*

All the model simulations are summarized in the Table 2.1. The AOCOUP experiment presented here started from a stable control simulation (a few thousand years). Estimated conditions in 1850 determine the external forcings of the piControl experiment and follow the CMIP5 protocol (http://cmip-pcmdi.llnl.gov/cmip5/). Instead, in AMIP, AMIPlike, AMIP-Aero and AMIPlike-Aero, the atmosphere reaches the equilibrium after 10 years of spin-up from 1940 to 1949. ASAs are from the CMIP5 project. In all model runs, External forcings well-mixed greenhouse gases, including CO2, CH4, N2O, and incoming solar irradiance (total value: 1367 Wm2) are from CMIP5 as well and vary every year; the seasonally varying ozone distribution is repeated every year. At the surface, vegetation is set constant and rivers are climatological at the mouth of the continents.

2.2 Description of the datasets used for comparison

Model simulation results are compared to available observation and reanalyzes datasets.

The SSTs are provided by the Met Office Hadley Center's Sea Ice and Sea surface Temperature (HadISST1, [61] Rayner et al.2003). It is a combination of monthly globally complete fields of SST and sea ice concentration on a 1° latitude-longitude grid from 1870 to 2011.

Precipitation field comes from the Climate research Unit (CRU) TS 3.00 dataset ([49] Mitchell et al.2004) and contains monthly global land precipitation on a regular grid (0.5° x 0.5°) for the period 1901-2000; the Global Precipitation Climatology Project (GPCP, [2] Adler et al.2003) is a globally complete, monthly analysis of surface precipitation at 2.5° latitude x 2.5° longitude resolution from January 1979 to the present. It incorporates precipitation estimates from low-orbit satellite microwave data, geosynchronous-orbit satellite infrared data, and surface rain gauge observations.

Wind fields and surface temperatures are from the European Center for Medium-Range

Weather Forecast Re-Analysis (ERA-Interim, [66] Simmons et al.2007a; [67] Simmons et al.2007b, [79] Uppala et al.2008). Data are globally complete fields of monthly zonal and meridional winds on a 1.875° latitude-longitude grid from 1989 to 2012.

Other fields are publicly available through the International Research Institute (IRI) for Climate and Society data library webserver (*http://iridl.ldeo.columbia.edu/index.htlm*). Specific humidity and temperatures are extracted from the NCEP-NCAR Climate Data Assimilation System I (CDAS-1) reanalysis dataset, [37] Kalnay et al.1996. NCEP-NCAR is a cooperated reanalysis project between the National Centers for Environmental Prediction (NCEP) and the National Center for Atmospheric Research (NCAR), to produce 40 years records (1957-1996) of global atmospheric fields. They are monthly globally fields on a 2.5° latitude x 2.5° longitude resolution from January 1949 to the present.

All the data (both model and observations) are interpolated into the HadISST1 dataset grid for comparison. All the Analyzes are done for the summer season from 1950 to 2004 and are limited to 1989-2004 when datasets are not available for longer time period.

2.3 Description of Analysis metrics/techniques used

2.3.1 Standard Deviation (STD)

A simple common approach to quantifying the magnitude and spatial distribution of the variability of a nonseasonal data is to map its dispersion from its mean. The more spread apart the data, the higher the deviation. The standard deviation map does not give any information on how the variations of the variable at one location are related to those at another location.

2.3.2 Empirical Orthogonal Function (EOF) and Linear Regression/Correlation

To ascertain the covariability of variable anomalies at different locations, alternative analysis methods are needed. One commonly used approach is the empirical orthogonal function - EOF ([82] von Storch and Zwiers, 1999). Conceptually, EOF analysis determines the most dominant modes of internal variability in a data set removing redundancy and multicollinearity. It filters out spatio-temporal pattern of variability that accounts for the maximum covariance between a variable anomaly time series at all pairs of grid points in the data set. Then, the remaining covariability is subject to the same decomposition with the constraint that the second spatio-temporal EOF pattern is orthogonal (e.g., uncorrelated) both in time and space to the leading EOF pattern. This procedure is repeated until all n EOF patterns have been computed, where n is equal to the number of grid points.

In practice, only the first few leading modes are robust as a result of the orthogonality constraint. EOF rotation may be used to circumvent this constraint; however, it may also result in patterns that are overly localized in space. Each EOF pattern is associated with a principal component (PC) time series, which describes the temporal evolution of the EOF pattern. The PC time series is obtained by projecting the EOF pattern onto the original field anomaly at each time step so as to find the sign and amplitude of the pattern at any given time. It should be noted that the sign of the EOF is arbitrary; however, the product of the EOF and the PC time series recovers the correct polarity of the mode at any given grid box and time. Although useful, EOF modes depend on the spatial domain considered and as they are subject to orthogonality constraints, they may not be separable if accounted for similar percentages of the total variance ([56] North et al.1982). EOFs are then empirically determined modes (due to dependence on the actual data set and values) and thus are not necessarily equivalent to the dynamical modes of the system. It is always prudent to confirm EOF patterns with simpler techniques such as compositing, linear regression/correlation maps. The general purpose of linear regression/correlation analysis beeing to find a (linear) relationship between a dependent variable and a set of explanatory variables.

2.3.3 Compisite Analysis

Composite analysis is one of the simplest analysis techniques applied to time series. It consists of sorting data carefully and logically into categories and comparing means for different categories. Composite analysis is useful when having many observations of some event and looking for responses to that event that are combined with noise from a lot of other influences. The idea is to average the data in a clever way in relation to the particular event such that all other influences are filtered out and only the event signal remains. Often, composite analysis reveals periodic phenomena with fixed phase that cannot be extracted from spectral analysis if the signal is small compared to the noise.

2.3.4 Maximum Covariance Analysis (MCA)

The Maximum Covariance Analysis - MCA ([6] Bretherton et al.1992) is also known as Singular Value Decomposition analysis ([83] Wallace et al.1992). The MCA can be considered as a generalization of the EOF Analysis, and indeed reduces to it when the two fields are identical. While the EOF analysis determines the dominant pattern of variability of one dataset, the purpose of the MCA is to find the pairs of coupled patterns explaining the largest covariance between two fields, for instance patterns of rainfall that go along with patterns of SST. It is usually used to study the coupling between parameters to understand physical mechanisms of climate variations, for instance, how are SST and West Africa rainfall related in terms of patterns of variability? The MCA yields two sets of singular vectors and a set of singular values associated with each pair of vectors. The

kth Expansion Coefficient (EC) for each variable is computed by projecting the respective data field onto the kth singular vector. The Correlation value between the kth ECs of the two variables indicates how strongly related the coupled patterns are.

Chapter 3

Results: Model African Climate Climatology and Rainfall Evolution

In this chapter, we focus on the validation of the CMCC model. We assess its capability to reproduce, in different SSTs configurations and prescribed varying anthropogenic sulfate aerosols, the mean summer West African climate in terms of rainfall and associated dynamical structures. The mean seasonal rainfall evolution is considered as well as its mean annual cycle.

3.1 Sea Surface Temperatures (SSTs)

The long-term June-July-August, JJA, summer mean global SSTs, averaged over 55 years from 1950 to 2004, for observation - Hadley (top panel) and model - AOCOUP (middle panel) is displayed on Figure 3.1. Overall, the coupled model reasonably depicts the main features of the global summer mean SSTs climatology; the upwelling zones along the equatorial Pacific and coastal Peru and the eastern tropical South Atlantic. The North eastern Pacific suffers with a warm bias which is particularly pronounced along the western coast of central Africa in the equatorial Atlantic. In general, the coupled model JJA-SST climatology presents a warm bias in the tropical ocean (20°S-20°N) and a cold bias in the extratropics, especially in the Mediterranean and the North Atlantic where differences exceed 4°C (bottom, Figure 3.1).

3.2 Surface Temperatures: West African Heat Low

The West African Heat Low (WAHL) has been identified as a key dynamical element of the WAM system ([44] Lavaysse et al.2009). It is an area of high surface temperatures associated to high insolation and low local evaporation. Over continental Africa, its associated upward motion generates a cyclonic circulation aloft which helps to strengthen and maintain (with the combination of the diabatically forced meridional circulation due to surface fluxes) the AEJ ([77] Thorncroft and Blackburn 1999). Figure 3.2 displays the mean boreal summer (JJA) surface temperature (colors) with the superimposed 925 hPa winds (vectors) from the ERAInterim reanalyzes Figure 3.2, a) and the different model runs. Overall, ERAInterim and the model are in good agreement even though the model's velocity tends to be overestimated. Over land, they all capture the temperaure peaks with the formation of the WAHL in the Sahara desert surrounded by a cyclonic circulation (North of the Sahel and South of the Sahara). The coupled run - AOCOUP, which takes into consideration the possible air-sea feedbacks and fluxes exchanged between the atmosphere and the ocean, underestimates the heat low intensity by ~ 3°C (Figure 3.2, b).

3.3 Surface Temperatures Biases

Figure 3.3 displays the model minus ERAInterim reanalyzes mean summer surface temperatures (colors) and winds (vectors) biases. In one hand, the reanalyzes are compared with the AMIP run (Figure 3.3, a) and in the other hand with the AOCOUP run (Figure 3.3, b). Over land, the model presents a cold bias over Sahara with higher values of ~ 4°C in the coupled run and over South Africa with higher values of ~ 4°C for AMIP. Warm surface temperature biases are present over the entire Sahel up to the red sea and

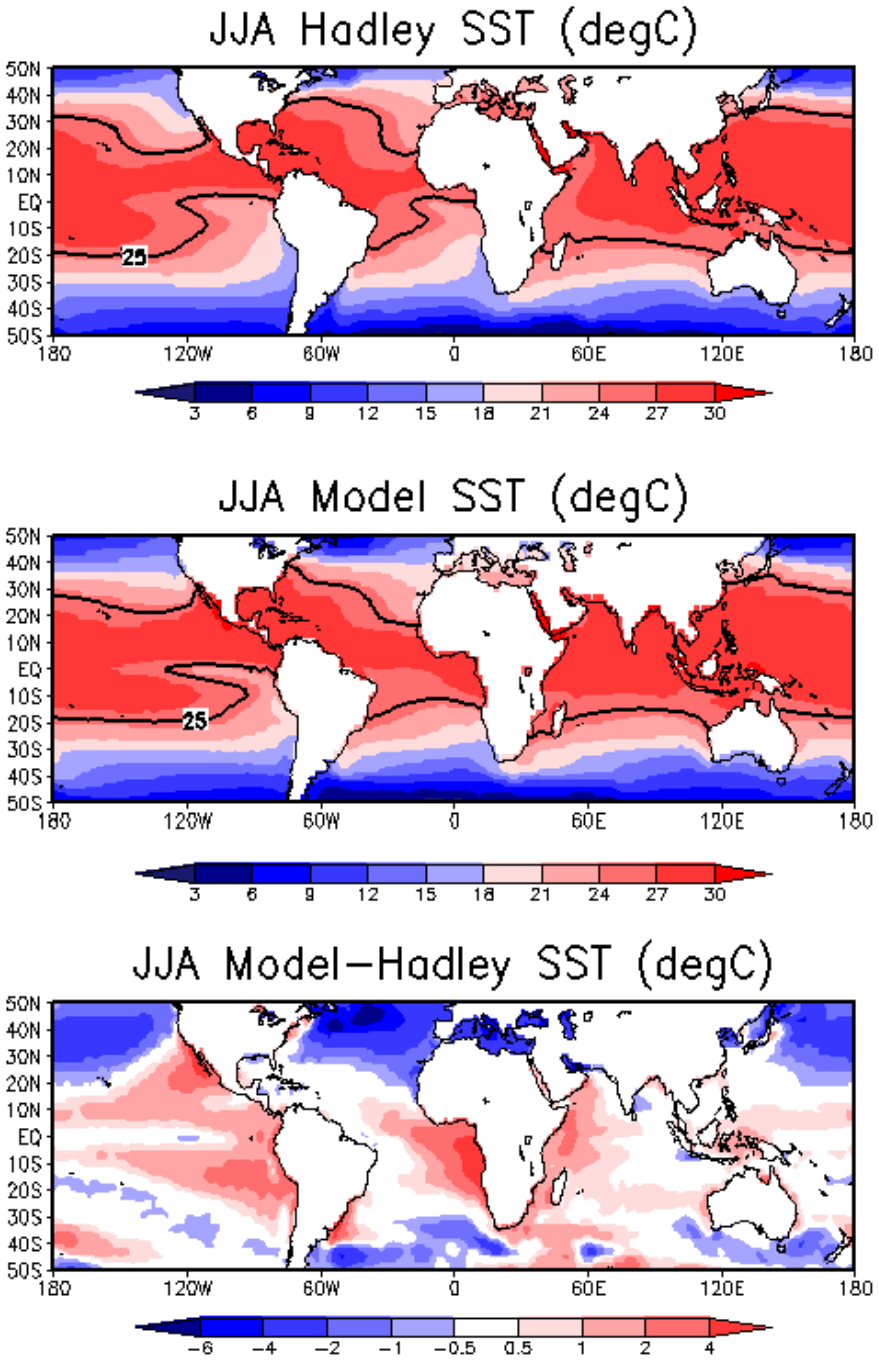

Figure 3.1: *1950-2004 June-July-August (JJA) Sea Surface Temperatures (SSTs) climatology: Observations-Hadley (top) and coupled Model (Middle). The black line represents 25°C. The bias (model minus observations) is shown at the bottom panel.*

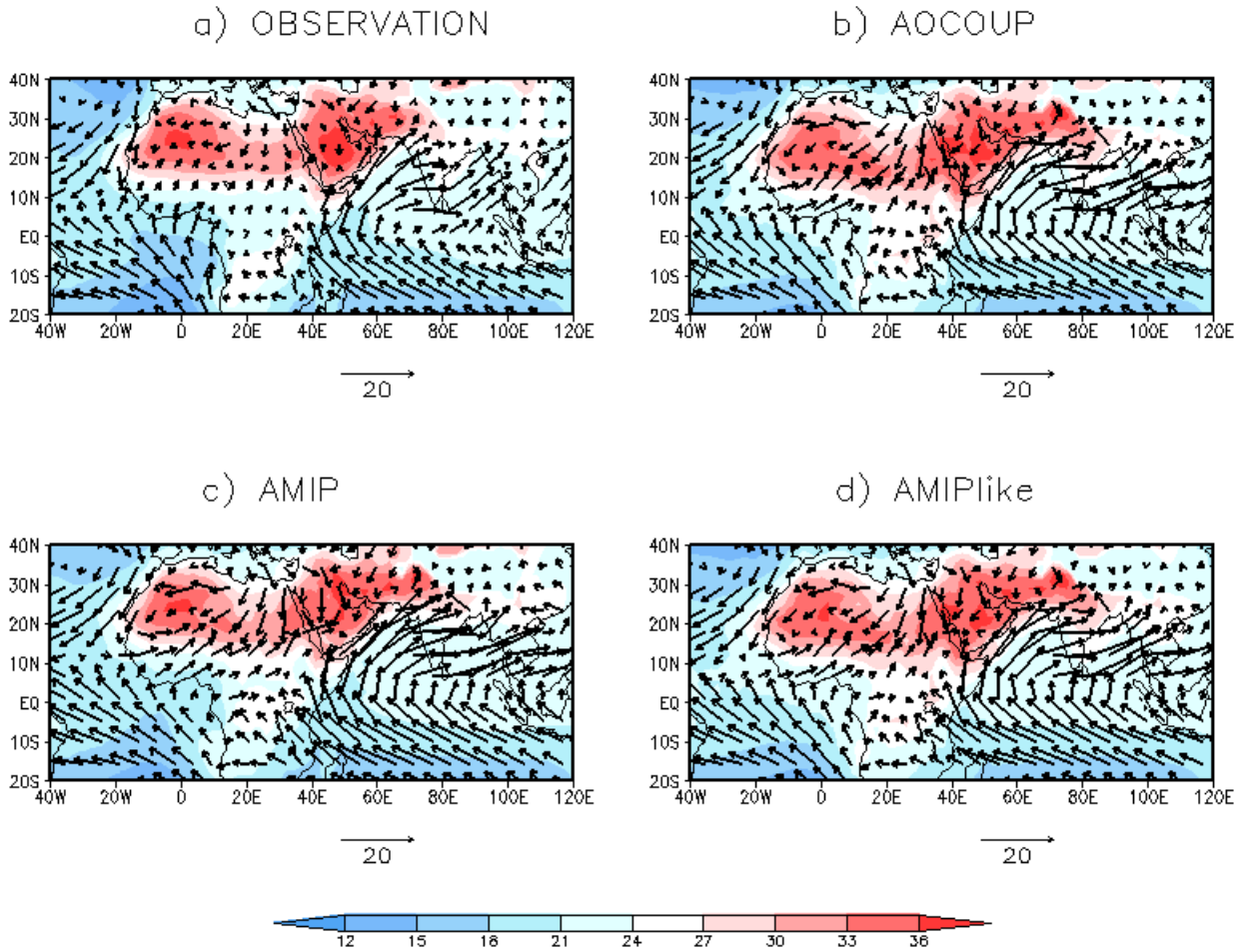

Figure 3.2: *1989-2004 June-July-August (JJA) Surface Temperature (colour) with superimposed 925 hPa winds (vectors). Observations-ERAInterim (a), AMIP(c), AOCOUP (b) and AMIPlike (d).*

the central equatorial Africa for AOCOUP run with highest values of $\sim 6°C$ located in the East Sahel. The warm biases are restricted to the East Sahel again till the red sea and the Central Equatorial Africa with values of $\sim 3°C$. Over the sea, warm temperature biases are present in the south tropical Atlantic with values up to 6°C and cold biases of $\sim 3°C$ in the North Atlantic. Cold temperature biases in North Africa act to strengthen the harmattan winds while warm biases over south tropical Atlantic reduce the strength of the monsoon which is clear for AOCOUP ([62] Rodriguez-Fonseca et al.2010). This special issue in [62] Rodriguez-Fonseca et al.2010 paper has been discussed when assessing the response of the West African monsoon to the SST forcing especially the tropical Atlantic at the interannual time scale. The authors concluded that warming of the tropical Atlantic will overall lead to a dipole anomalous precipitation over West Africa with positive anomalies over the Gulf of Guinea and negative anomalies in the Sahel. In fact, warming of the tropical Atlantic will decrease the land-ocean temperature and latitudinal pressure gradients that will lead to the maximum convection to the South and decrease the Sahelian convergence with the final result of a decrease of the Sahelian rainfall and an increase of rainfall in the Gulf of Guinea.

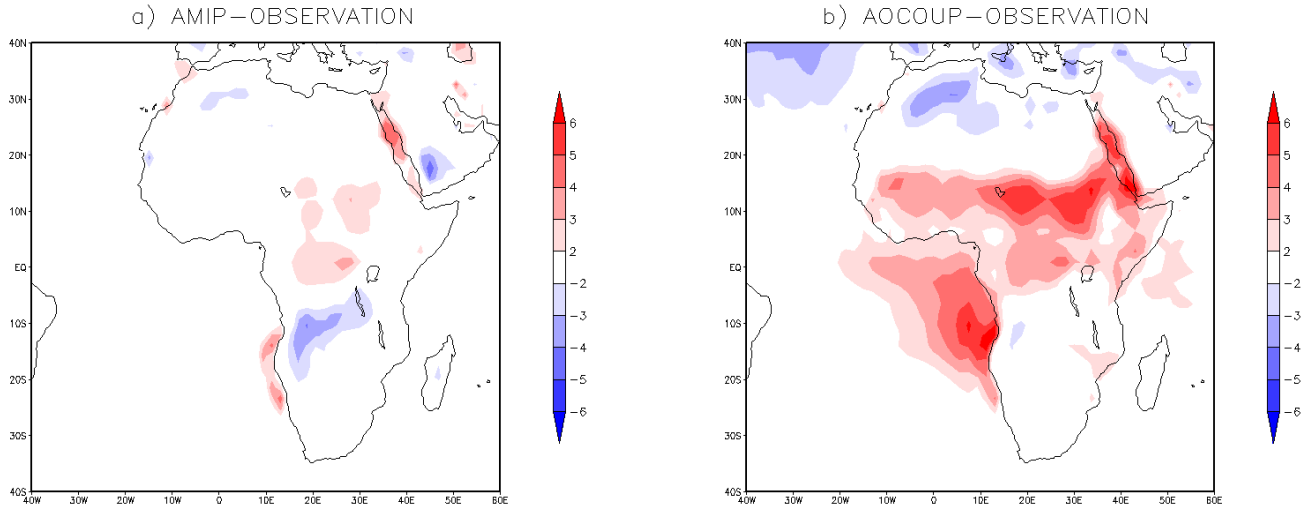

Figure 3.3: *1989-2004 Boreal Summer (June-July-August, JJA) surface temperature biases in °C: AMIP minus ERAInterim (a) and AOCOUP minus ERAInterim (b).*

3.4 African Easterly Jet - AEJ

During the monsoon season, the African Easterly Jet, AEJ, prevails over west Africa and is located at about 15°N (Figure 3.4, a, observations). It extends longitudinally from the Atlantic ocean towards west African inland where it reaches an average velocity of 15m/s. It lies in a region of strong latitudinal temperature gradient in the lower troposphere

between the northern Sahara and the Guinean coast. The model is overall able to capture the general characteristics of the AEJ (Figure 3.4, AMIP(c), AMIPlike(d), AOCOUP(b)).

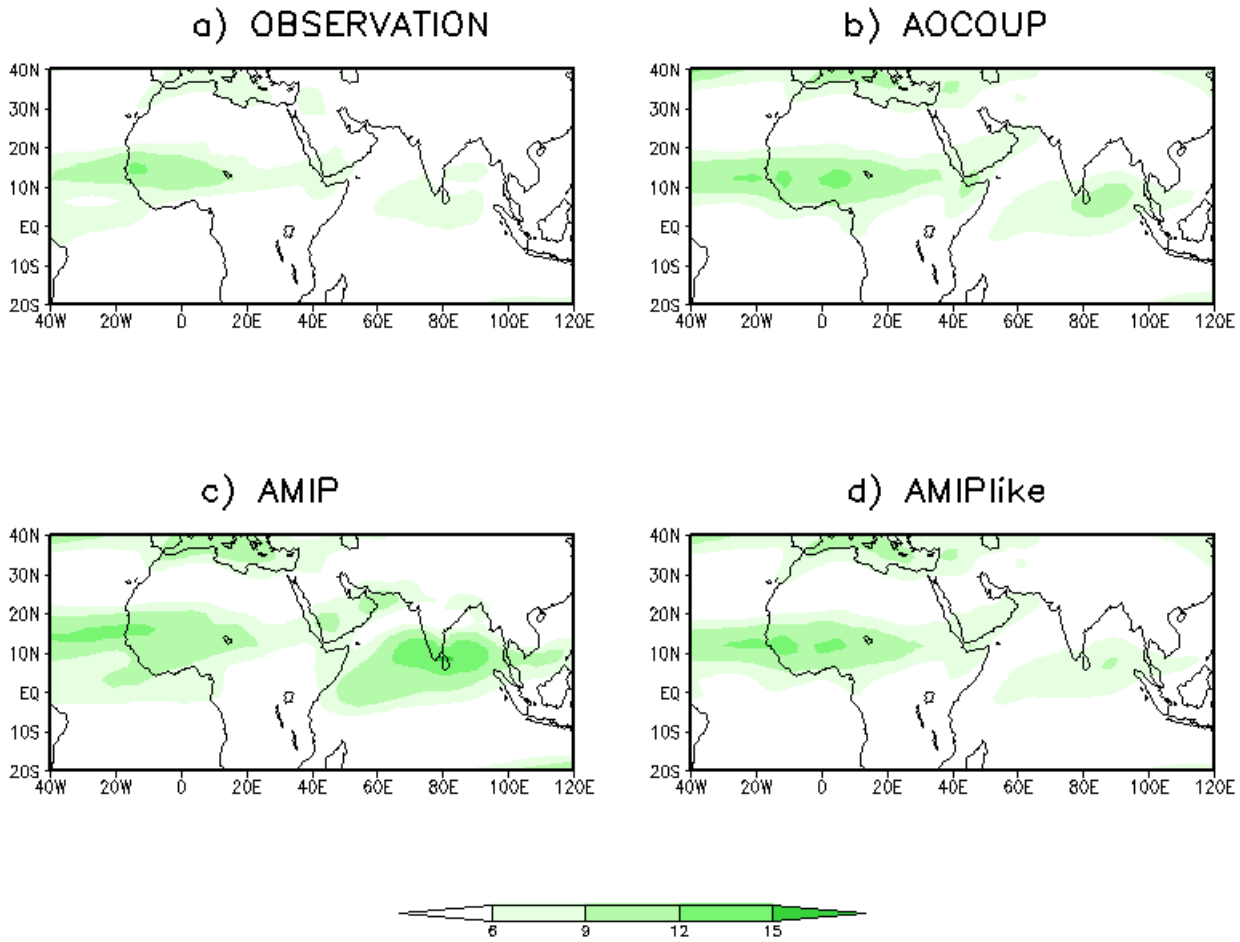

Figure 3.4: *1989-2004 June-July-August (JJA) Modulus of the wind at 600hPa. a - Observations: ERAInterim, AMIP(c), AOCOUP (b) and d) AMIPlike (d).*

3.5 Tropical Easterly Jet - TEJ

In boreal summer, strong easterlies in the upper troposphere prevail over the entire WAM area as shown in Figure 3.5, a). The mean flow is dominated by the TEJ, which peaks over the Indian ocean and is best developed at about 200hPa. While the AEJ is stronger over the western portion of African continent, the TEJ instead is stronger over east Africa. The mean TEJ latitudinal position and intensity are successfully simulated by the model despite some deficiencies. When the atmospheric component of the model is forced with prescribed observed SSTs (AMIP, Figure 3.5, c), its captures well the position of the TEJ but slightly overestimates its intensity. Instead, when forced with prescribed model SSTs

(AMIPlike, Figure 3.5, d) and in the coupled run (AOCOUP, Figure 3.5, b), its intensity appears weak and the TEJ is mainly limited to the indian ocean.

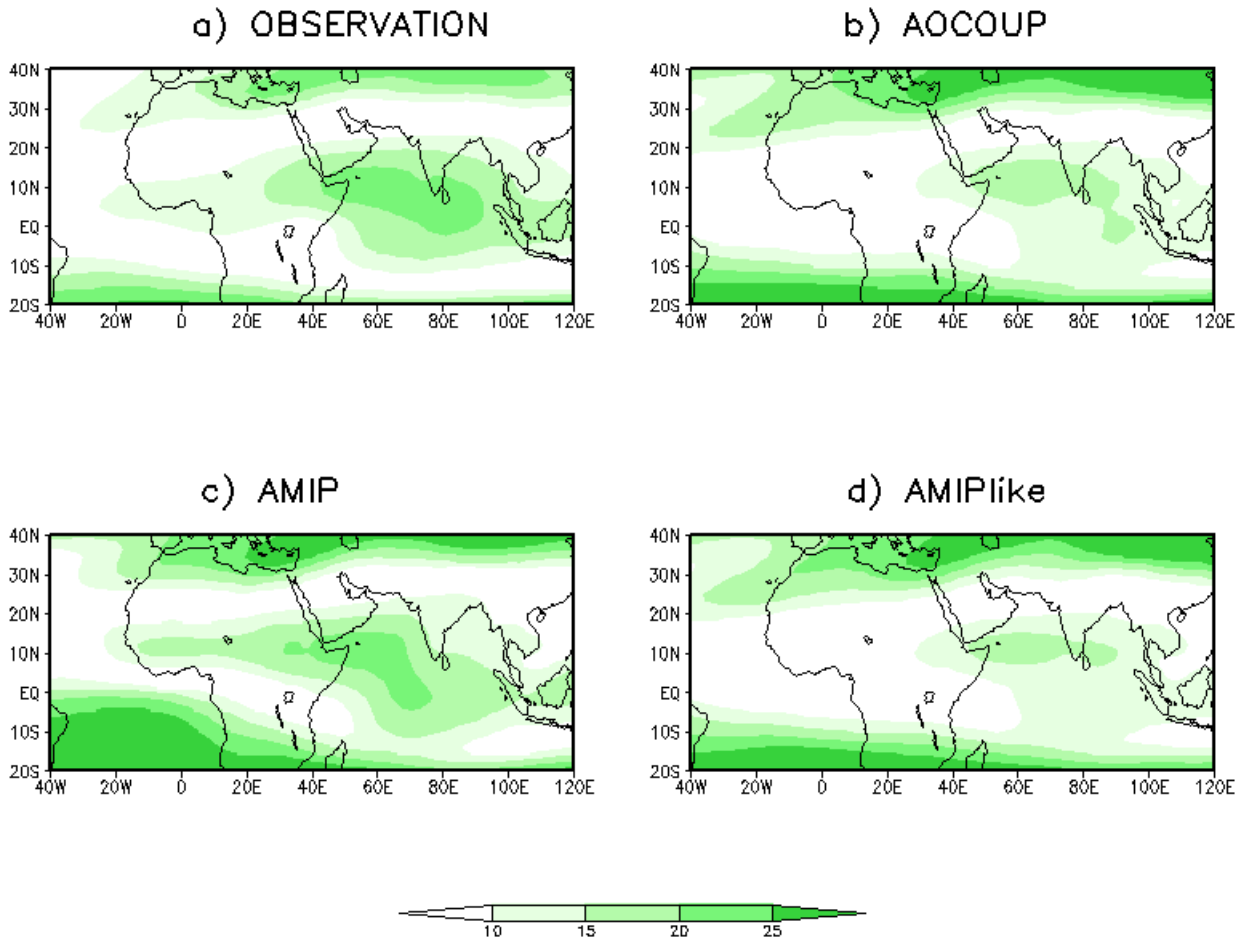

Figure 3.5: *1989-2004 June-July-August (JJA) Modulus of the wind at 200hPa. a - Observations: ERAInterim, AMIP(c), AOCOUP (b) and d) AMIPlike (d).*

3.6 Zonal Wind profile

The observed zonal wind profile during boreal summer (June-July August, JJA) averaged between 10°W and 10°E (Figure 3.6, a) illustrates the main dynamical large-scale feature associated with precipitation over Africa. The near surface monsoon flow is located between 0°-15°N, the dry southward Harmattan airflow from the Sahara between 20°N and 30°N at the low-level between the surface and 850hPa. The AEJ is instead located at the mid-level at 600hPa centered around 13°N and the TEJ in the upper troposphere at 200hPa and around 10°N.

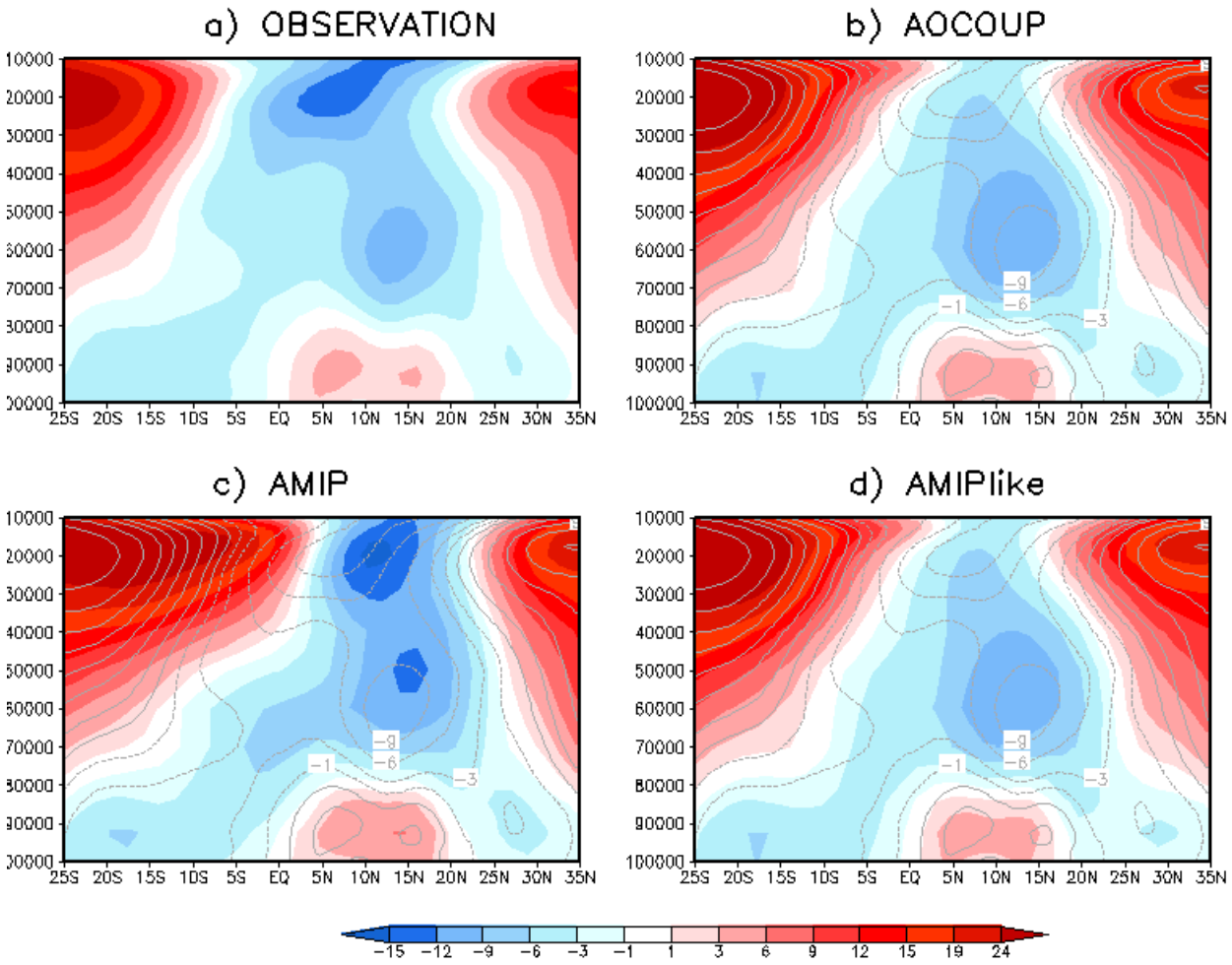

Figure 3.6: *Vertical cross section of the zonal wind during 1989-2004 boreal summer (June-July-August, JJA) averaged between 10°W-10°E for ERAInterim (a), AMIP(c), AOCOUP (b) and AMIPlike (d). Grey contours on model plots are the same as for ERAInterim.*

As in any monsoon system, the monsoon flow is a major source of water vapor for West Africa, as it brings evaporated water over the Gulf of Guinea. Previous studies ([20] Cook 1999; [77] Thorncroft and Blackburn 1999) have shown that the AEJ is a result of the strong meridional surface moisture and temperature gradients between the Sahara and Equatorial Africa, and the TEJ, a result of the reversal in the mid-tropospheric thickness gradient due to the heating over the Tibetian plateau and the Himalayas; so is associated with the upper-level outflow from the Asian monsoon.

Overall, AMIP (Figure 3.6, c) captures the main features that characterized the atmospheric circulation over Africa. The monsoon flow is reasonably simulated both in latitudinal extent and intensity but it is less penetrative around the Equator. The core of the AEJ is well isolated but its intensity is slightly overestimated and slightly shifted northward and upward as well. The core of the TEJ is well captured around 200hPa but its strength is slightly overestimated and shifted northward. The shift of the core and the overestimation of the easterlies have been shown to be related to strong surface temperature gradients ([20] Cook 1999).

The coupled model (Figure 3.6, b) as well as AMIPlike (Figure 3.6, d) also simulate less penetrative monsoon but capture well its intensity. The isolated core of the TEJ is almost missing in both simulations. The weakness of TEJ has been shown to be a common problem of state of the art coupled models. Additionally, [14] Chen and Van Loon, 1987 have shown that it tends to be weaker during warm phase of the Pacific ENSO. AOCOUP and AMIPlike both show a wider latitudinal extension of the AEJ with a right position of the core but the intensity is slightly overestimated in AMIPlike.

3.7 Precipitation

In this section, we examine the spatial patterns of boreal summer precipitation and the associated low-level circulation. Figure 3.7 compares CRU precipitation and 925 hPa ERAInterim winds climatologies (a) in JJA with the corresponding model fields over the period 1989-2004. At this time of the year, the ITCZ is at its northernmost location and the WAM rainfall is at its maximum. Observations show a band of maximum rainfall, centered along 10°N, that spans the African continent, with three maxima connected to orographic features over the Guinean, the Cameroon and the Ethiopian highlands. The associated low level circulation shows north and south Atlantic anticyclonic flows, the WAM flow as well as northerlies and easterlies around the Sahara thermal low region. Rainfall in the India and Indian ocean is associated to the lower tropospheric Somali jet which is developed as a response to the land-sea gradient of large-scale heating ([74] Sperber et al., 2000).

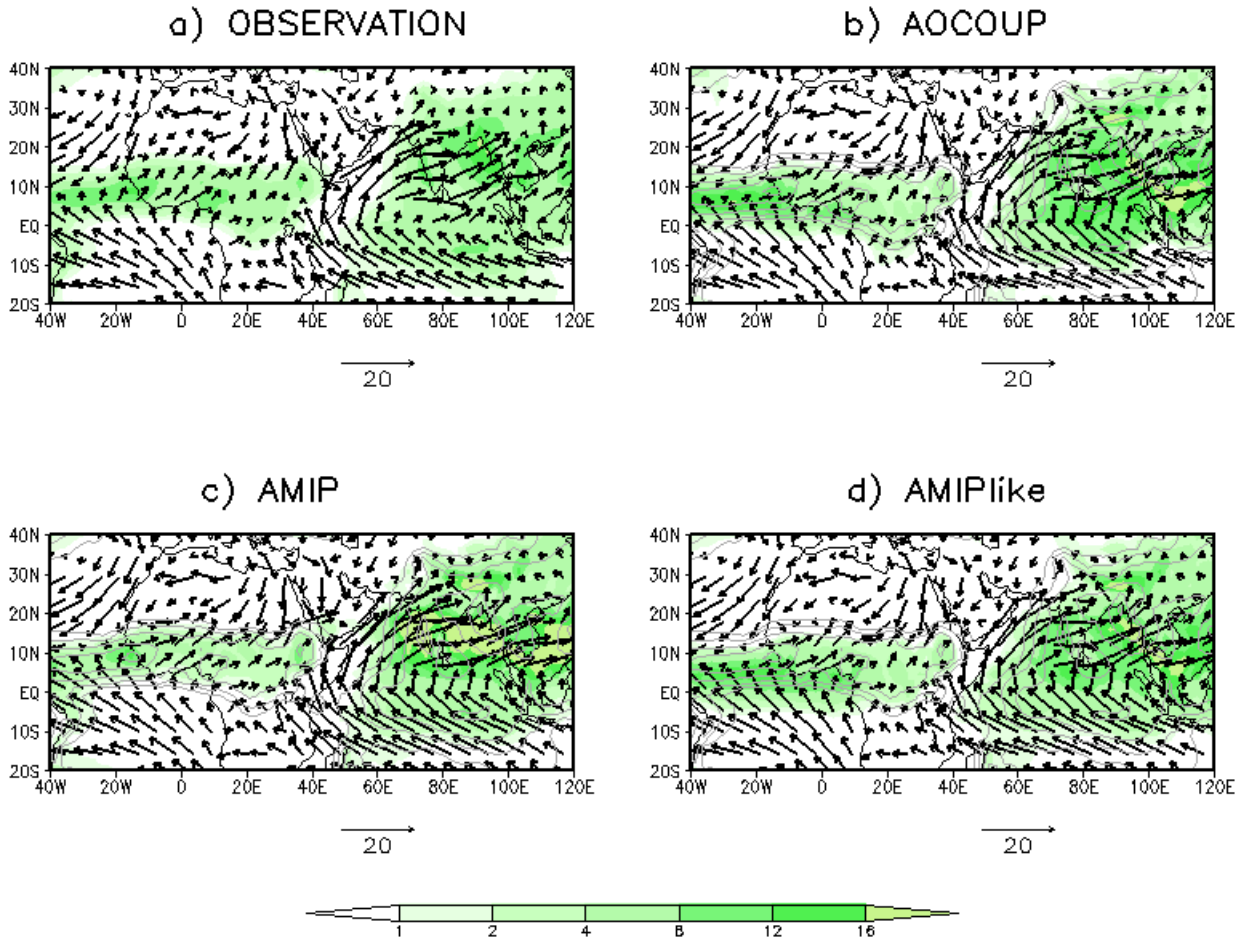

Figure 3.7: *1989-2004 June-July-August (JJA) Rainfall (colour) with superimposed 925 hPa winds (vectors). a - Observations: GPCP (colour) and ERAInterim (vectors), AMIP(c), AOCOUP (b) and AMIPlike (d).*

Overall, all three model simulations reasonably depict the main features of precipitation and low level wind climatologies for African and Indian monsoon systems. In general, the model overestimates the rate of the Asian monsoon rainfall mainly along the coast of Asia but its spatial spread is well reproduced. The seasonal reverse in direction and the intensification of the Somali jet are also well captured. The low level circulation features of the WAM are well reproduced with a slight overestimation of wind intensity in the northern Sahel in all model runs. The intensity of precipitation is well captured but the rainbelt seems to be narrow in AMIP (Figure 3.7, c) and fails to capture the Cameroon highlands maxima. On the other hand, the position of the ITCZ seems to be shifted southward in AOCOUP (Figure 3.7, b) and AMIPlike (Figure 3.7, d) runs and the monsoon flow is less penetrative, locating the maximum of rainfall mostly in the Atlantic ocean. However, AOCOUP and AMIPlike capture well the three maxima both in position and intensity. The southward shift of the whole rainfall monsoon system in AOCOUP and AMIPlike seems to be a common problem to the other state of the art coupled general circulation models ([31] Hourdin et al.2010).

3.8 Analysis of the African Rainfall Evolution

In this section, we focus on the seasonal migration of the ITCZ over West Africa as well as the rainfall annual cycle in different African subregions.

3.8.1 Seasonal Evolution

Figure 3.8 displays the Hovmoëller diagram of the seasonal migration of the ITCZ over west Africa. In the observations (contours, a, b, c, top row), the first transit of the ITCZ over the Guinean coast occurs in spring between May and June (onset of the monsson), followed by a short dry season in July - August over the region, which contrasts with the establishment of the rain season over the Sahel. During Fall, from the end of September to the beginning of October, the ITCZ quickly withdraws, re-watering the Guinean coast. AMIP (Figure 3.8, a) AMIPlike (Figure 3.8, b) and AOCOUP (Figure 3.8, c) runs are able to reproduce the seasonal migration of the ITCZ with a one month phase shift. While AMIP is characterized by a weaker penetration of the monsoon, AMIPlike and AOCOUP seem to shift the ITCZ to the South as mentioned before. These biases in the model could be related to the convection scheme used, which has been shown to play an important role in rainfall representation in GCMs ([31] Hourdin et al.2010). Obviously, a higher rainfall variability associated to the North and South migration of the ITCZ is depicted where (position) and when (time phase) rain rates are higher (Figure 3.8, d, e, f, bottom row).

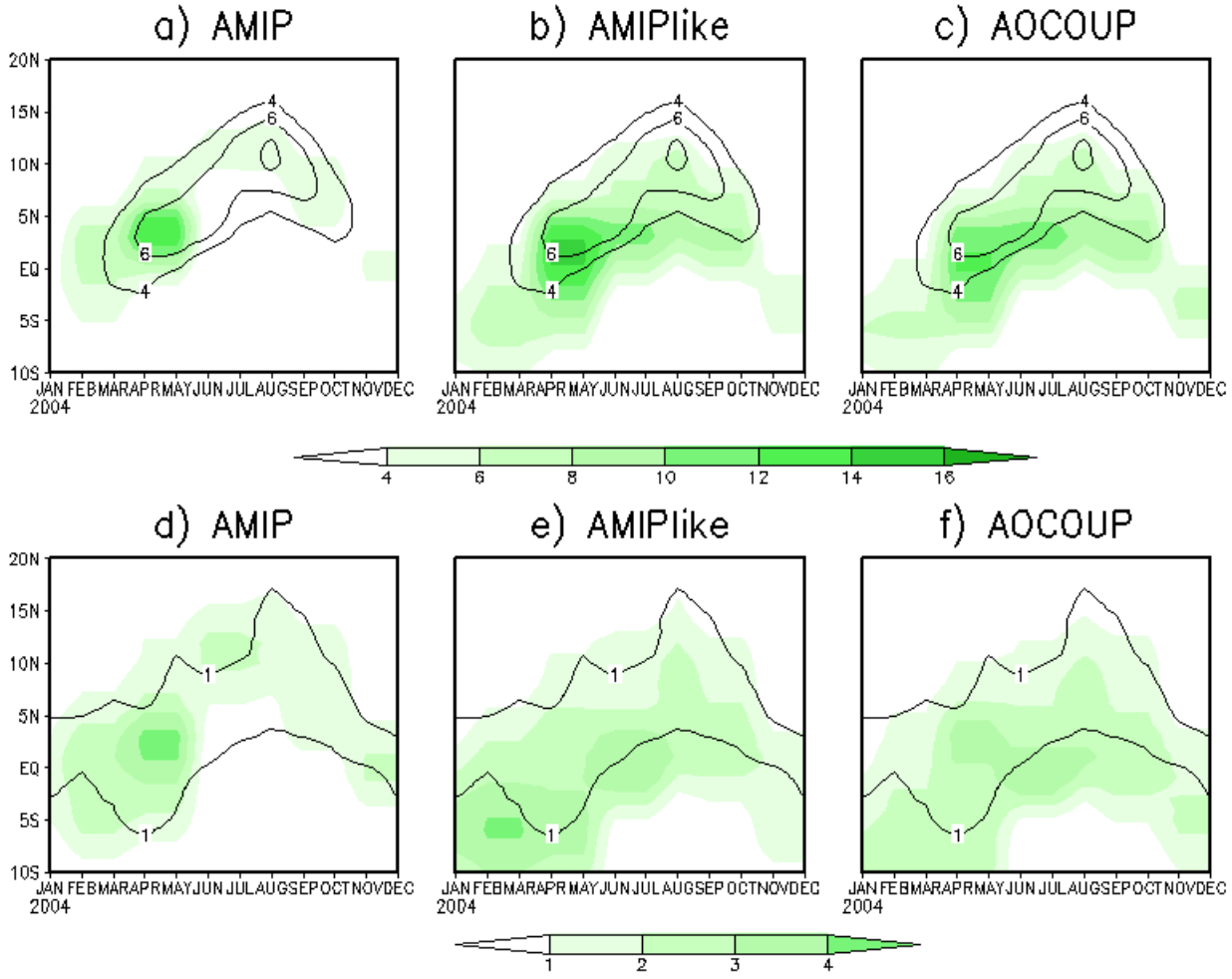

Figure 3.8: *Hovmoëller diagram of rainfall in mm/day averaged between 10° W-10° E for GPCP (black solid) and model simulations. (a), (b) and (c) represent the mean rainfall for AMIP, AMIPlike and AOCOUP respectively and (d), (e) and (f) the corresponding standard deviations.*

3.8.2 Mean annual cycle

According to GPCP and CRU (Figure 3.9, a, dot and solid black lines respectively), West Sahel precipitation annual cycle peaks in August with some slight differences in the intensities among the observed estimates. AMIP (Figure 3.9, a, green) and AOCOUP (Figure 3.9, a, grey) both reproduce the observed peak in August but tend to underestimate its magnitude with AMIP closer to observation. AMIPlike (Figure 3.9, a, red) captures also the West Sahel rain season but it peaks in September.

Over the East Sahel (Figure 3.9, b), the same annual phase is found with the difference that the observed intensities are lower than than in West Sahel. All model runs underestimate the precipitation peaks but capture their phases in August.

Over the Guinean coast (Figure 3.9, c), all the observational datasets show a primary maximum during Spring in May-June, a secondary one during Fall in September-October and a relative minimum in mid-summer. AMIPlike and AOCOUP capture the phase of the two maxima, but tend to overestimate precipitation compared to the two observational datasets. AMIP captures the two rain seasons but overestimates the spring maximum which peaks one month earlier and underestimates the mid-summer minimum which peaks in October. The two rain seasons are separated by a very pronounced dry season during summer with almost no rain as all the rainfall migrates in the Sahel.

Two precipitation maxima are also found in the North Equatorial Central Africa (Figure 3.9, d) with the summer maxima more pronounced than the one in spring. AMIPlike and AOCOUP again capture the phase of the spring peak and delay the second one by two months. In general, they both underestimate the rainfall intensities. AMIP captures the double peaked seasonal structure as well separated by a dry point structure in July. The rainfall magnitudes are underestimated.

The general observation that comes out from this analysis is that AMIP looks closer to observations over the Sahel while the coupled model as well as AMIPlike seem to performing better in the Equatorial regions.

3.9 Summary and conclusions

The CMCC general circulation model is able to reproduce the mean features that characterize the West African Monsoon system but few biases emerge. One should cite the weakness of the simulated AEJ and the widening of its latitudinal extension, the underestimation of the westward extension of the TEJ over the African continent in AMIPlike and AOCOUP. As many state of the art coupled GCMs, the main WAM system is shifted southward in the coupled and AMIPlike runs. This last issue might be related to the convection scheme used ([31] Hourdin et al., 2010) . In general, the mean anuual cycle

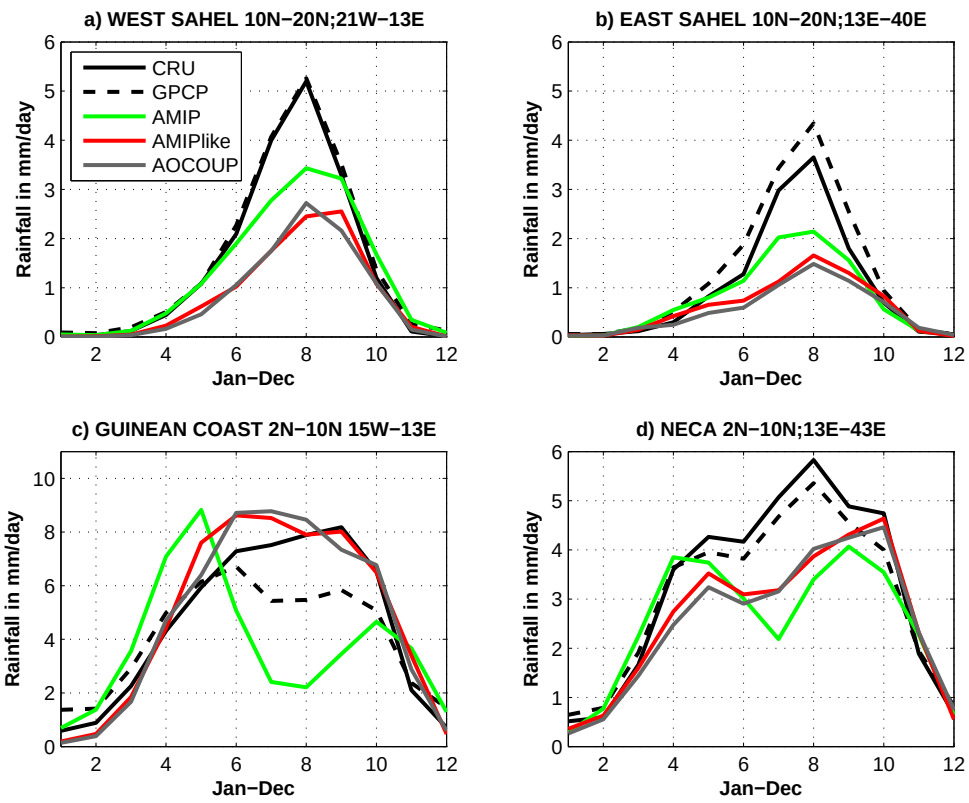

Figure 3.9: *Annual cycle of standardized precipitation (mm/day) for CRU (black solid), GPCP (black dot), AMIP (green), AMIPlike (red) and AOCOUP (grey), averaged over West Sahel (a); East Sahel (b); Guinean Coast (c) and North Equatorial Central Africa - NECA (d).*

of precipitation , including single and multiple rain seasons, is well captured over most of African subregions, even though AMIP seems to performing better in the Sahel and the coupled model as well as AMIPlike in the equatorial Africa. Overall, it is assessed that the performance of model used here is of sufficient quality for application to climate change and climate variability studies over west Africa .

Chapter 4

Results: Interannual and Interdecadal Rainfall Variability and the associated mechanisms

In this chapter, we focus on the dominant SSTs and West African rainfall coupled patterns of variability. A link between those patterns of variability in terms of mechanisms is determined. This is assessed both at the interannual and multidecadal time scales. Furthermore, because of the great similarity between the AMIPlike and AOCOUP climatology results, only few results from AOCOUP are shown as we verified the same is true for variability.

4.1 Results: Patterns of Variability

In order to describe patterns of rainfall co/variability in the Sub-Saharan Africa during the establishment of the Monsoon, EOF and MCA analysis techniques as described in Chapter 2 are applied.

4.1.1 SST-Rainfall coupled modes: Multiple Covariance Analysis

a) Observations

MCA is employed to identify areas in WA where rainfall covariates with SSTs and to extract the corresponding variation in time. Figure 4.1 represents the dominant first two leading modes of covariability between the two variables.

The first mode (Figure 4.1, a) explains 48% of the total covariance between July-September, JAS, precipitation over WA and global SSTs. It statistically links Sahelian rainfall variability (hereafter, Sahelian mode) with an interhemispheric SSTs pattern (Figure 4.1, c). The sign of the loadings shows that Sahelian droughts are significantly correlated to positive tropical SSTs anomalies and negative extratropical SSTs anomalies. The associated SSTs and rainfall expansion coffecients (ECs) (Figure 4.2, a) are dominated by variability at the interannual time scale and present a correlation number of 0.71.

The second mode of covariability (Figure 4.1, b) pictures the influence of the Gulf of Guinea (Figure 4.1, d) on the monsoon, and explains 14% of the total covariance. The precipitation pattern reveals that warmer than average SSTs in the Gulf of Guinea are strongly correlated with higher than average precipitation along the coast. The corresponsing ECs Figure 4.2, b, highly correlate (0.81) and are also dominated by variability at the interannual time scale. While the first mode might correspond to a modulation of the monsoon activity by interhemispheric SSTs, the second mode can be interpreted as a local modulation of the latitudinal position of the African rainbelt through Gulf of Guinea SSTs. These two observed teleconnections are fully consistent with the results of previous result in [27] Giannini et al.2003. The robustness of this MCA method has been largely assessed in the [33] Joly et al., 2007 paper.

b) AMIP

In the AMIP run, the interhemispheric SSTs pattern, which is the first dominant pattern, covariates (at 35%) with a Sahelian zonal dipole (Figure 4.3, a). Positive tropical

(a) (b)

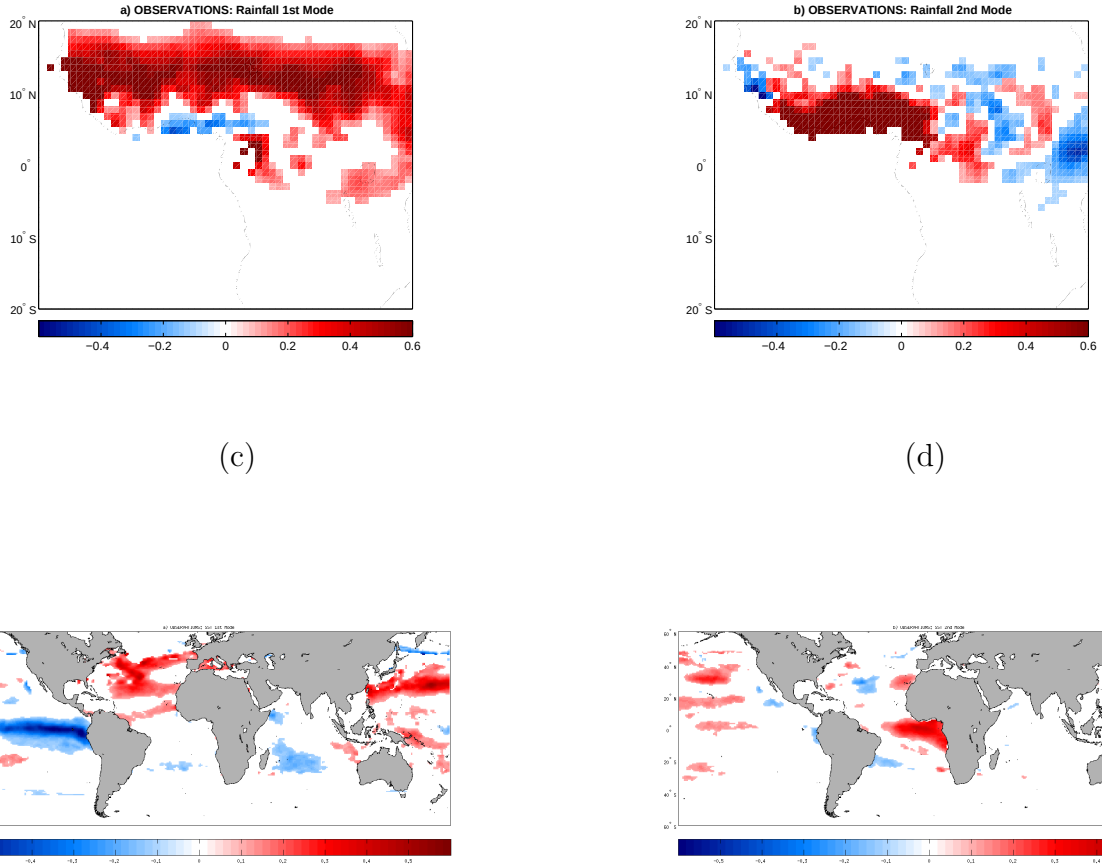

(c) (d)

Figure 4.1: *Maximum covariance analysis (MCA) of observed CRU WAM rainfall (20S-20N, 20W-30E) and global Hadley SSTs during July-August-September, JAS, 1950-2004, for the First (a and c) and second dominant modes (b and d). The correlations, significant at the 95% level, are colour shaded.*

(a) (b)

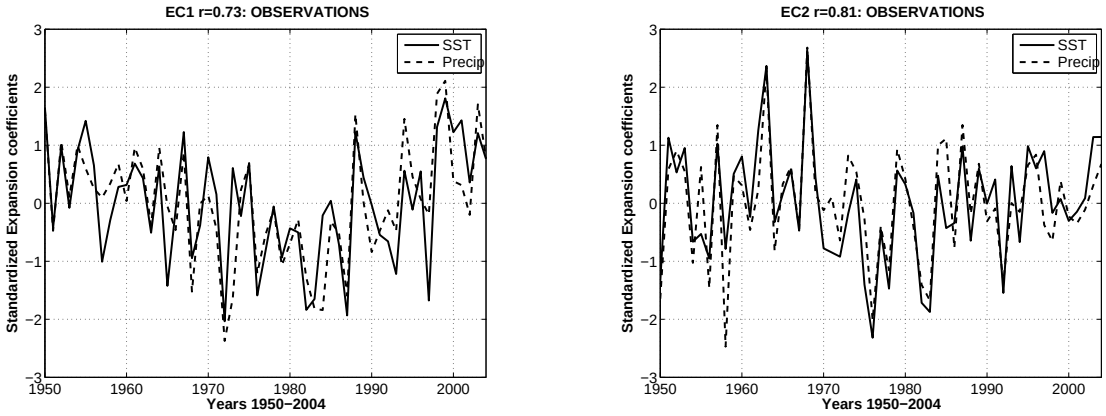

Figure 4.2: *Normalized expansion coefficients - ECs associated with the observed coupled mode of covariability between SSTs and WAM rainfall in Figure 4.1. EC1 (a) and EC2 (b)*

(a) (b)

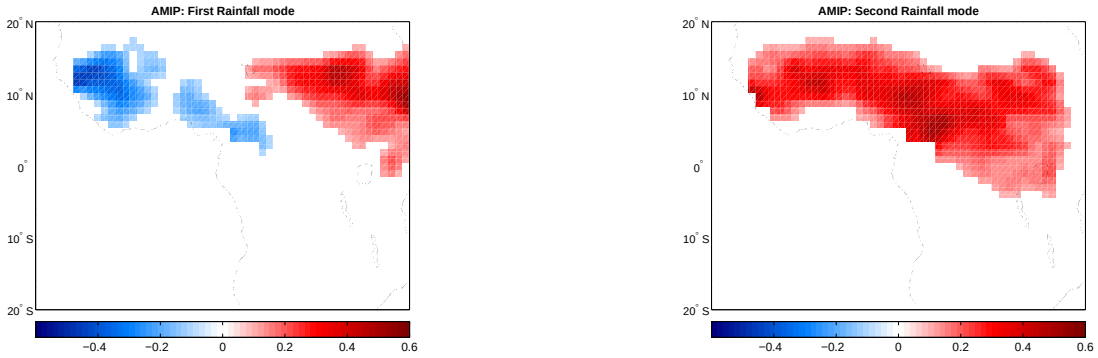

(c) (d)

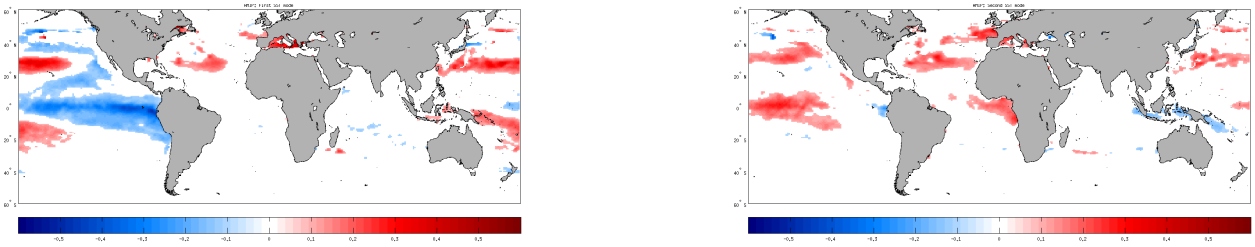

Figure 4.3: *Same as Figure 4.1 but for AMIP.*

SSTs anomalies (mainly in the Pacific) and negative northern extratropical SSTs covariate with dry rainfall anomalies in the east Sahel and wet rainfall anomalies in the west. The associated ECs are displayed on Figure 4.4, a. They are highly correlated (0.81) and dominated by variability at interannual time-scale. AMIP second dominant SSTs and rainfall covariability patterns explain 30% of of the total covariance and are shown on Figure 4.3, b. Guinean coast rainfall pattern positively covariates with SSTs in the tropical eastern Atlantic, northern Atlantic and part of the west Pacific (Figure 4.3, d). The corresponding ECs (Figure 4.4, b) highly correlate (0.73) and are dominated as well by variability at the interannual time scale. In general, we can assert that there is no clear seperation between the two dominant modes of covariability, given the numbers of the explained total covariance (35% for the first mode and 30% for the second).

(a) (b)

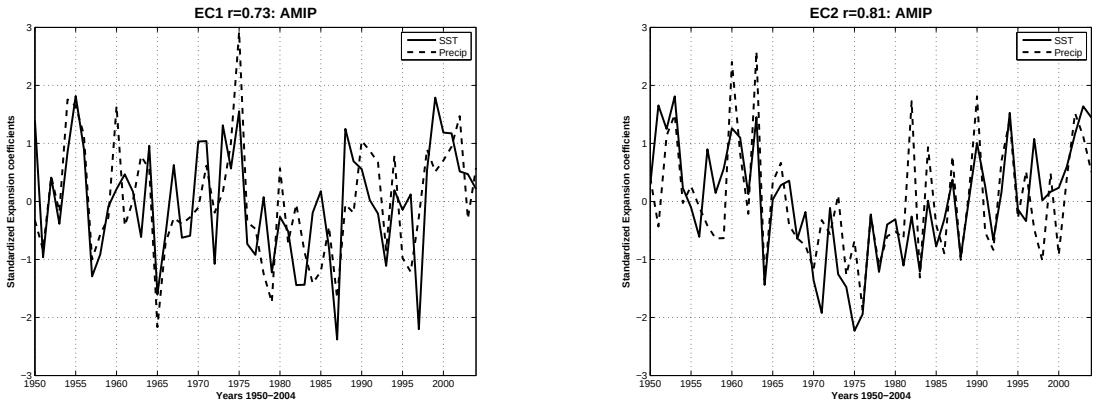

Figure 4.4: *Same as Figure 4.2 but for AMIP.*

c) AMIPlike

AMIPlike first dominant pattern of covariability explains 64% of the total covariance, Figure 4.5, a. A meridional rainfall pattern over west Africa (negative anomalies in the Guinea coast and positive anomalies over south tropical Africa) is shown to be related to negative SSTs anomalies over tropical ocean (especially in the Pacific and western Indian ocean) and a dipole SST pattern in the Atlantic (Positive anomalies in the north and

(a) (b)

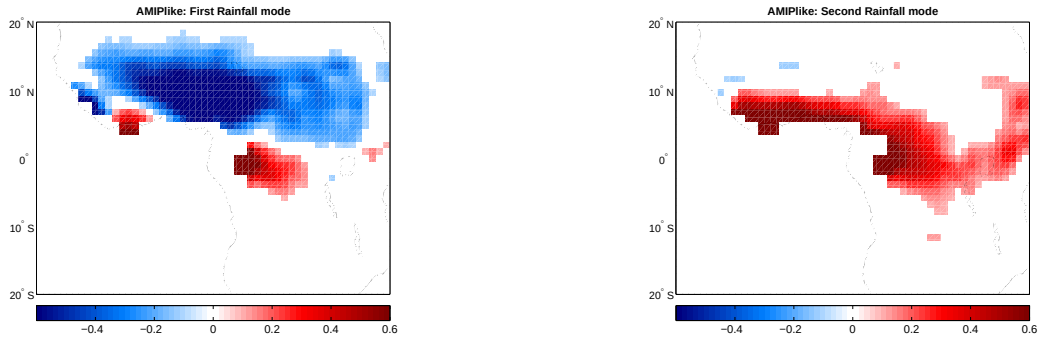

(c) (d)

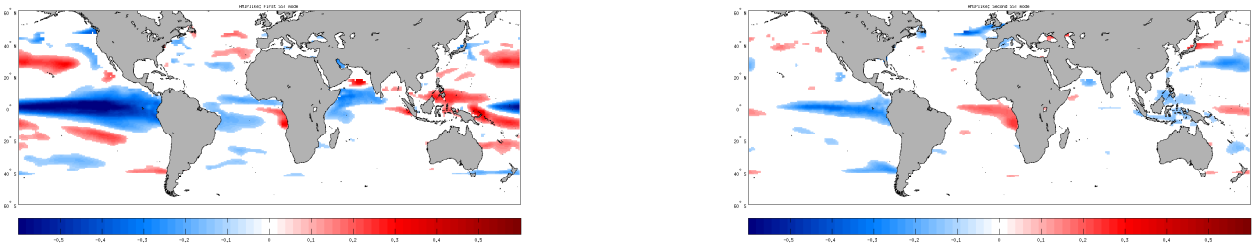

Figure 4.5: *Same as Figure 4.1 but for AMIPlike.*

negative in the south equatorial Atlantic). The corresponding ECs (Figure 4.5, a) are highly correlated (0.81) and covariate mainly at the interannual time scale. The second patterns (Figure 4.5, b) of covariability (14%) show that Guinean coast rainfall (Figure 4.5, d) is positively influenced by SSTs over the Gulf of Guinea and negatively influenced by the Pacific SSTs mainly at the interannual time scale.

(a) (b)

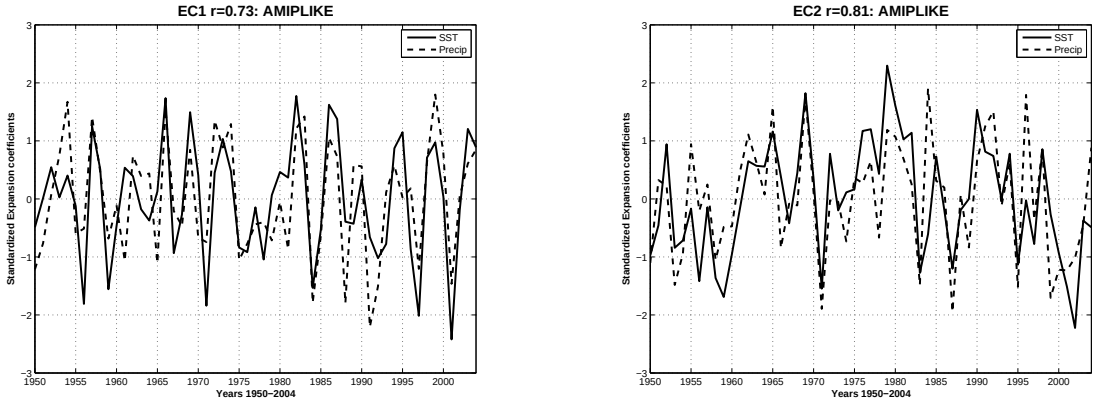

Figure 4.6: *Same as Figure 4.2 but for AMIPlike.*

4.1.2 SST-Rainfall coupled modes: Empirical Orthogonal Function

Figure 4.7 compares the first two leading EOF modes of rainfall variability over Africa. Observation shows a clear separation between the variability in the continental Sahel (Figure 4.7, a) precipitation between 10N and 20N represented by the first EOF (that explains 27% of the total variance) and the oceanic Intertropical Convergence Zone (ITCZ), and its extension along the Gulf of Guinea coast (Figure 4.7, b), between the equator and 10°N, represented by the second EOF (that explains 14% of the total variance). This separation is in accordance with the previous applied MCA technique. Furthermore, [28] Giannini et al.2005 showed that the anomalies of opposite sign in Figure 4.7, a, between Sahel and Guinean coast, are not significant.

The temporal structures of precipitation variability are shown on Figure 4.8. CRU PC1 (Figure 4.8, black line, top row) is mainly dominated by variability at the interannuall tendency. On the other hand, CRU PC2 (Figure 4.8, black line, bottom row) is dominated by variability at the interannual time scale and characterizes the rainfall variability over the coast of Guinea.

In the AMIP run, the first mode (Figure 4.7, c), seems to exhibit the Sahelian (5N-20N) mode, explaining 29% of the total variance, with rainfall restricted to the central eastern part of Sahel. The second mode instead, (Figure 4.7, d), exhibits an east-west zonal dipole mode of 22% of total variance, with negative anomalies located over the Guinea coast and positive anomalies in the East Sahel. As we can notice, the percentages of variance show that there is no clear separation between the continental (Sahelian) and oceanic (Guinean coast) modes of rainfall variability in this run. Applying rotated EOF (not shown) analysis doesn't give any meaningful result. Despite the fact that AMIP EOF1 spatial pattern seems to corresponding the most to the Sahelian mode of rainfall variability, its corresponding PC1 (Figure 4.8, dot blue lines, top and bottom rows) does not seem to exhibit the same behaviour given the low correlation between the two PCs is: r(CRU PC1 - AMIP PC1)=0.17. Instead, the correlation between AMIP PC2 and CRU PC1 is higher (0.47) (Figure 4.8, dot green lines, top and bottom rows) and the observed Sahelian mode seems to be more represented in the AMIP EOF2.

The same behaviour is present in the Guinean coast mode as well: r(CRU PC2 - AMIP PC1)=-0.24; r(CRU PC2 - AMIP PC2)=0.24. The rainfall zonal (east-west) dipole noticeable in the AMIP Sahel rainfall variability can be relied to previous studies by [65] Rowell 2001 and [3] Bader 2003. They related a significant change in east Sahel rainfall but no impact on the west Sahel mainly due to El Nino Southern Oscillation (ENSO). We will pay more attention to this zonal AMIP rainfall pattern later on in this thesis.

AMIPlike run (as well as AOCOUP, not shown), exhibits a clear separation between the first rainfall dominant mode (Figure 4.7, e) that explains 38% of the total variance and the second rainfall dominant mode (Figure 4.7, f) explaining 18% of the total variance. Interestingly, the second mode exhibits a meridional dipole, with positive rainfall anomalies in the west Sahel contrasting negative anomalies in the equatorial Africa. On the other hand, AMIPlike EOF2 looks similar to the observed EOF1 while AMIPlike EOF1 resembles the CRU Guinean coast EOF2 pattern. The separation of the two modes of rainfall variability over Africa is quite clear in the AMIPlike PCs as well (Figure 4.8, last column, dot darked orange), even though the correlation is low.

These results are summarized in the Table 4.1.

The correlation maps of the associated PCs with the global SSTs are shown in Figure 4.9. In observations (Figure 4.9, a), positive Sahel rainfall is connected to negative SSTs anomalies in the entire tropics and to positive anomalies in the northern Atlantic as confirmed by the MCA analysis. Positive correlation values connect the Gulf of Guinea

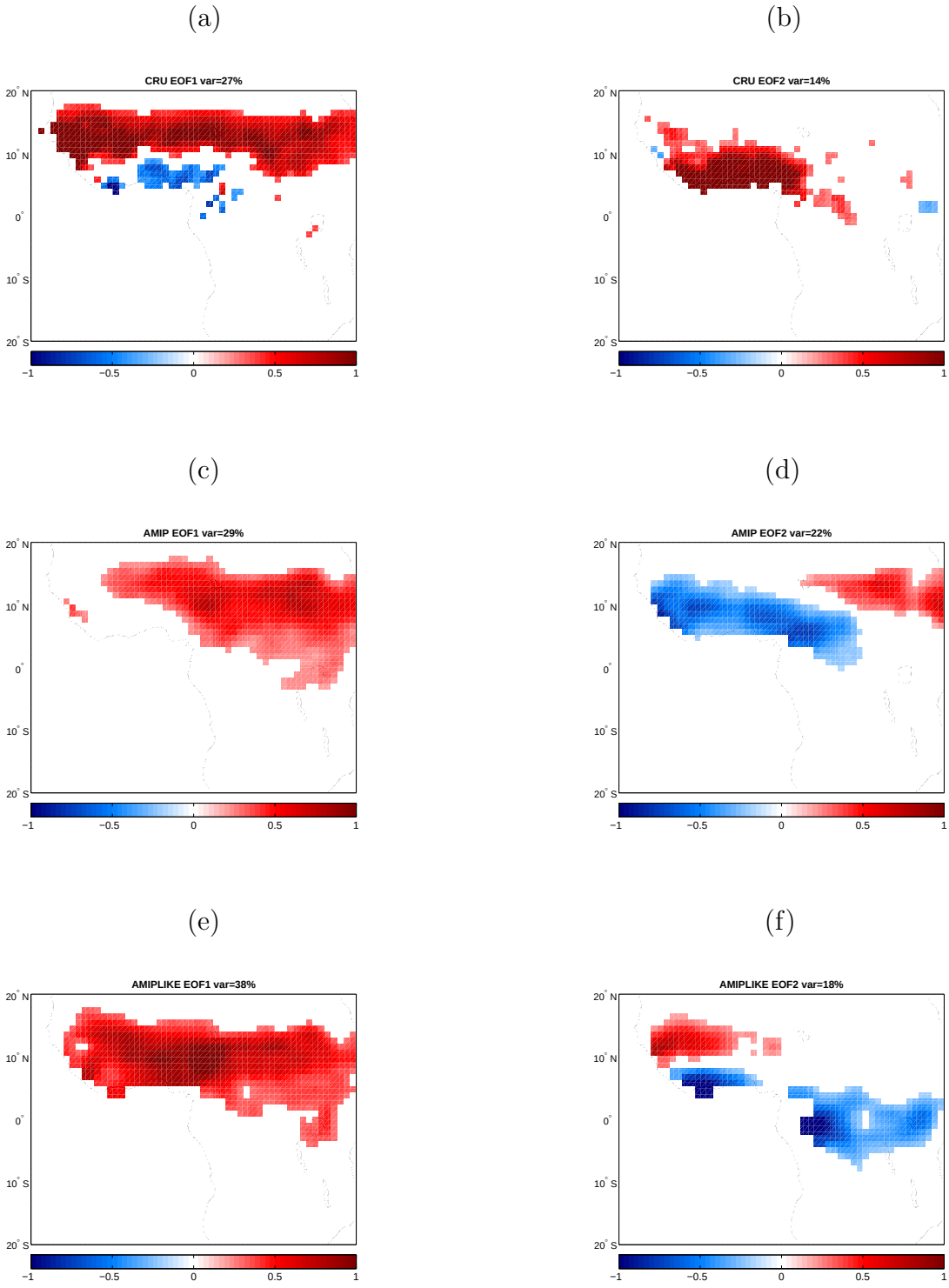

Figure 4.7: *EOF1 (left) and EOF2 (right) rainfall Spatial patterns for the summer JAS 1950-2004 period. CRU: EOF1(a), EOF2 (b); AMIP: EOF1(c), EOF2 (d); AMIPlike EOF1(e), EOF2 (f); Units are in mm/day per standard deviation of the associated principal components (Figure 4.8). Only 95% significant results are shown.*

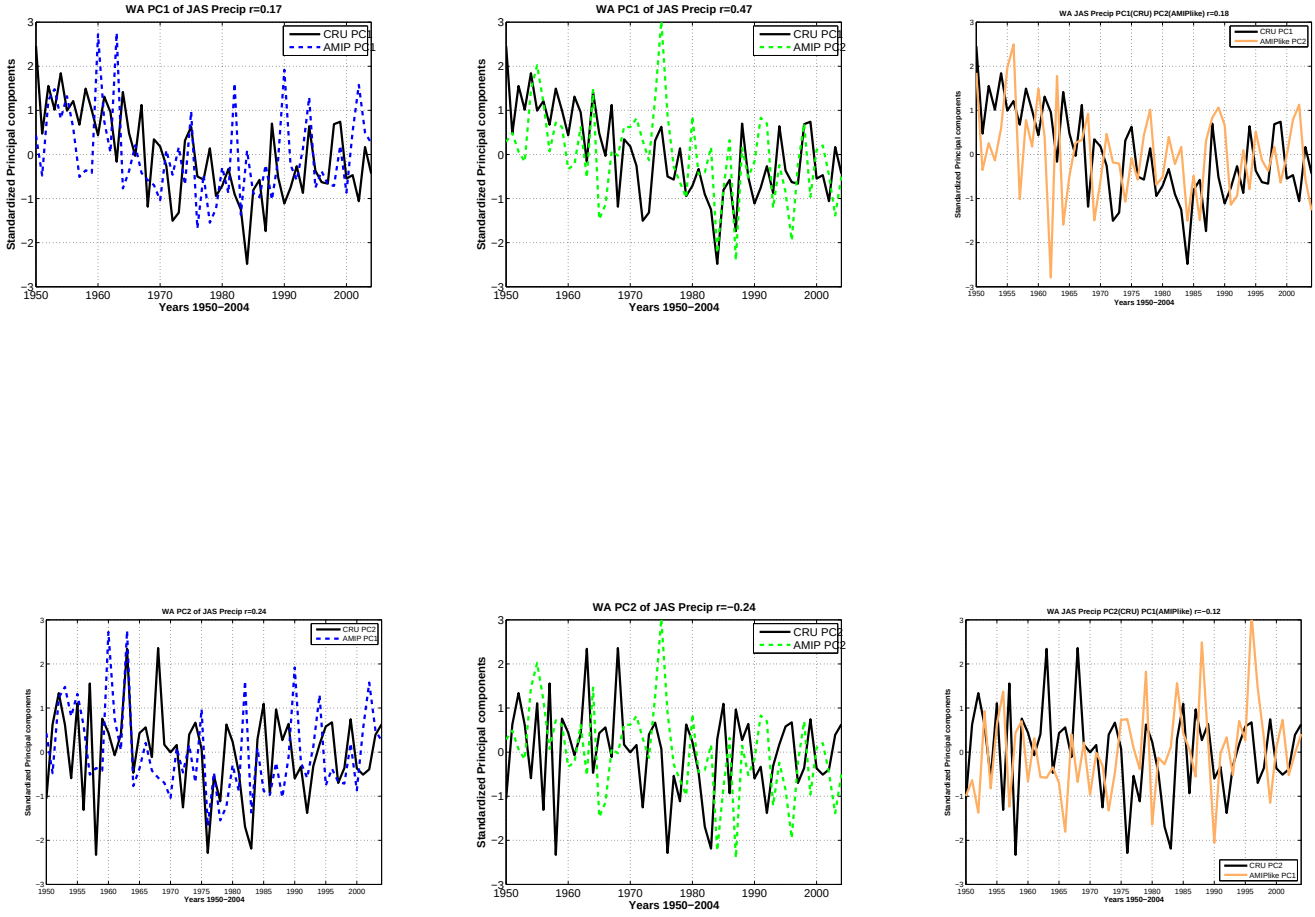

Figure 4.8: *Standardized PCs. Black lines: observations (CRU), Dark orange line: AMIPlike, Dashed blue line: AMIP PC2, Dashed green line: AMIP PC1. Top row represents time series between CRU PC1 and AMIP PC1 (left) and PC2 (middle) on one hand, and CRU PC1 and AMIPlike PC2 (right) on the other hand. Bottom row displays the same but is for PC2 and AMIPlike is for PC1. The correlations between observed and modeled PCs are given in the title: r(CRU PC1 - AMIP PC1)=0.17; r(CRU PC1 - AMIP PC2)=0.47; r(CRU PC2 - AMIP PC1)=-0.24; r(CRU PC2 - AMIP PC2)=0.24; r(CRU PC1 - AMIPlike PC1)=0.12; r(CRU PC1 - AMIPlike PC2)=0.18; The remaining correlation numbers is listed in the text.*

(a)

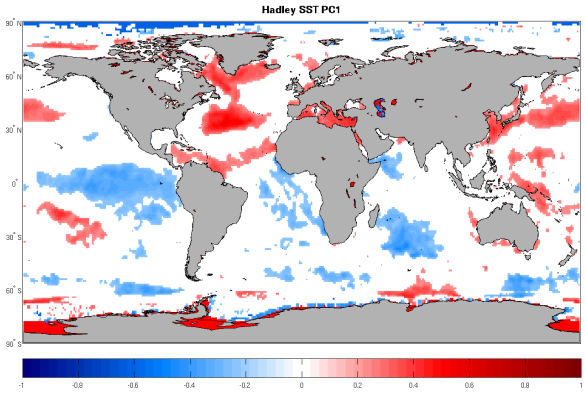

(b)

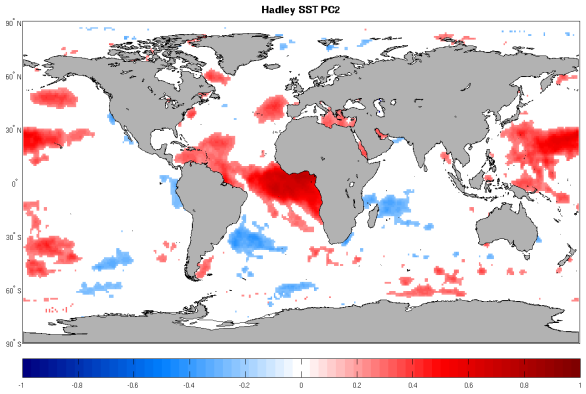

(c)

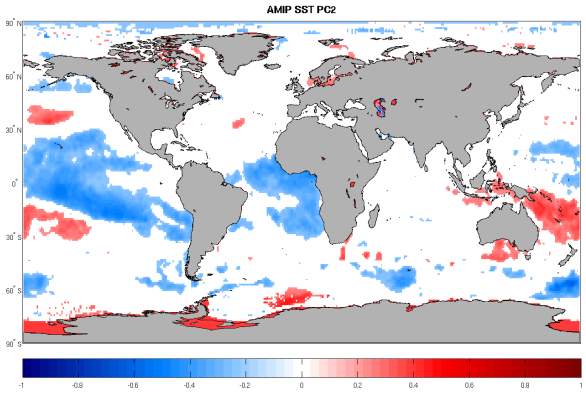

(d)

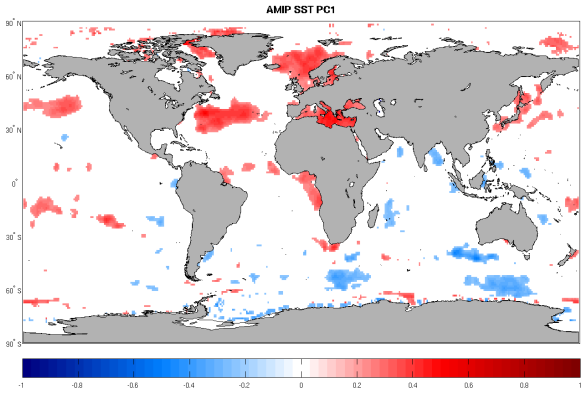

(e)

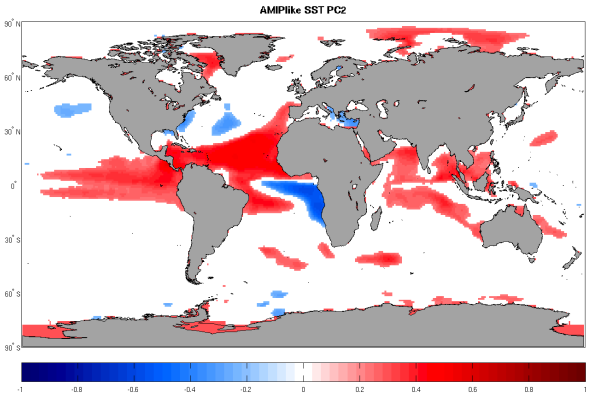

(f)

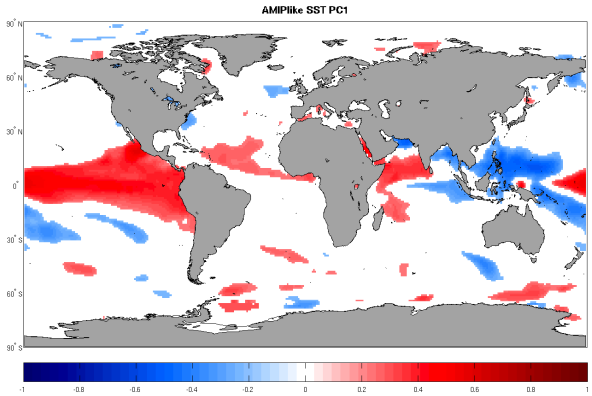

Figure 4.9: *Regression of the 1950-2004 global summer SSTs onto the differents PCs: PC1 (left) PC2 (right) for Observations (a and b) AMIP (c and d) and AMIPLike (e and f).*

PC Correlation Numbers

	$CRU - PC1$	$CRU - PC2$
$AMIP - PC1$	0.17	-0.24
$AMIP - PC2$	**0.47**	**0.24**
$AMIPlike - PC1$	-0.05	-0.12
$AMIPlike - PC2$	**0.18**	**-0.01**
$AOCOUP - PC1$	-0.06	-0.001
$AOCOUP - PC2$	**0.16**	**0.001**

Table 4.1: *Correlation of Model rainfall PCs with the Observed rainfall PC1*

Rainfall to the eastern tropical Atlantic ITCZ (Figure 4.9, b). To summarize, positive rainfall anomaly in Sahel is associated with negative SST anomalies in the tropical Pacific and Indian Oceans and interhemispheric SSTs anomalies in the Atlantic (positive in the North and negative in the South). Positive rainfall anomalies in the Guinea coast are associated with positive SSTs anomalies in the eastern equatorial Atlantic.

As mentioned above, AMIP second mode of rainfall variability (the zonal dipole) is explained by the interhemispheric SSTs variability (Figure 4.9, c) and AMIP first mode of rainfall variability (Figure 4.9, d) is explained by SSTs variability over East tropical Atlantic. AMIPlike rainfall instead seems to be mainly related to tropical SSTs especially to the Pacific in any cases ((Figure 4.9, e and f).

4.1.3 Variability of the East and West Sahel in the AMIP run

[65], Rowell (2001) and [3], Bader and Latif (2003) found that the tropical SSTs anomalies appear to driving the drying trend more in the eastern Sahel than in the western Sahel. To verify this assumption, given the east-west structure of AMIP rainfall variability, we split the AMIP Sahel into two subregions: West Sahel (10N-20N, 21W-10E) and East Sahel (10N-20N, 13E-40E). Rainfall indices (ESRI and WSRI for East and West Sahel Rainfall Index, respectively) are then computed by averaging the JAS rainfall anomalies over each of the two separated Sahel subregions. We also compute the Sahel rainfall index (SRI) for the entire Sahel (10N-20N;21W-40E) for both observations and AMIP. Time series are then normalized by their corresponding unit standard deviation. The results are given in Figure 4.10.

The interesting remark is the higher correlation of r = 0.43 between the observed SRI (black) and AMIP ESRI (red), Figure 4.10, b, compared to the AMIP entire SRI Figure 4.10, a, r = 0.28. There is no correlation between the observed SRI and the AMIP WSRI, Figure 4.10, c, -0.16.

We then applied a 21-year running mean to each index to extract the "low-frequency"

(a)

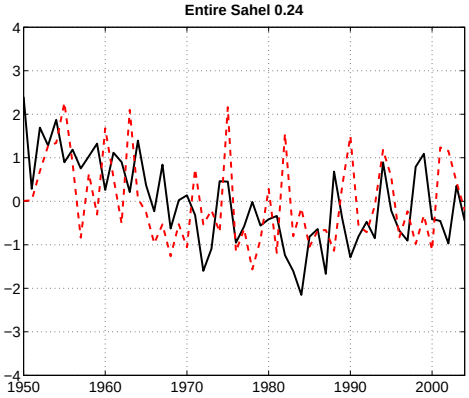

(b)

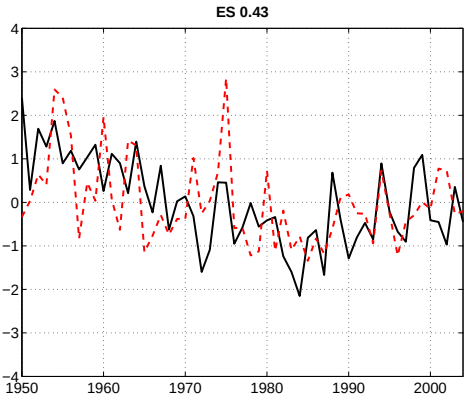

(c)

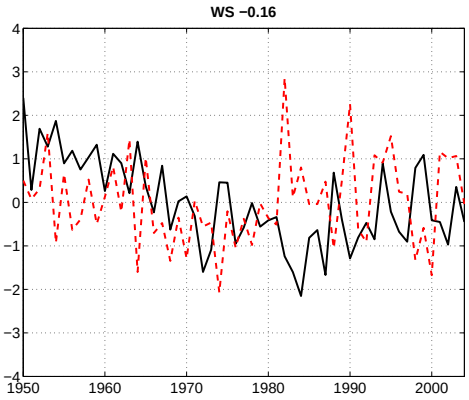

Figure 4.10: *Time series of Summer rainfall indices for CRU (black) and AMIP (red). Rainfall is averaged over Sahel (21W-40E, 10N-20N) for: CRU (a, b and c) and AMIP (a); over two subregions for AMIP: East Sahel (21W-10E, 10N-20N) - ESRI (b) and West Sahel (13E-40E,10N-20N) - WSRI (c). Correlation numbers are given in the title.*

(a)

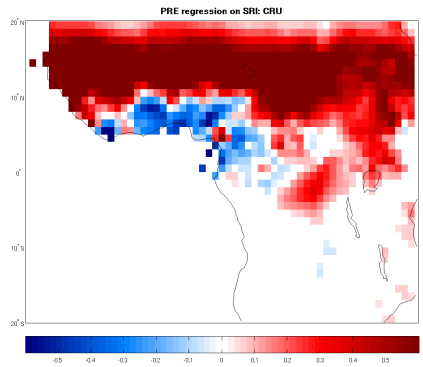

(b)

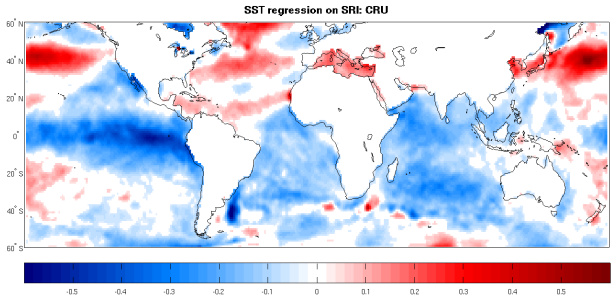

(c)

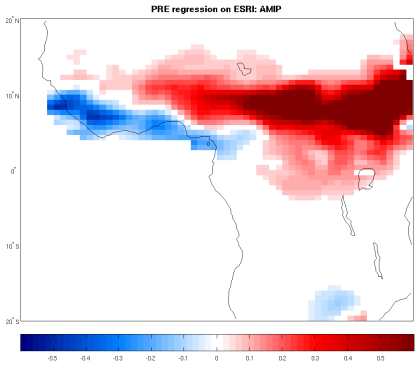

(d)

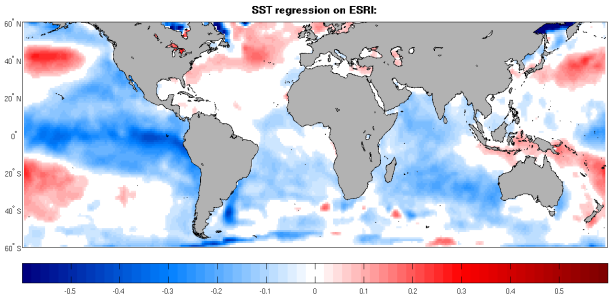

(e)

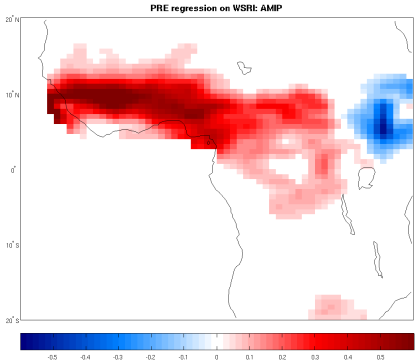

(f)

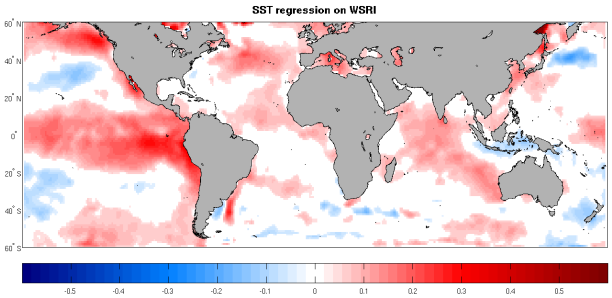

Figure 4.11: *Regression of 1950-2004 JAS summer WA rainfall (left) and global SSTs (right) onto the different indices computed in Figure 4.10 for observed SRI (a and b) AMIP ESRI (c and d) and AMIP WSRI (e and f).*

AMIP	Non Filtered	Decadal Component	Interannual Component
SRI	0.28	0.95	0.03
ESRI	0.43	0.97	0.21
WSRI	-0.16	0.001	0.26

Table 4.2: *Correlation numbers between AMIP and observed Sahel rainfall indices (SRIs). AMIP SRI (second row, second column) is correlated with observed SRI as well as their low (second row, third column) and high (second row, fourth column) frequency components of variability. SRI is computed by averaging the JAS rainfall anomalies over 10N-20N;21W-40E. The low component of variability is obtained by applying a 21-year running mean (third row) and the residual results to be the high component. The same procedure is applied for AMIP East SRI (ESRI) and West SRI (WSRI) where the average is done between 10N-20N, 13E-40E and 10N-20N, 21W-10E respectively.*

variability of the time series. In this way, we are able to decompose time series into their decadal and interannual components of variability (Not shown).
There is a net increase in the correlation numbers both at the high and low frequency of variability for the East Sahel: from 0.95 to 0.97 (low frequency) and from 0.03 to 0.21 (high frequency) for non-filtered and filtered data respectively. West Sahel rainfall presents only the interannual variability and is positively correlated to the observed SRI (0.26). These results are summarized in the Table 4.2.

The regression of the global summer SSTs into those indices in Figure 4.11 shows that the traditional Sahel rainfall variability and the SSTs interhemispheric influence is fulfilled and restricted to east Sahel in the AMIP run (Figure 4.11, c and d). The AMIP ESRI variability follows observed SSTs influence (Figure 4.11, a and b) as it is negatively correlated with an interhemispheric SSTs pattern . This result of Sahel rainfall variability restricted in the east was also found by [9] Caminade et al.2010 using another model. The main assertion we can make is that the basic structure of the Sahel rainfall variability at the decadal time scale can be simulated when the model only uses the observed SSTs as lower boundery conditions. The interannual variability still presents some difficulties.

4.1.4 Decomposition of rainfall PCs into high and low frequencies of variability

To investigate the effect of SSTs influence on Sahel rainfall at the decadal time-scale, we performed a 21-year running mean of the principal components as discussed earlier, Figure 4.12. Figure 4.12 (a and b) shows that the model, when forced with observed SSTs, is able to reproduce the long term drought that governed the Sahel during 1970s-1980s. A very high correlation exists between the AMIP two PCs and the observed PC1: CRU PC1 (black) and AMIP PC1 (Figure 4.12, dot blue) : 0.89; CRU PC1 (black) and AMIP

(a) (b)

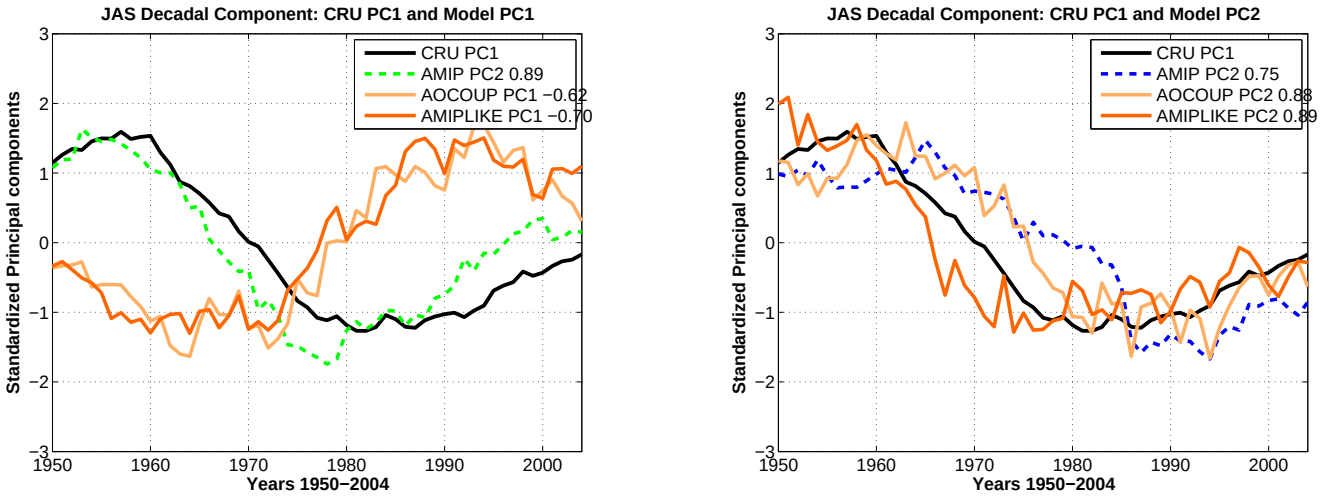

Figure 4.12: *Low frequency component of the Standardized principal components for: CRU PC1 (black line) and Model PC1 (a); CRU PC1 (black line) and Model PC2 (b). The correlation numbers between observed and modeled PCs are given in legend.*

Model PC Correlation Numbers with CRU PC1

Runs	$PC1$	$PC2$
$AMIP$	**0.89**	**0.75**
$AMIPlike$	**-0.70**	**0.89**
$AOCOUP$	**-0.62**	**0.88**

Table 4.3: *Correlations between the decadal components of the model PCs and CRU PC1: Sahelian mode.*

PC2 (Figure 4.12, dot green) : 0.75. On the other hand, very interesting and surprisingly as reproduced in Figure 4.12,b, despite the absence of realistic SSTs, AMIPlike PC2 (dark orange) as well as AOCOUP PC2 (light orange) are also able to reproduce the low frequency variability of the Sahel rainfall with high correlation of 0.89 to observation for both of them. AMIPlike and AOCOUP PC1 instead show a negative correlation to SSTs. The summary of these correlations is done in Table 4.3.

The above results imply that SST is not the only dominant factor able to shape the variability in the Sahel. AMIP was expected to reflect this long drought behaviour in the Sahel rainfall as forced to follow observations through SSTs. Many factors can be guessed to be playing a role. According to the model settings performed in the present work, one possible player is the impact of anthropogenic sulfate aerosols (ASAs) onto Atlantic SSTs, which may have had an effect on the low frequency variability of Sahel precipitation through radiative forcing.

In the next chapter, we will verify our hypothesis and if it is revealed true, investigate the possible linkage, in terms of mechanisms, between ASAs and the Sahel rainfall.

4.1.5 Regression of global SSTs into Sahel PC Components

In order to identify the oceanic parts that influence the most Sahel rainfall at decadal and interannual time scales, we regress the global SSTs into the low-frequency (Figure 4.13, a) and the high-frequency (Figure 4.13, b) components of the observed Sahel PC. This decomposition highlights the role of the slower oceanic variability characteristic of the dipolar SST mode in the Atlantic and west Indian oceans in forcing the trend.
At the interannual time-scale, the Sahel rainfall is influenced by the tropical oceans. In particular, main impact is imparted by the pacific ocean, the tropical Atlantic and the west indian.

For AMIP run, results are summarized on Figure 4.14. Central east Africa rainfall (corresponding to EOF1) variability mainly owns its existence to a dipolar SST patterns of negative signs in the Atlantic and the indian ocean at the decadal time scale (Figure 4.14, a). It has no evident link to SSTs at the interannual time scale (Figure 4.14, b).

(a) CRU PC1 Decadal

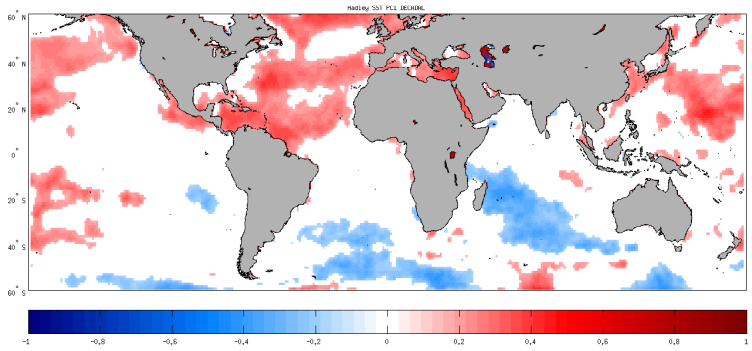

(b) CRU PC1 Residual

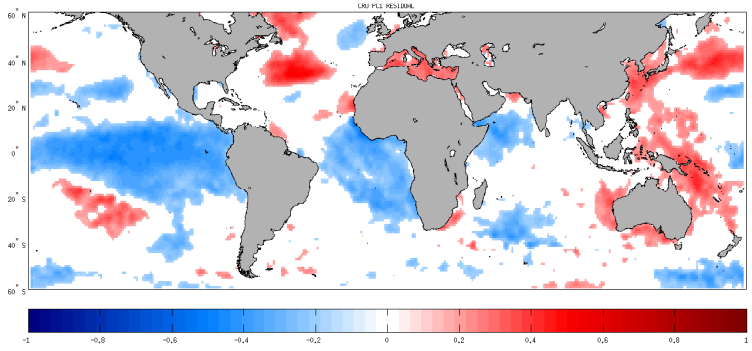

Figure 4.13: *Regression of the global 1950-2004 Summer SSTs into the Low (a) and High (b) frequency components of the Standardized Observed PC1 for CRU precipitation. SSTs are from the Hadley dataset.*

The variability in east-west rainfall (corresponding to EOF2) instead has no SSTs influence at the decadal time scale (Figure 4.14, c) and is mainly influenced by the tropical Pacific and Atlantic at the interannual time scale (Figure 4.14, d).

On the other hand, the meridional rainfall dipole in AMIPlike (corresponding to EOF2) is mainly due to the influence of the North Atlantic, at the decadal time-scale (Figure 4.15, c) and the influence of the Pacific and the east Indian at the interannual time-scale (Figure 4.15, d). In the same time, AMIPlike EOF1 seems to be mainly related to tropical SSTs additionally to the tropical east Atlantic upwelling zone at the interannual time-scale (Figure 4.15, b) and has almost no link to SSTs at the decadal time scale (Figure 4.15, a).

(a) AMIP PC1 Decadal

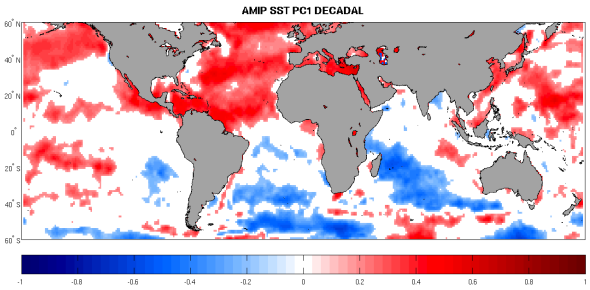

(b) AMIP PC1 Residual

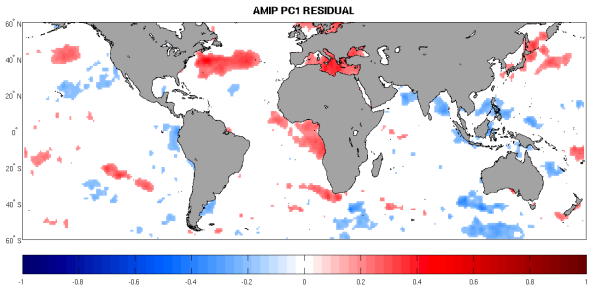

(c)AMIP PC2 Decadal

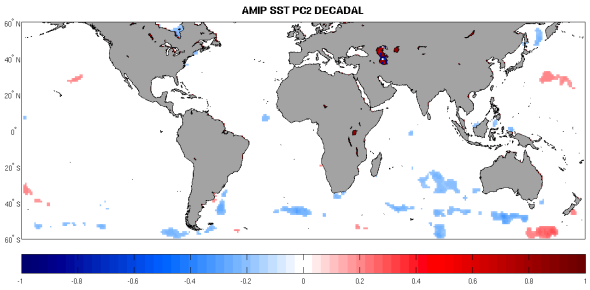

(d) AMIP PC2 Residual

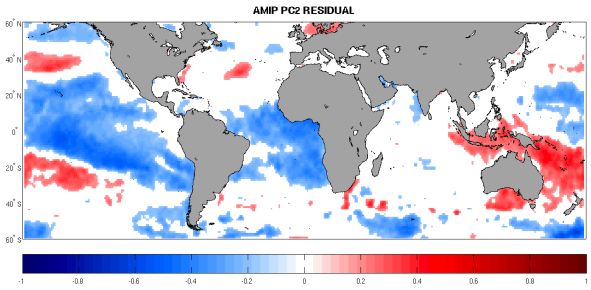

Figure 4.14: *Same as Figure 4.13 for AMIP PC1: (a) for low and (b) for high frequency of variability and AMIP PC2: (c) for the lower and (d) for the higher one.*

(a) AMIPlike PC1 Decadal

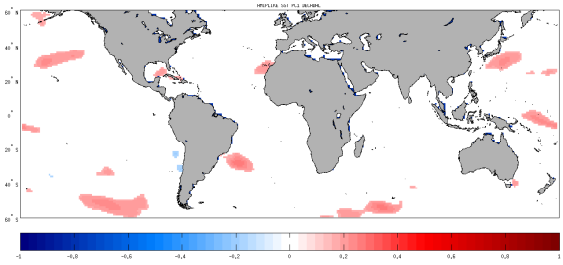

(b) AMIPlike PC1 Residual

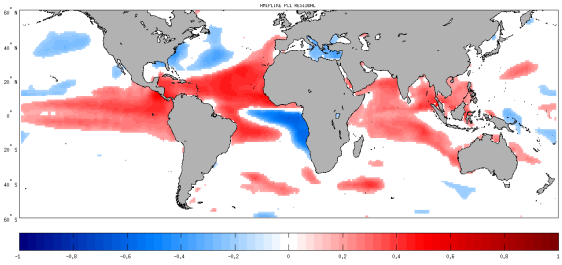

(c) AMIPlike PC2 Decadal

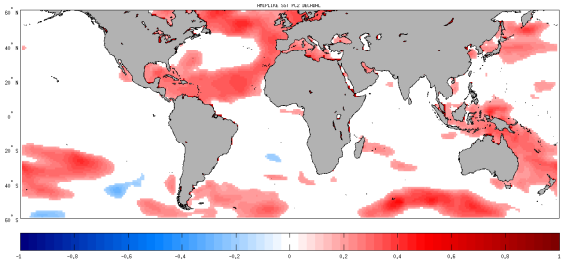

(d) AMIPlike PC2 Residual

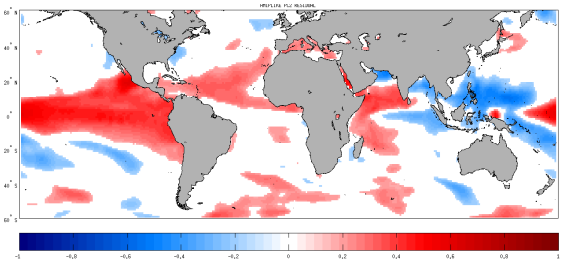

Figure 4.15: *Same as Figure 4.13 for AMIPlike PC1: (a) for low and (b) for high frequency of variability and AMIPlike PC2: (c) for the lower and (d) for the higher one.*

4.2 Mechanisms of the Rainfall Variability: Interannual time scale

A coupled of mechanisms have been identified in the literature to induce anomalous precipitation over Africa. Here in the following, we discuss about two of them, which in general, involve two competing aspects: the Dynamics and the Thermodynamics.

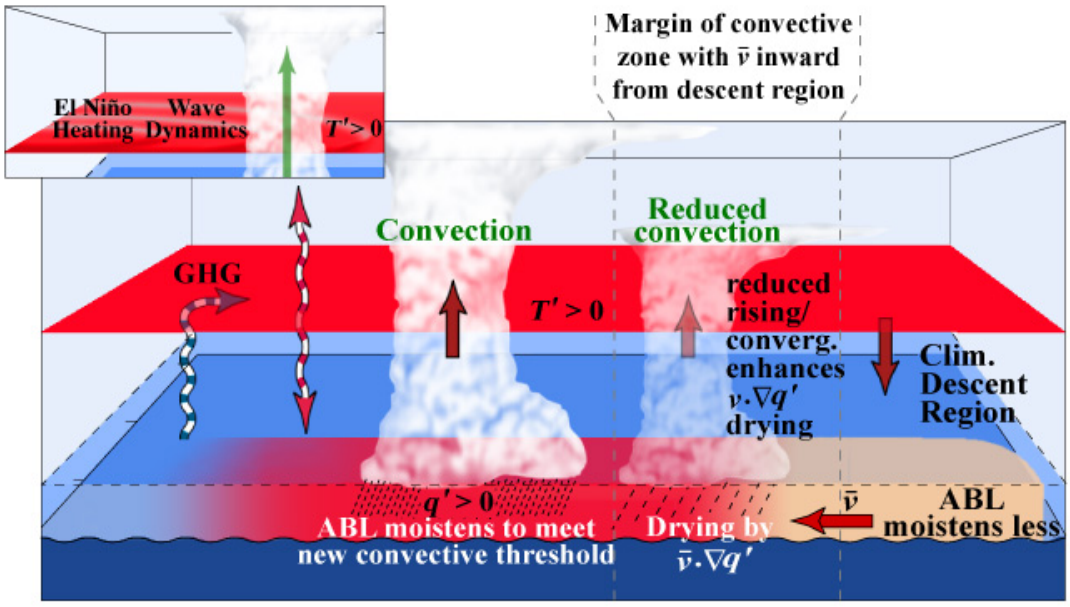

Figure 4.16: *Schematic of the upped-ante mechanism for negative precipitation anomalies for global warming and El Nino cases as proposed by [51] Neelin et al.2003. For the global warming case, the tropospheric temperature warms due to increased absorption of infrared radiation (dashed curves) by greenhouse gases (GHG). For the El Nino case (inset) warming is spread from the Pacific by wave dynamics. The rest of the pathway via convective interactions is common to both. Adjustment of atmospheric boundary layer (ABL) moisture in convective regions, to meet the new convective ante, establishes a gradient of ABL moisture anomalies q' relative to nonconvective regions. This creates a drying tendency where low-level flow v moves into the margin of a convective zone. Feedbacks reducing upward motion and low-level convergence enhance this drying tendency.*

4.2.1 Dynamics due to ENSO teleconnection or the upped-ante mechanism

Great interest has been given to the influence of Pacific ocean as one of the oceanic major source of heat/energy important for the atmospheric global circulation. A few authors focused on the linkage between the Pacific ocean and the persistence of drought in the

Dataset	AMIP	AMIPlike	NCEP-NCAR
El Nino Years	1965, 1972	1959, 1971	1972, 1987
	1987, 1997	1984, 1997	1997
La Nina Years	1955, 1973	1957, 1969	1964, 1973
	1975, 1989	1982, 1998	1993

Table 4.4: *Retained El Nino and La Nina years for the composite analysis.*

Sahel ([25] Folland et al.1986, [35] Janicot et al.2001). A Sahelian rainfall reduction has been related to warming over the tropical pacific ([33] Joly et al.2007, [27] Giannini et al.2003, among others). Relative mechanisms have been attributed such as the stabilization mechanism, also called the upped-ante mechanism described in [51] Neelin et al.2003 and a schematic picture of the mechanism is summarized in Figure 4.16. In general, during El Nino, there is an anomalous ascending motion over the equatorial Pacific. The troposphere over the Pacific then warms and Moisture rises to maintain precipitation. In the same time, the moisture gradient relative to neighboring subsidence regions increases. Because the tropical atmosphere can not support large temperature and moisture gradients between the Pacific and its neighboring regions, the anomalous convective heating over the tropical Pacific spreads rapidly through the entire atmosphere and warms up the higher layers as the latent heat is released. This higher-level warm temperature anomalous extends eastward right over margins of convection zones (where subsidence occurs) through equatorial waves and preferentially Kelvin waves [29], Gill 1980. Strong inflow of dry air from the subsidence regions (including Africa) then favors rainfall reduction.

Selection of the appropriate ENSO years

An index is defined as the time series of the linearly detrended summer JAS SSTs anomalies averaged over the region (190°E- 240°E, 5°S-5°N) over the period 1950-2004. Then the time series is normalized by its standard deviation. A year is defined as El nino year when the resulting index is greater than one standard deviation and as La nina when it is less than one standard deviation. According to this procedure, four years have been chosen for both El Nino and La Nina events, for AMIP and AMIPlike. Due to the availability of "observed" datasets with large set of variables, the NCEP-NCAR reanalysis dataset is used to compare with the model dataset and three years are chosen as corresponding to El Nino and La Nina events as well. The chosen years for each dataset are summarized in Table 4.4.

For observations, the stabilization mechanism is summarized in the Figure 4.17. During El Nino events, low layers warm up over the equatorial Pacific, up to 2°C, Figure 4.17, c. The warmer and moister conditions of the boundary layer then enhances the local convection. This leads to a warm anomaly in the higher levels ($\sim$ 1°C) that extends, due to the stabilition mechanism, eastward right over Africa where anomalous subsidence

(a) 200hPa Temperature

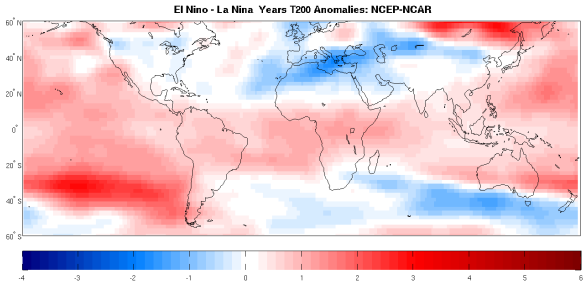

(b) Precipitation

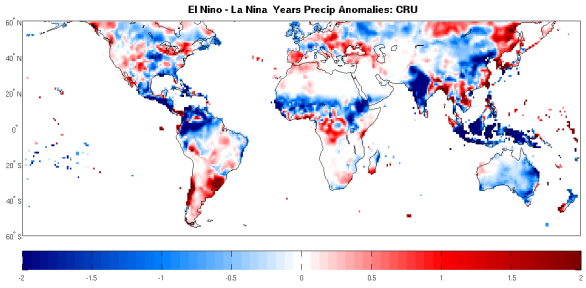

(c) Vertical Temperature

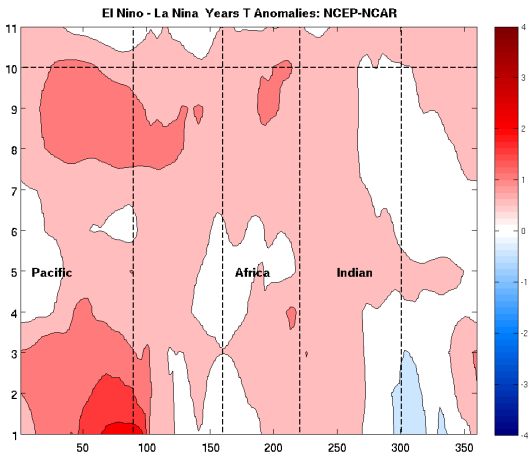

Figure 4.17: *JAS NCEP-NCAR ENSO composites (difference between El Nino minus La Nina anomalies) for: (a) 200hPa Temperature, (b) precipitation and (c) Temperature vertical cross section (averaged between 10S-10N). The horizontal dashed line at 10 corresponds to 200hPa and the vertical dashed lines separe different regions.*

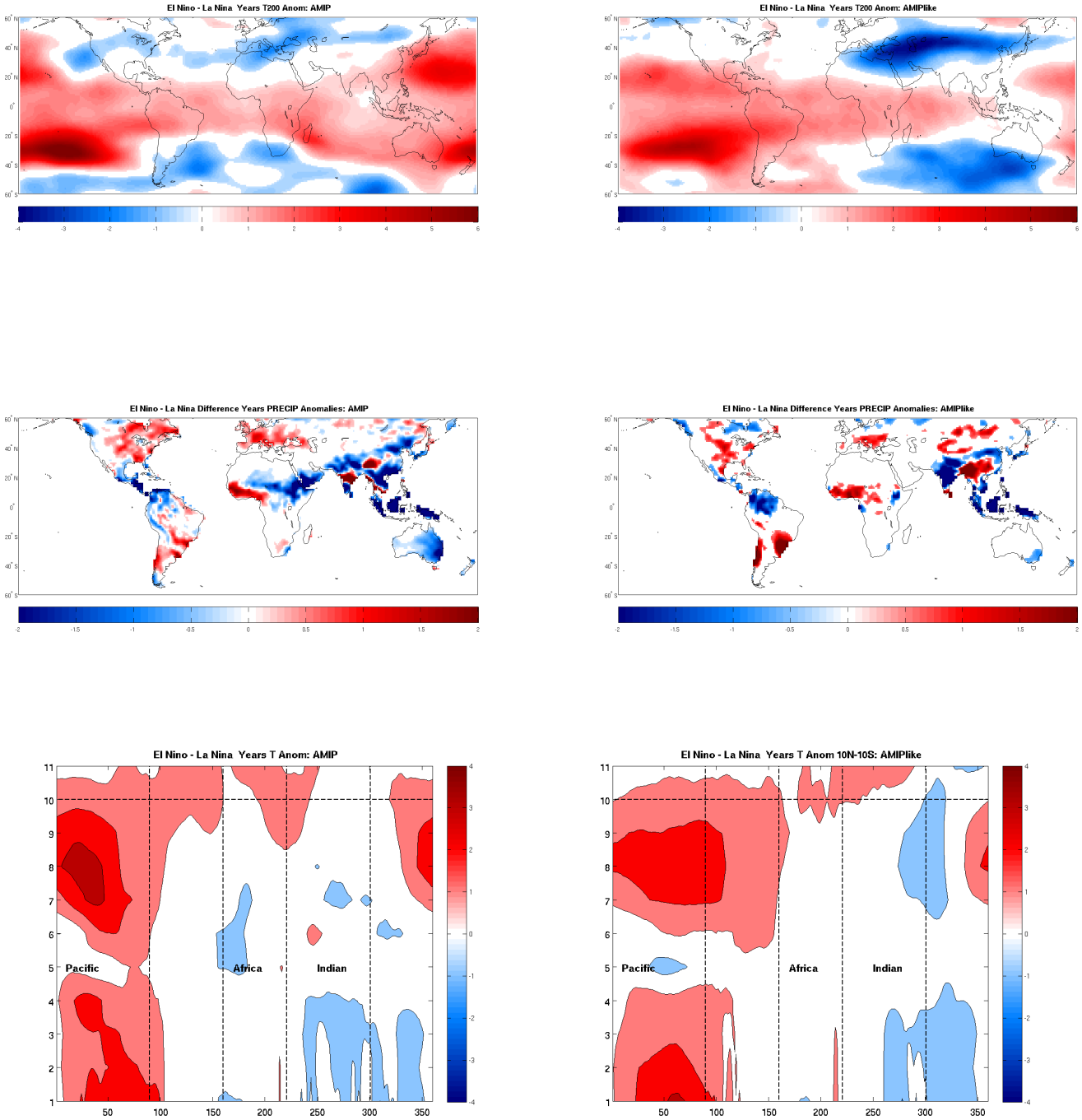

Figure 4.18: *Same as Figure 4.17 for AMIP (Left) and AMIPlike (Right).*

occurs. This is clearly shown at Figure 4.17, a, with a widespread and significant westerly anomaly originating eastward from the enhanced convective heating over central east Pacific. As a consequence of this direct atmospheric ENSO influence, rainfall is reduced as a whole over Africa, as shown in Figure 4.17, b.

Despite the fact that higher levels of the model composite are considerably warmer compared to NCEP-NCAR reanalysis ($\sim 3°C$ for AMIP (Figure 4.18, bottom left) and $\sim 1°C$ for AMIPlike, Figure 4.18, bottom right), the dry rainfall anomalies in AMIP Sahel is restricted to the central eastern Sahel. Furthermore, the AMIP west Sahel (not shown) and AMIPlike African rainfall seem not to follow the stabilization mechanism (opposite sign of rainfall, Figure 4.18, middle right) and the rainfall variability of those regions might instead own its explanation to non dynamical processes.

4.2.2 Thermodynamics: Anomalous gross moist stability mechanism

The dynamics of the stabilization or the upped-ante mechanism described above is based on the warming of the troposphere. To compensate the warm tropospheric temperature, atmospheric boundary layer (ABL) moisture must normally increase to maintanin positive convective available potential energy (CAPE) in convective regions. In the upped-ante mechanism, increase in ABL moisture is opposed by imported dry air wherever inflow from nonconvective regions over margins of convective regions. The ABL is not enough to meet the higher convective ante induced by the warmer tropospheric temperature, so precipitation is decreased. In the anomalous gross moist stability mechanism, gross moist stability is reduced due to increased ABL moisture. As a result, convection is enhanced and precipitation becomes heavier over convective regions [19], Chou and Neelin, 2004. While the upped-ante mechanism induces negative precipitation anomalies over the margins of convective regions, the anomalous gross moist stability mechanism induces positive precipitation anomalies within convective regions.

In observations as represented in Figure 4.19, during El Nino years, in the Sahel, the boundary layer (BL) is warmer than the free atmosphere (a) while the specific humidity decreases (b). The BL beeing warmer than the free atmosphere, deep convection should be enhanced as the moisture supply significantly decreases at the edge of the convection zone Sahara. This leads to a decrease of humidity/precipitation over Sahel as shown Figure 4.20, a. El Nino events are associated with negative specific humidity anomalies over the entire Sahel and positive anomalies in the equatorial regions (Eastern Atlantic and coastal and central Africa). This is also marked by weakening of the monsoon flow inside the African continent. Similarly for AMIP East Sahel, decrease in precipitation is explained by the stabilization mechanism as represented in Figure 4.21 and Figure 4.20, b.

In the AMIP west Sahel (Figure 4.22, a), despite the fact that the BL is warmer than the free atmosphere, the specific humidity instead decreases. Again as the BL is warmer,

(a) Temperature

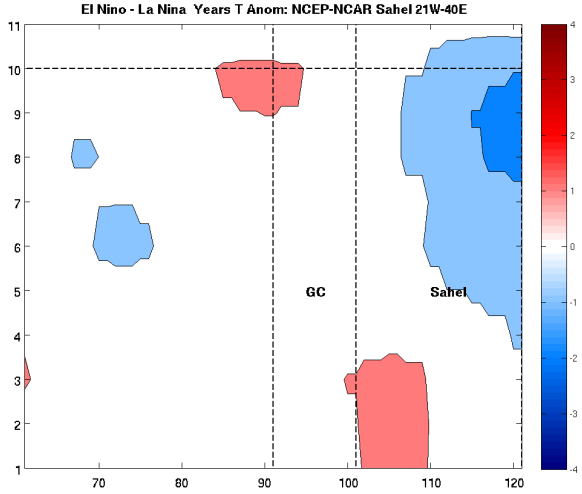

(b) Specific Humidity

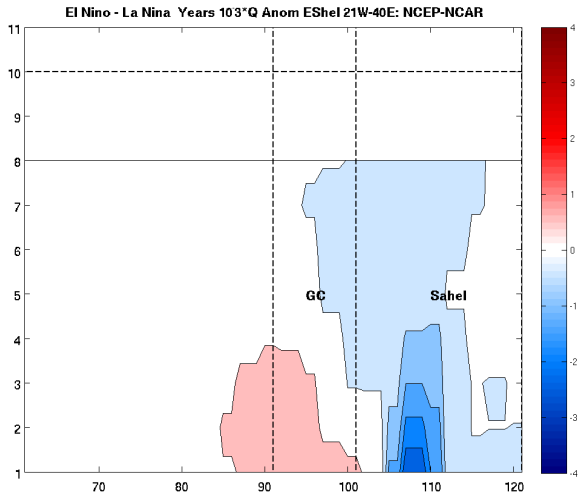

Figure 4.19: *JAS ENSO composites (difference between El Nino minus La Nina anomalies) for the vertical cross section (latitude-height) of: temperature (a) and Specific humidity (b), averaged over the entire Sahel (21W-40E) for NCEP-NCAR. The x axis represents latitude from 30S-30N. The horizontal dashed lines at 10 represent 200hPa and the vertical ones separe the different regions*

(a) Observations

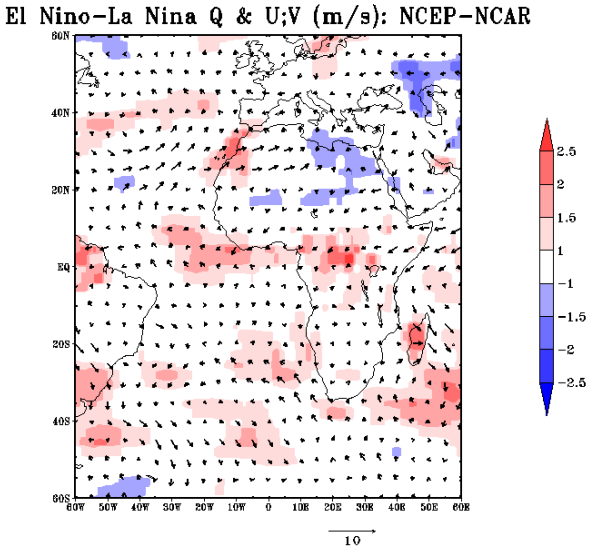

(b) AMIP

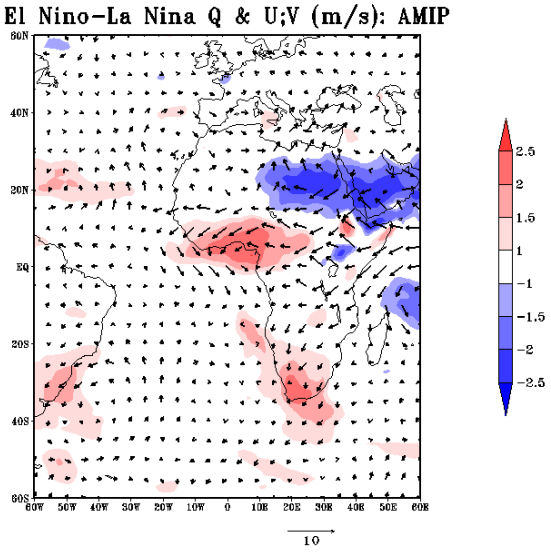

(c) AMIPlike

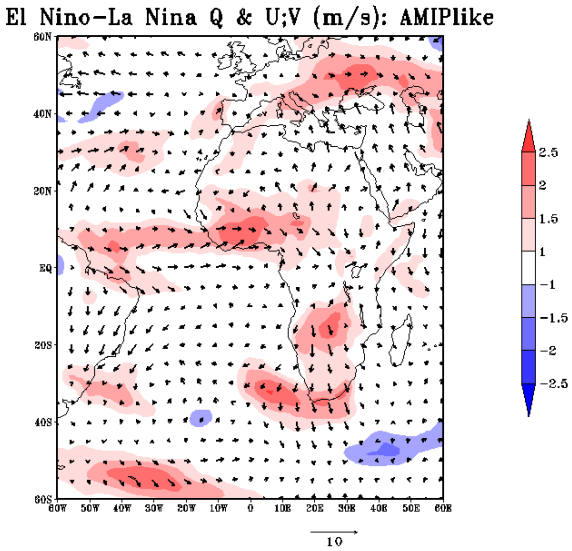

Figure 4.20: *JAS ENSO composites (difference between El Nino minus La Nina anomalies) of Specific Humidity (color) and 925hPa winds (vectors) for: NCEP-NCAR (a) AMIP (b) and AMIPlike (c).*

deep convection should be enhanced but due to the fact that the moisture supply significantly increases at the edge of the convective zone (here Gulf of Guinea), this leads to an increase precipitation over West Sahel as shown in Figure 4.20, b, western African side. Again, dynamical effects (weakening of the monsoon flow) are still involved but the thermodynamical effects through the moisture supply are strong enough to overcome the dynamics.

We should note that in AMIPlike Figure 4.22, b, despite the fact that moisture supply in the lower levels originates from the Sahel instead from the Gulf of Guinean (Figure 4.22, b) as in the case of AMIP West Sahel, the same result persists: wetter Sahel (Figure 4.20, c).

In general, one of the problems of the coupled model/AMIPlike, is that it is able to reproduce the observed features of variability but in the opposite sign. The sensitivity of the zonal dipole rainfall pattern in AMIP to ocean SSTs has been tested in the [9] Caminade et al.2010 using another model. They found that the model was very sensitive to the SST warming over the Gulf of Guinea, rather than the Atlantic SST dipole itself. This had leaded to increased convergence (and precipitation) over west Africa and decrease convection over eastern Africa as reproduced here.

4.3 Summary and conclusions

The model used here is capable to reproduce the low frequency Sahel rainfall variability and still has problems for higher frequency of variability. Our hypothesis is that competing forcings between dynamics and thermodynamics are playing the role. Furthermore, the ability of the model when forced with model SSTs to reproduce the long term Sahel drought enhances this last hypothesis. Model seems to exhibit a strong relationship to radiative forcing at the low frequency variability mainly due to ASAs. If this hypothesis is true, this could be an important result for the future global warming studies. We will pay more attention on this issue in the following chapter.

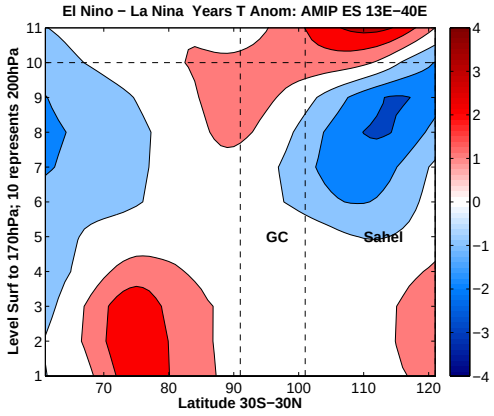

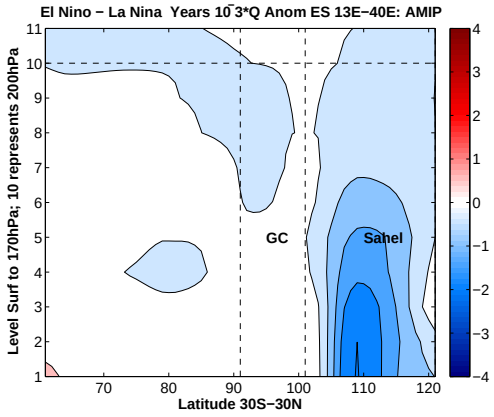

Figure 4.21: *Same as Figure 4.19 but AMIP East Sahel (13E-40E).*

(a) AMIP West Sahel

(b) AMIPlike Sahel

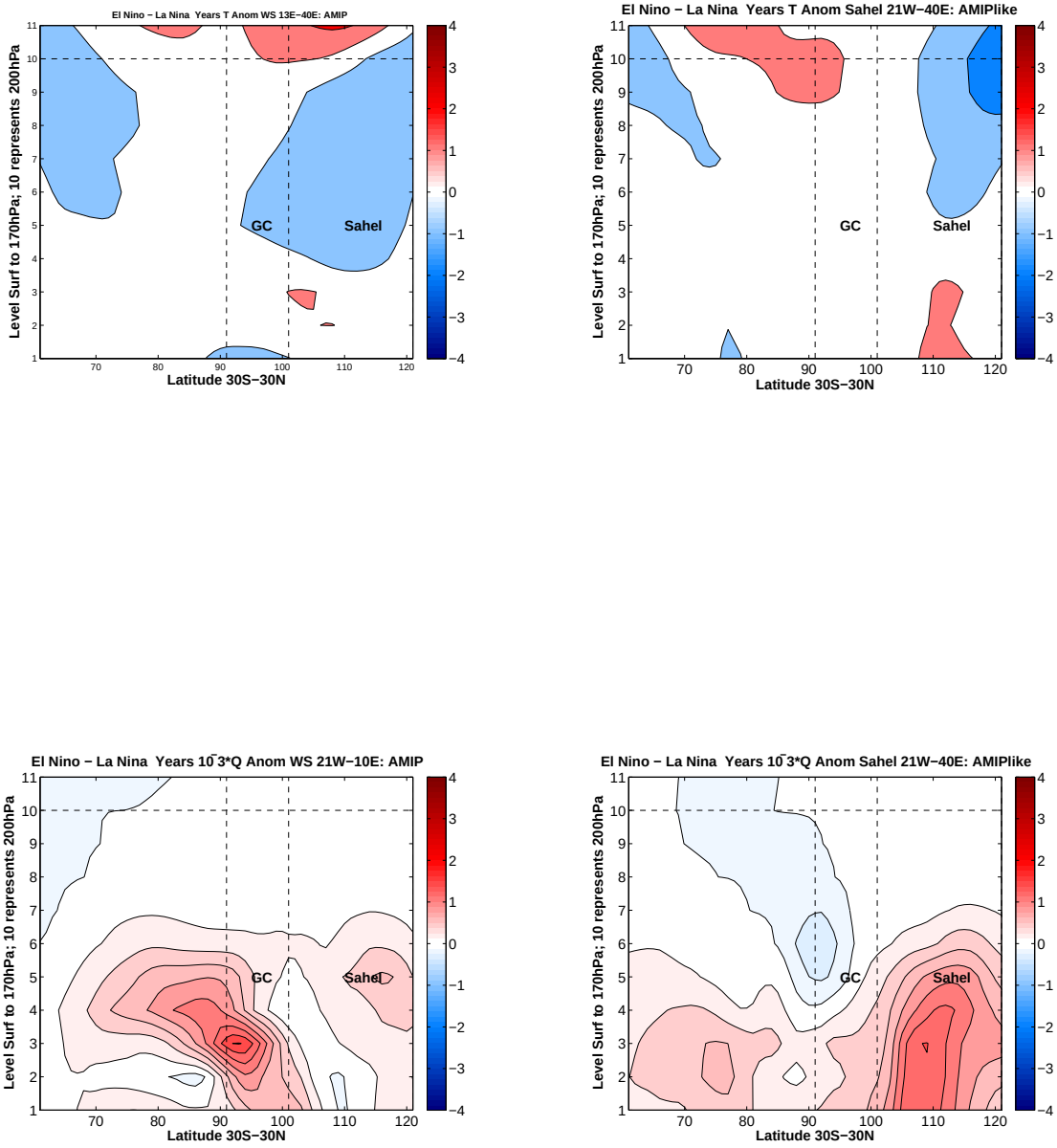

Figure 4.22: *Same as Figure 4.19 but for AMIP West Sahel (21W-10E), left and AMIPlike entire Sahel (21W-40E), right.*

Chapter 5

Results: Role of Anthropogenic Sulfate Aerosols

In this chapter, additionally to the analyses of AMIP and AMIPlike runs, AMIP-Aero and AMIPlike-Aero, runs with climatology Anthropogenic sulfate aerosols, are examined to evidence their role on the Sahel rainfall at the decadal time scale. For the purpose, two indices (following [10] Chang and Chiang et al.2011) are computed in order to highlight the Atlantic interhemispheric SSTs/Aerosols loading gradient and their impact on Sahel rainfall.

5.1 State of the Art of model Sulfate Aerosols influence on WAM

As concluded in the previous chapter and accordingly to other works ([25] Folland et al.1986, [80] Ward 1998, [27] Giannini et al.2003), the multidecadal fluctuations of Sahel summer rainfall in the 20th century do not appear to be related to El Nino Southern oscillation (ENSO). A few works have explained the long-term decrease of 20th century Sahel rainfall with the combination of external anthropogenic forcing and internal variability ([30] Held et al.2005, [5] Biasutti and Giannini 2006, [38] Kawase et al.2010). In fact, [30] Held et al.2005 analyzed initial condition ensembles of two versions of a coupled model, and concluded that the drying Sahel trend is partly anthropogenically forced (aerosol loadings and GHGs emissions) and partly due to internal variability of the ocean-atmosphere climate system. The comparison between the GHGs and Aerosol forcing on the African climate leads to the conclusion that: global warming due to GHGs exhibits a minor but positive impact on precipitation. On the contrary, seasonal rainfall amount is largely reduced in response to increased atmosphere aerosol burden from biomass burning, fossil fuel combustion ([58] Paeth and Feichter 2006).

Sulfate aerosols influence climate directly (via the direct radiation effect) by scatter-

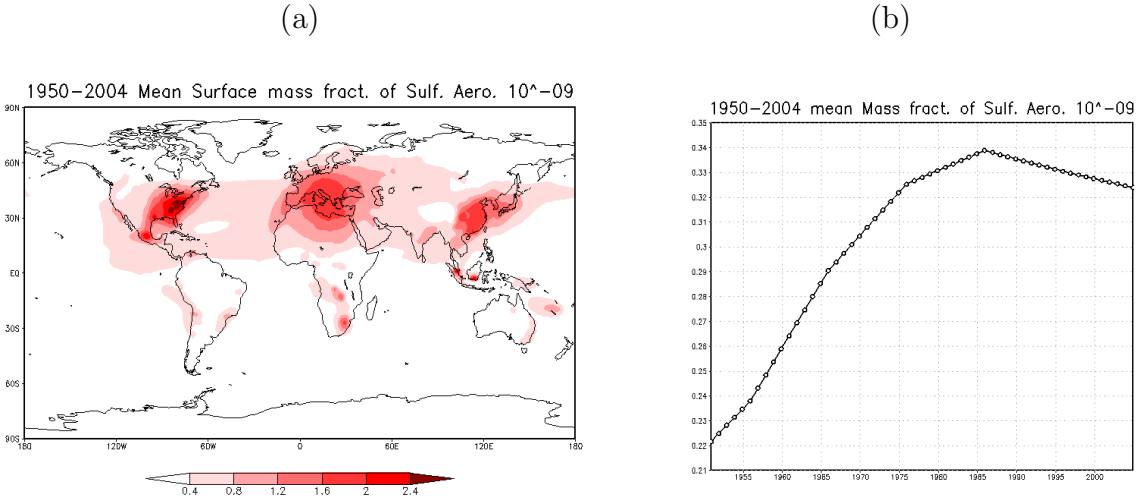

Figure 5.1: *1950-2004 Spatial distribution of the surface summer ASAs (mass fraction of sulfate dry aerosol in air expressed in sulfur kg/kg) - (a) and the time series of the corresponding global surface summer mean - (b)*

ing or absorbing solar radiation, and indirectly, by changing the microphysical properties of clouds. The indirect impact acts in two different ways:
1- the ability of aerosol to change cloud albedo by changing the number of cloud droplets, which can subsequently scatter a different amount of solar radiation, making the cloud more or less reflective (the first indirect effect, [78] Twomey 1977);
2- changing the precipitation characteristics of clouds and increasing cloud lifetime (the

second indirect effect, [1] Albrecht 1989).

Modelling work by [36] Jones et al.2001 suggests that the first indirect effect may have a greater impact on climate than the direct effect which is to cool the climate.

Sulfate aerosols are concentrated mainly in the Northern hemisphere as illustrated by Figure 5.1, a, and have increased much during the second half of the 20th century due to human activity, Figure 5.1, b. Their overall effects decrease the absorbed solar radiation

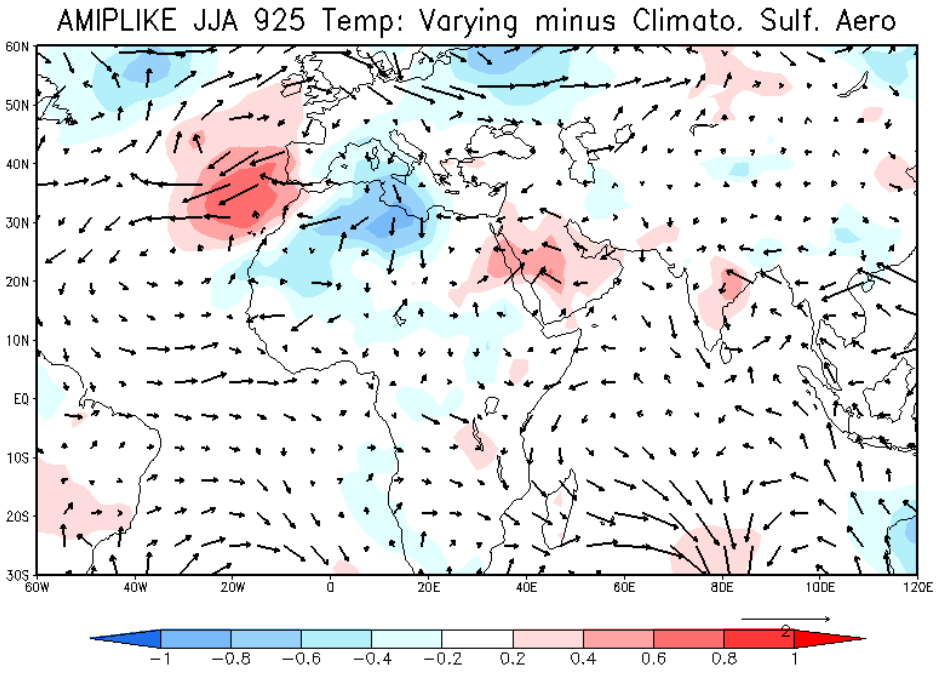

Figure 5.2: *Mean Summer 1950-2004 925hPa Temperature difference between: AMIPlike with Varying ASAs minus AMIPlike-Aero with Climatological ASAs.*

and induce a strong local cooling as evidenced in Figure 5.2 where the mean summer 1950-2004 surface temperature difference between AMIPlike and AMIPlike-Aero is displayed. On average, AMIPlike has more ASAs that AMIPlike-Aero and Figure 5.2 indicates the impact of increased aerosol. There is cooling over North Africa, Europe, far North Atlantic and in the Sahel but there is actually warming off the coast of Spain and North West Africa. This could be relevant for Sahel rainfall. The idea is that their location in the Northern hemisphere could have significantly contributed to an interhemispheric SST gradient (North ocean colder than South), which substantially have altered lower circulation and rainfall ([32] Hulme and Kelly 1993, [85] Williams et al.2001, [63] Rotstayn and Lohmann 2002, [4] Baines and Folland 2007). Especically, Tropical Atlantic and the interhemispheric gradient of SSTs have been shown to be impacted by ASAs ([63] Rotstayn and Lohmann, 2002) and consequently, have leaded to a southward shift of the tropical rainfall including Sahel rainfall as represented in Figure 5.3. Increased

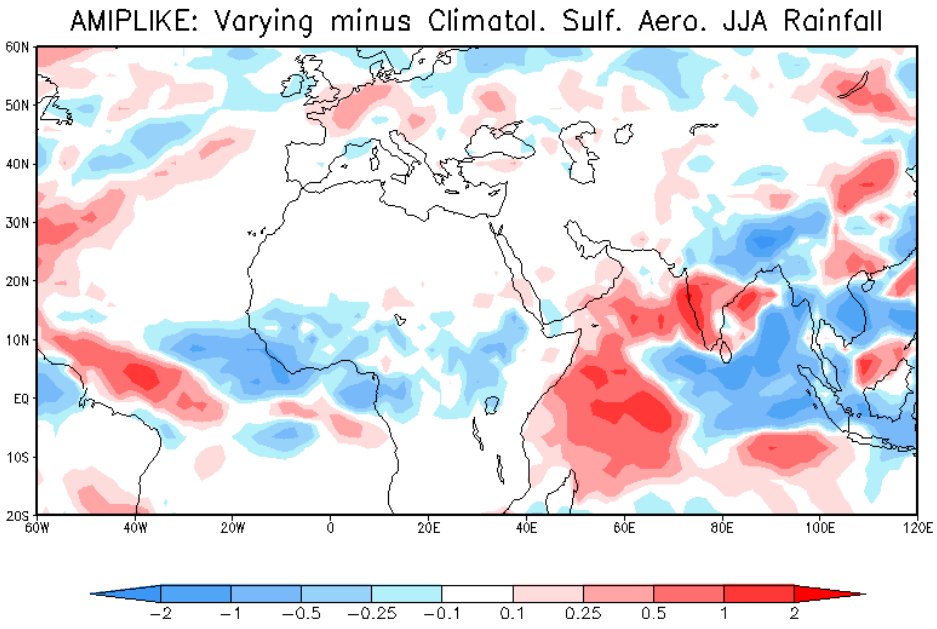

Figure 5.3: *Mean Summer 1950-2004 Precipitation difference between: AMIPlike with Varying ASAs minus AMIPlike-Aero with Climatological ASAs.*

ASAs has a huge impact in the indian Ocean / South-East Asia sector as well and may be a response to aerosol forcing. Consequently, the diabatic heating anomalies in this sector may have impacted into West Africa and increased rainfall over there. This point needs more investigation in the future research.

5.2 Results of the EOF Analysis

When prescribing ASAs to climatological (Figure 5.4), the spatial patterns of rainfall variability look very similar to the ones discussed in the previous chapter with varying ASAs, Figure 4.7. AMIP-Aero EOF1 represents the Sahelian mode and its variability explains 29% of the total variance (a) and AMIP-Aero EOF2, the zonal dipole representing 22% of the total variance (b). AMIPlike-Aero EOF1 (c) explains 29% of the total variance and seems to represent the Sahelian mode and AMIPlike-Aero EOF2 (22%), presents a meridional dipole (d).

The decadal components (21-year running mean) of the corresponding PCs are given in Figure 5.5 for PC1 (a) and PC2 (b). Interestingly, only AMIP-Aero PC1 (Figure 5.5, a, green) is able to reproduce the long Sahel drought and highly correlates (0.86) with the observed PC1 (black line). AMIP-Aero PC2 (blue) and AMIPlike-Aero PC2 (dark orange)

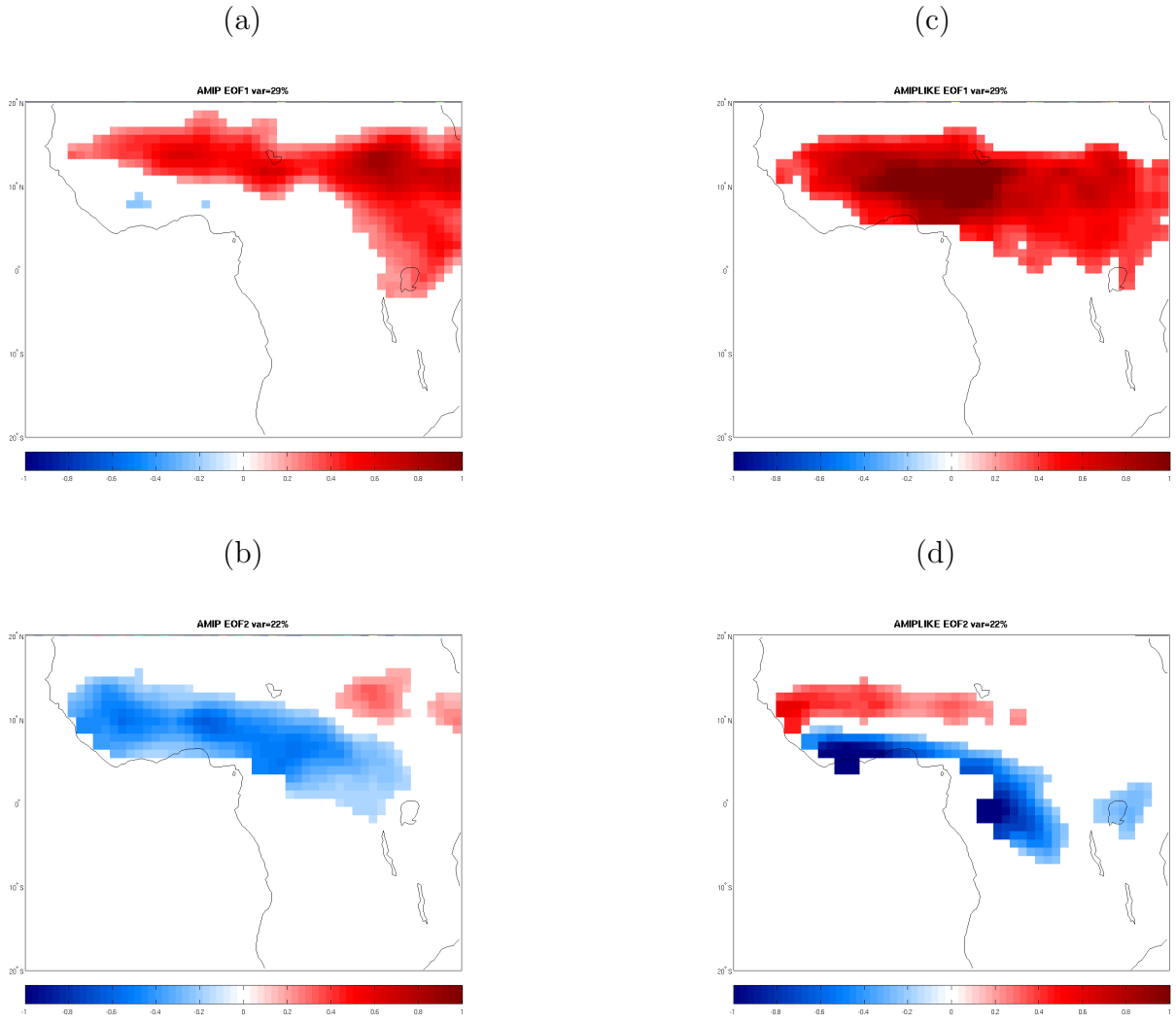

Figure 5.4: *AMIP-aero: EOF1 (a); EOF2 (b) and AMIPlike-Aero: EOF1 (c); EOF2 (d) applied for the same area and time period as in Figure 4.7. Units are mm/day per standard deviation of the associated principal components (PCs). The explained variances are given in the text. Only 95% significant results are shown.*

(a) (b)

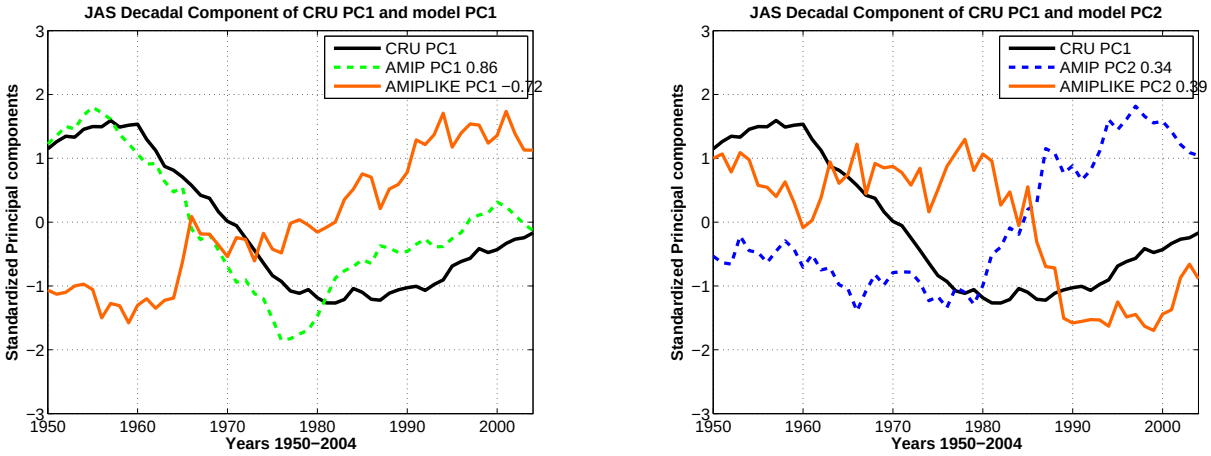

Figure 5.5: *Low frequency component of the Standardized principal components (PCs) for runs with prescribed climatological aerosols. In both plots, black line represents CRU PC1. Model PC1 (a) and PC2 (b): AMIP-Aero (dashed blue), AMIPlike-Aero (dark orange). Model Correlations with CRU PC1 are given in the legend.*

on Figure 5.5, b, do not reproduce the long Sahel drought anymore and have low correlations with observation (0.39 and 0.34 respectively). AMIPlike-Aero PC1 (Figure 5.5, a, dark orange) instead negatively correlates with observation (-0.72). These results illustrate the evidence that, additionally to SSTs, ASAs have played a role in shaping the long Sahel drought as well and should be considered as an important component in GCMs especially when used in coupled mode.

Regression of the global summer SSTS onto the decadal and residual components of the corresponding PCs for AMIP-Aero is shown Figure 5.6 and for AMIPlike-Aero in Figure 5.7. At the decadal time scale, when forced only with prescribed observed SSTs, AMIP-Aero Sahel drought is forced by an interhemispheric SSTs pattern: warm SSTs anomalies in the northern hemisphere and cold SSTs anomalies in the South (Figure 5.6, a). The Gulf of Guinea SSTs plays a great role at the interannual time scale (Figure 5.6, b). The second mode of rainfall variability (zonal dipole) seems to be related to an interhemispheric SSTs pattern of variability in the Atlantic at the decadal scale (c) and in the western Pacific and eastern equatorial Atlantic at the interannual time scale (d).

Similarly, the regression of AMIPlike-Aero global summer SSTs onto the corresponding PCs components is shown in Figure 5.7. As expected, the model does not show any evident relationship to SSTs at the decadal time scale (a and c) and most of the African rainfall variability is mainly related to the SSTs variability in the Pacific and in the tropical Atlantic at the interannual time scale (b and d).

In conclusion, when the model is set in uncoupled mode with climatological ASAs, it is important to force it at the bottom boundaries with prescribed observed SSTs in order to reproduce the long drought that governed the Sahel region in 1970s-1980s. AMIPlike-Aero run, forced with model SSTs and no realistic (climatological) ASAs, is not able to reproduce the Sahel drought anymore.

5.3 Mechanism of the Rainfall Variability: Interdecadal time scale

[10] Chang and Chiang et al.2011 concluded that the tropical Atlantic interhemispheric SST gradient significantly influences the rainfall climate of the tropical Atlantic sector, including droughts over West Africa. This secular trend is exhibited from the beginning of the twentieth century until the 1980s, with stronger warming in the south relative to the north. They showed that the trend behavior is on top of a multidecadal variation associated with the Atlantic multidecadal oscillation (AMO). We follow the procedure they used to derive two indices of the Atlantic interhemispheric SST and sulfate aerosol gradients hereafter AIHG and SIHG indices respectively. AIHG is obtained by substracting the average SST across the entire tropical North Atlantic basin (5-35N, 0-80W) from the tropical south Atlantic (5S-20S, 60W-20E) and applying a 21-year running mean to

(a) AMIP-Aero PC1 Decadal

(b) AMIP-Aero PC1 Residual

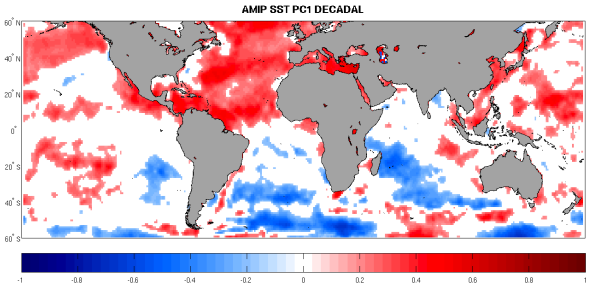

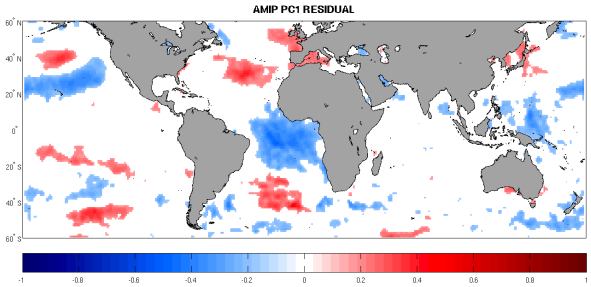

(c) AMIP-Aero PC2 Decadal

(d) AMIP-Aero PC2 Residual

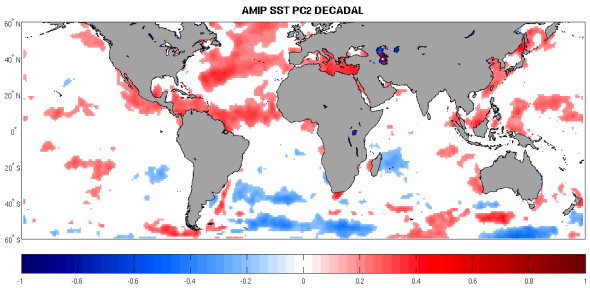

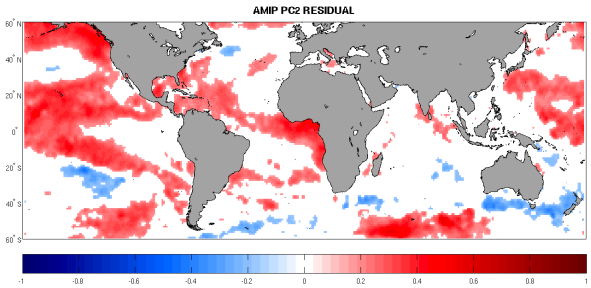

Figure 5.6: *Same as Figure 4.14 but for AMIP-Aero with climatological ASAs.*

(a) AMIPlike-Aero PC1 Decadal

(b) AMIPlike-Aero PC1 Residual

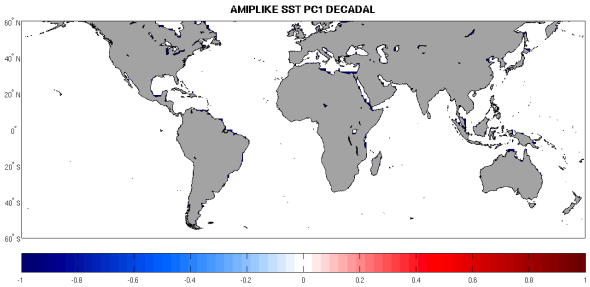

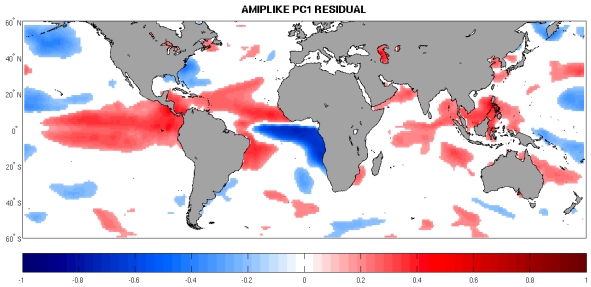

(c) AMIPlike-Aero PC2 Decadal

(d) AMIPlike-Aero PC1 Residual

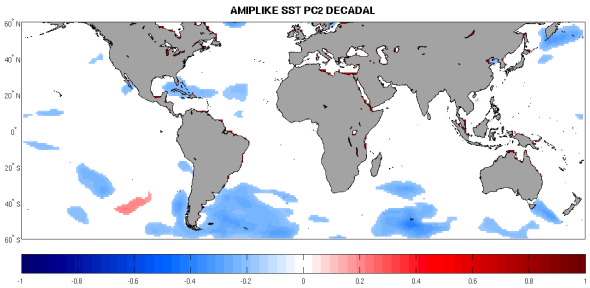

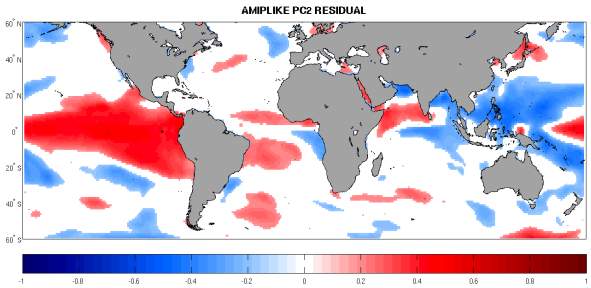

Figure 5.7: *Same as Figure 4.15 but for AMIPlike-Aero with Climatological ASAs.*

emphasize multidecadal and longer time-scale variations. The same is done (now North minus South) for SIHG, difference between two boxes: North Atlantic (20N-60N, 0-80W) minus South Atlantic (20S-60S, 60W-20E).

Over North America and Europe as shown in Figure 5.1, b, sulfate emissions continuously increased until late 1970s (Figure 5.8, black line) and then started declining ([72] Smith et al.2001) because of legislation in North America and Europe in the 1960s and 1970s that mandated reductions in atmospheric pollution. Overall, the interhemispheric SST gradient - AIHG (same plot, dark orange (model) and dashed blue lines (observations)), exhibits a long-term increasing trend (south warmer than north) superimposed on a pronounced multidecadal variation throughout the twentieth century. The observed AIHG peaks in the 1980s and follows the variations of the sulafte aerosols with a delay phase. The model AIHG follows the SIHG in the early 1950s till mid-1960s where it seems to be leading the sulfate aerosols variations (probably due to the internal variability of the model) till mid-1970s when it started following the SIHG. The correlations between the AIHG and SIHG time series are relatively high: 0.87 for Model (AMIPlike) and 0.80 for observation (AMIP), both simulations forced with varying aerosols. Despite some evident differences noted on Figure 5.8, we can conclude that sulafte aerosol forcing has been one of the leading cause of the twentieth century trend in the AIHG.

5.3.1 Direct Sulfate Aerosols influence on SSTs

Correlations of the global SSTs and ASAs with the multidecadal index AIHG are shown in Figure 5.9. In AMIP/observation, Figure 5.9, a, a strong interhemispheric SST gradient pattern in the Atlantic is evidenced: Southern Atlantic warmer than Northern hemisphere. The corresponding correlation with the SITG reflects also the interhemispheric ASAs gradient (b): more sulfate loadings in the northern hemispere compared to the southern hemisphere.

AMIPlike somehow reproduces the interhemispheric gradient in SSTs (Figure 5.9, c) and in ASAs (Figure 5.9, d).

As discussed in some studies ([50] Moura et al.1981, [16] Chiang et al.2000, [17] Chiang et al.2002), the interhemispheric SST gradient has a strong dynamical control on the ITCZ position and as a result, shifts the Atlantic ITCZ southward. This could also be, one of the reason why the coupled model and AMIPlike runs shift the global precipitation Southward as discussed in the third chapter of this work.

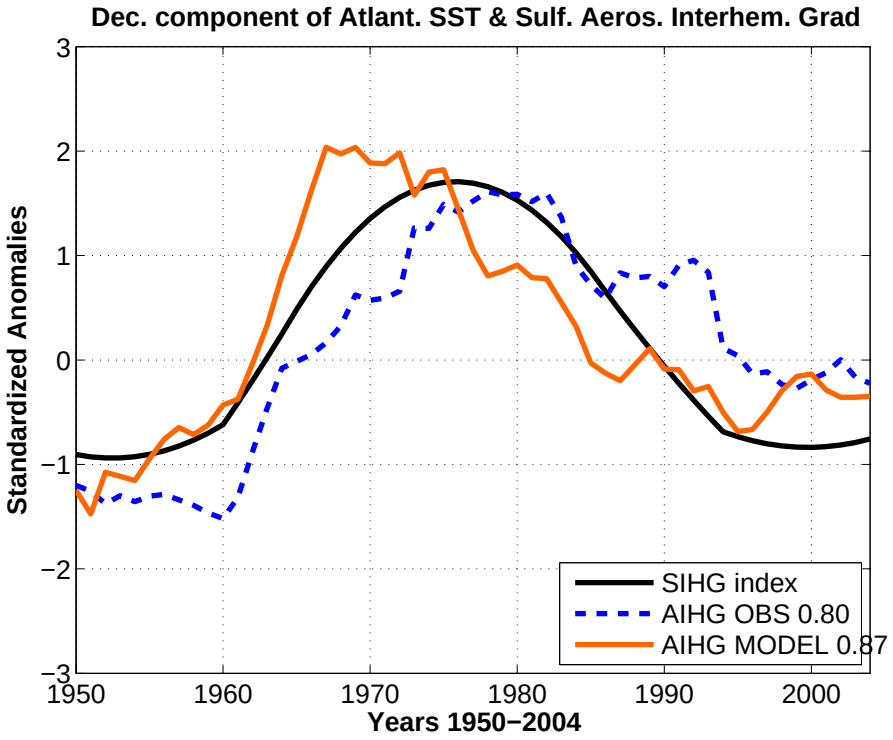

Figure 5.8: *Area-averaged Atlantic SSTs and surface sulafte aerosol emissions from the forcing applied for AMIP and AMIPlike. Black line, difference between North Atlantic (20N-60N, 0-80W) minus South Atlantic (20S-60S, 60W-20E) surface sulafte aerosol emissions. Dark orange (model) and green (observed) lines correspond to the difference between tropical south Atlantic (5S-35S, 60W-20E) and tropical North Atlantic basic (5-35N, 0-80W), south minus north. A 21-year running mean is applied to the two time series to emphasize multidecadal and longer time-scale variations.*

(a) Observations AIHG

(b) Observations SIHG

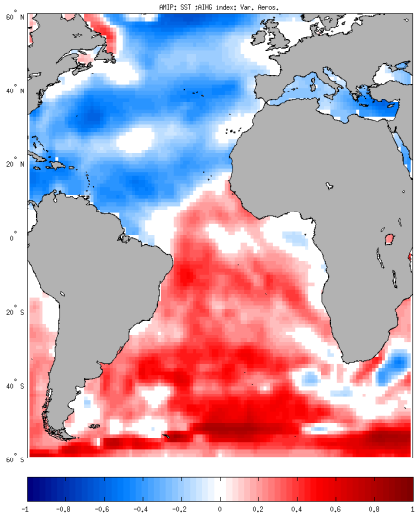

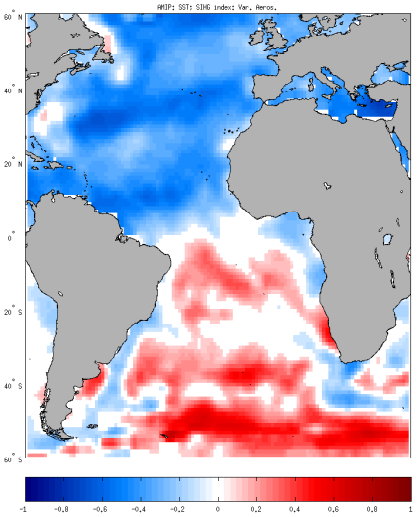

(c) Model AIHG

(d) Model SIHG

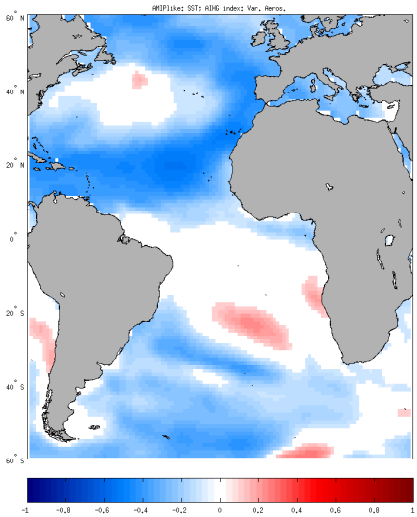

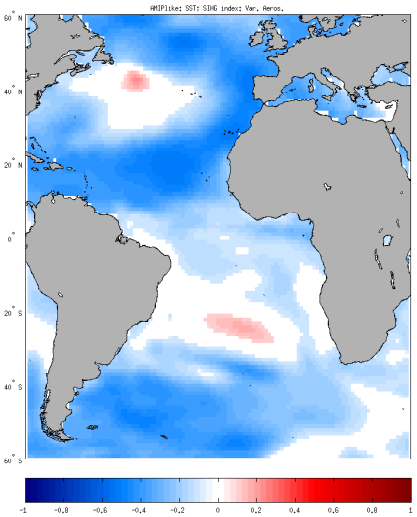

Figure 5.9: *Correlation of AIHG (left) and SIHG (right) indices with AMIP/observed (a and b) and modelled (c and d) SSTs .*

(a) AMIP AIHG

(c) AMIP-Aero AIHG

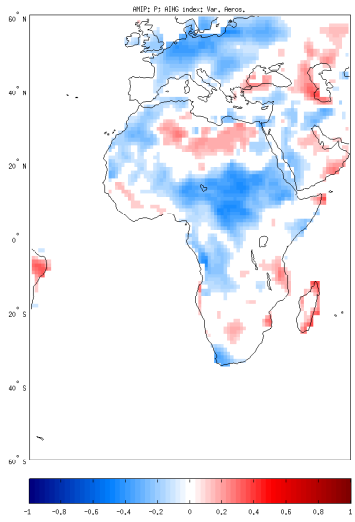

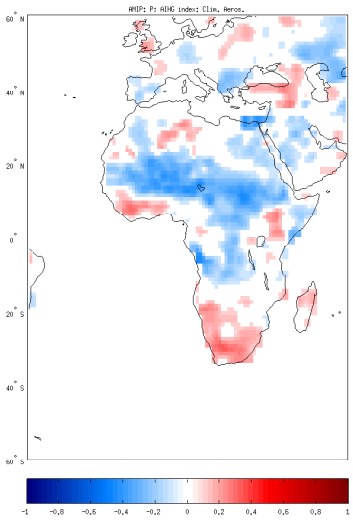

(b) AMIP SIHG

(d) AMIP-Aero SIHG

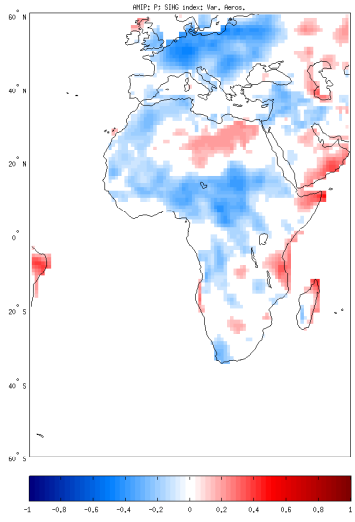

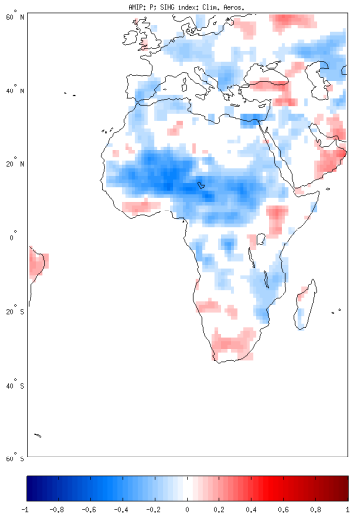

Figure 5.10: *Correlation of global precipitation (snapshot on Africa) for AMIP (a and b) and AMIP-Aero (c and d) with the corresponding AIHG (top row) and SIHG (bottom row) indices.*

5.3.2 Indirect Sulfate Aerosols influence on rainfall

The terminology **Indirect** is employed here to refer to the influence that Sulfate aerosols might have on African rainfall by means of the Atlantic SSTs, given their strong relationship through the above computed indices. The correlation maps of the global precipitation focusing on Africa with the multidecadal AIHG and SIHG indices for runs with varying and climatological sulfate aerosols are displayed in Figure 5.10 and Figure 5.11, where SSTs are forced to follow observations and model respectively.

Figure 5.10, a, shows that when the AMIP run is performed with prescribed varying sulfate aerosols, a negative correlation exists between the AIHG index and rainfall over Central Eastern Africa and Europe. There is a zonal dipole in the Sahara rainfall variability with negative correlation to AIHG in the West Sahara and positive correlation in the east Sahara. These correlation patterns between AIHG and Africa rainfall are similar when considering the Sulfate aerosol interhemispheric gradient index (Figure 5.10, b). On the contrary, when the AMIP run is performed with prescribed climatological sulfate aerosols, AMIP-Aero, (Figure 5.10, c), the negative correlation between AIHG and rainfall still exists over central eastern Sahel. Additionally, there is an increase of negative correlation over West Sahel. The negative correlation over Europe disappeared. The same results are found when correlating the SITG and the rainfall (Figure 5.10, d). So indirectly, via Atlantic SSTs, the loading of the ASAs has dried up the entire Sahel region.

The same analyses are performed for AMIPlike runs. AMIPlike run, (with prescribed modelled varying SSTs and ASAs), Figure 5.11, a, presents a negative correlation between AIHG index and rainfall over the entire Sahel and West Europe. A positive correlation instead exists over South Africa. The same conclusions are true for correlations between SIHG index and rainfall. AMIPlike with no real forcings, AMIPlike-Aero (with prescribed modelled varying SSTs and climatological ASAs) reflect, as expected, no Sahel rainfall relationship to Atlantic SSTs (c) and Sulfate aerosols (d) at the multidecadal time scale. A negative link instead exists between the two indices and the East Europe rainfall.

5.4 Summary and conclusions

We have shown that atmospheric model forced with prescribed model SSTs, is also able to reproduce the long term Sahel drought as far as the SSTs contain an imprint of varying ASAs. There is a strong correlation between the tropical Atlantic interhemispheric SSTs and sulfate aerosols gradients indices, which negatively correlate with Sahel rainfall. The mechanism through which this occurs can be described as follows: the larger loadings of ASAs in the atmosphere during 1970s-1980s in the northern hemisphere compared to the south, has created an interhemispheric SSTs gradients in the Atlantic. This Atlantic interhemispheric ASAs loading gradient has locally modified the oceanic and atmospheric circulations that has consequently, additionally to the global ocean SSTs effect, caused

(a) AMIPlike AIHG

(c) AMIPlike-Aero AIHG

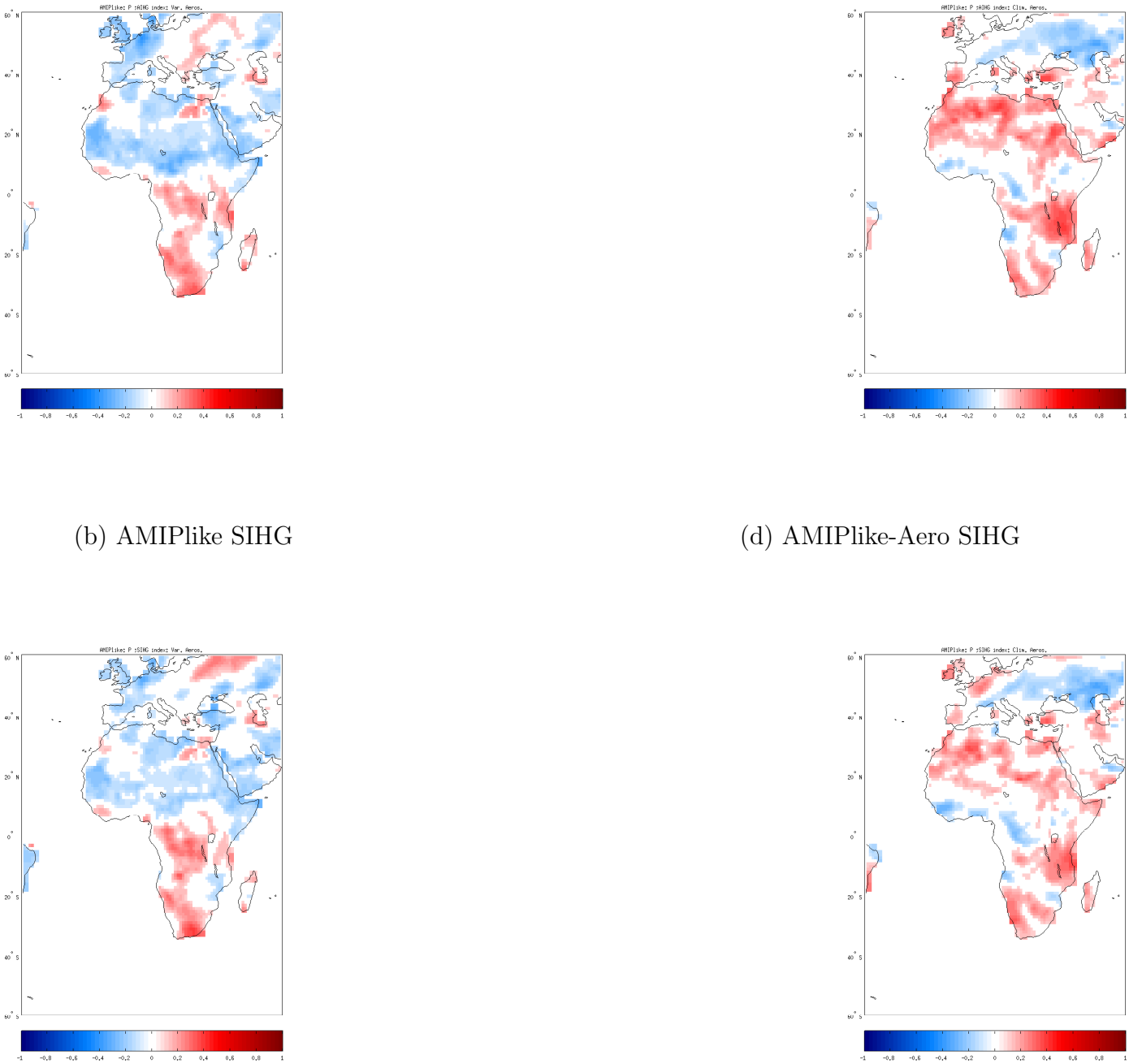

(b) AMIPlike SIHG

(d) AMIPlike-Aero SIHG

Figure 5.11: *Correlation of global precipitation (snapshot on Africa) for AMIPlike (a and b) and AMIPlike-Aero (c and d) with the corresponding AIHG (top row) and SIHG (bottom row) indices.*

the drying of the Sahel and reduction of rainfall over Europe. These results additionally to the traditional southward shift of the Atlantic ITCZ belt found in the litterature, show , for the first time, an evidence of Sulfate aerosol impacts on the Sahel drought.

Conclusion and Outlook

5.5 Summary and Conclusions

In this thesis, we first investigated the Summer West African Climate in terms of climatology, variability and associated main mechanisms that governed the climate of the region during the second half of the last century, at the interannual and decadal time scales. Then, We focused on the understanding of the role that the main contributors (Sea Surface Temperatures, SSTs, and Anthropogenic Sulfate Aerosols, ASAs) have played in shaping the climate of West Africa - WA. This has been done through model simulations performed in coupled (ocean-atmosphere) and uncoupled (prescribed SSTs) modes with ASAs set in different configurations. All the simulated results have been compared to observations.

1. The results show that the basic structure of the WA climate, such as the monsoon flow in the lower troposphere, the AEJ and the TEJ in the mid and upper troposphere, may be reasonably simulated by the model forced with observed SSTs.

2. The AMIP run systematically overestimates the strength of the AEJ inland due to the overestimation of the low level temperature gradients between Sahara and Tropical Africa. Besides, the simulated monsoon flow does not penetrate enough inland, because of an underestimation of the low level temperature gradients between ocean and land.

3. In coupled atmosphere-ocean mode or with prescribed SSTs from coupled model, the WA summer mean climate features are also captured. The strength of the monsoon flow is well captured; the strength of the AEJ as well, although, its core is too wide. The strength of the TEJ is underestimated and its flow, limited to the Indian Ocean and does not propagate westward. This could be related to the convection scheme used or can be the hallmark sign of years of reduced Sahel precipitation as proposed by [52] Newell and Kidson 1984; [54] Nicholson anf Grist 2001.

4. Simulated seasonal rainfall climatologies are generally consistent with observations. Model captures the rainfall spatial variability, the north-south migration of the ITCZ and the associated low-level circulation and phase. On the other hand, it shows a clear southward shift of the ITCZ and underestimates the amplitude of the Sahel rain season. AMIPlike and AOCOUP capture well the phase of the two rainy seasons in the equatorial Africa but overestimate their magnitudes in the western region and underestimate them in the east. In general, AMIP seems to perform better in the Sahel, while AOCOUP and AMIPlike show higher skill in the equatorial region.

5. SSTs - WA rainfall first pattern of covariability relies, at the decadal time-scale, negative Sahel rainfall with an nterhemispheric global SSTs pattern (warm in the North and cold in the South). At the interannual time-scale, Sahel drought is related to SSTs variability in the Pacific mainly related to ENSO. The second pattern of covariability relies guinean coast rainfall to variability in the eastern equatorial

Atlantic at the interannual time-scale. This is inextricably tied to the Atlantic marine ITCZ which in turn is related to the local walker circulation.

6. The AMIP run forced with climatological ASAs is able to reproduce very well the drying tendency of the Sahel. The varying ASAs limit the drying trend to the central east Sahel, and the EOF analysis does not show a clear separation between the continental Sahel and the oceanic guinean coast rainfall patterns of variability anymore. The reproduced drying trend in the Sahel rainfall on one hand, and the Central East Sahel rainfall on the other, has been linked in general to an interhemispheric large scale SST mode at the multidecadal time scale plus the effect of the Pacific at the interannual time-scale.

7. The warming of the Pacific Ocean leads to a homogeneous increase of the tropospheric temperature over the tropics, that in turn leads to an anomalous inflow of dry air (originating from the subsidence region Sahara) into the Sahel (central east Sahel). This chain of processes is called upped-ante mechanism. At the interannual time scale, SSTs and ASAs influence west Sahel rainfall variability (through the so-called anomalous gross moist stability mechanism) as local anomalous moisture supply at the edge of the convection zone (Gulf of Guinea) is strong enough to overcome large-scale dynamics.

8. When the model is forced by prescribed AOCOUP SSTs and climatological ASAs, the two dominant patterns of rainfall variability over WA seem to be mostly linked to La Nina events in the Pacific. The drying trend in Sahel rainfall is not reproduced. Interestingly, when uses in coupled mode or uncoupled mode prescribed coupled model SSTs, the model is able to reproduce the drying trend in Sahel rainfall when the effect due to varying ASAs is added.

9. Teleconnection between ASAs and WA rainfall has been established through the computation of AIHG and SIHG indices. This indirect impact of ASAs on the WA rainfall has been revealed to be possible through the modification of the AMO: the asymmetric increase of ASAs in the two hemispheres has induced, an asymmetric modification of SSTs in the Atlantic, that in turn affected the Atlantic multidecadal oscillation (AMO) and tropical rainfall accordingly.

5.6 Discussion and Outlook

Some outlooks are proposed.

- The results presented in the last chapter of this work demonstrate that ASAs may play a potentially major role in the Sahel rainfall decadal variability : ASAs seem to have substantially altered low-latitude circulation (especially in the Atlantic) that in turn has led to negative rainfall trend in the Sahel. Further studies are desirable,

with more complete treatment of aerosols. For instance, it has been shown in [68] Ramaswamy et al.2001 that dust aerosols, which are mainly produced in the Sahara, have a potential impact on both shortwave and longwave radiations through aerosol-cloud interactions.

- More work is still needed to assess the relative role of internal ocean-atmosphere generated SSTs versus ASAs driving, using for example AMIP and AMIP-Aero to identify what fraction of the role of SSTs was (i) attributed to internal ocean-atmosphere process, (ii) driven by aerosol variations.

- Additionally, land surface properties, such as the vegetation dynamics and land use change, should be included as forcing as it has been shown to amplify the variability of Sahel precipitation ([40] Kucharski et al.2012).

- The possible role of varying ASAs on Sahel drought found in this work suggests that, on the other way, regreening conditions observed in the Sahel at the end of the 20th century could be due to the decrease in ASAs emissions after 1980s as imposed by the world legislation laws. This possibility should be taken into consideration in future studies dealing with climate change scenarios.

- Finally, every experiment performed in this work, made use of one member only. It would be interesting to extend our experiments making use of a set of multiple members simulations. Besides, some sensitivity experiments with the same model configuration but focusing, for instance on different ocean basins, could also be a good exercise. A particular interest could be dedicated to the role of the North Atlantic with respect to global tropical ocean on the WA rainfall as an evident imprint of ASAs has been particularly revealed in the area. Additionally, plannification of multi-model comparison that includes the same experimental design we used here could be important.

Bibliography

[1] B. Albrecht, Aerosols, cloud microphysics and fractional cloudiness, Science, **245**, 1227-1230 (1989).

[2] R. F. Alder, G. J. Huffman, A. Chang, R. Ferraro, P.P Xie, J. Janowiak, B. Rudolf, U. Schneider, S. Curtis, D. Bolvin, A. Gruber, J. Susskind, P. Arkin, E. Nelkin, The version-2 Global Precipitation Climatology Project (GPCP) Monthly Precipitation Analysis (1979-Present), J. Hydrometeor., **4**, 1147-1167 (2003).

[3] J. Bader, M. Latif, The impact of decadal-scale Indian ocean sea surface temperature anomalies on Sahelian rainfall and the north Atlantic oscillation, Geophys Res Lett., **30**, 2169 (2003)

[4] P. G. Baines, C. K. Folland, Evidence for a rapid global climate shift across the late 1960s. J. Climate **20**, 2721-2744 (2007).

[5] M. Biasutti, A. Giannini, Robust Sahel drying in response to late 20th century forcings. Geophys. Res. Lett., **33**, L11706 (2006)

[6] C. S. Bretherton, C. Smith, J. M. Wallace, An Intercomparison of Methods for Finding Coupled Patterns in Climate Data. J. Climate, **5**, 541?560 (1992).

[7] C. Cagnazzo, E. Manzini, M. A. Giorgetta, P.M. De F. Forster, J. J. Morcrette, Impact of an improved shortwave radiation scheme in the MAECHAM5 General Circulation Model. Atmos Chem Phys **7**, 2503-2515 (2007).

[8] C. Cagnazzo, and E. Manzini, Impact of the stratosphere on the winter tropospheric teleconnections between ENSO and the North Atlantic and European region, J. Clim., **22**, 1223?1238, doi:10.1175/2008JCLI2549.1., (2009).

[9] C. Caminade and L. Terray, Twentieth century Sahel rainfall variability as simulated by the ARPEGE AGCM, and future changes, Climate Dynamics **35**, 75-94 (2010).

[10] C. Y. Chang, J.C.H. Chiang, M. F. Wehner, A. Friedman, R. Ruedy, Sulfate aerosol control of tropical Atlantic climate over the 20th century, J. Climate **24**, 2540-2555 (2011).

[11] A. J. Charlton, L. M. Polvani, J. Perlwitz, F. Sassi, E. Manzini, K. Shibata, S. Pawson, J. E. Nielsen, and D. Rind, A new look at stratospheric sudden warmings. Part II: Evaluation of numerical model simulation, J. Clim., 20, 470?488, doi:10.1175/JCLI3994.1. (2007).

[12] J. G. Charney, Dynamics of deserts and drought in the Sahel, Quart. J. Royal Meterol. Society **101**, 193-202 (1975).

[13] J. G. Charney, W. J. Quirk, S. H. Show and J. Kornfield, A comparative study of the effects of albedo change on drought in semiarid regions, Journal of Atmospheric Science **34**, 1366-1385 (1977).

[14] T.C Chen and Van Loon, Interannual Variation of the Tropical Easterly Jet, Mon. Weather Rev., **115**, 1739-1759 (1987).

[15] A. Cherchi and A. Navarra, Reproducibility and predictability of the Asian summer monsoon in the ECHAM4-GCM, Clim. Dyn., **20**, 365-379 (2003).

[16] J. C. H. Chiang, Y. Kushnir, C. Bitz, Interdecadal changes in eastern Pacific ITCZ variability and its influence on the Atlantic ITCZ, Geophys. Res. Lett. **27**, 3687-3690 (2000).

[17] J. C. H. Chiang, Y. Kushnir, A. Giannini, Deconstructing Atlantic ITCZ variability: Influence of the local cross-equatorial SST gradient, and remote forcing from the eastern equatorial Pacific. J. Geophys. Res., **107**, 4004, doi:10.1029/2000JD000307 (2002).

[18] C. Chou, J. D. Neelin, H. Su, Ocean-Atmosphere-Land feedbacks in an idealized monsoon. Q. J. Roy. Meterol. Soc. **127**, 1869-1891 (2001).

[19] C. Chou, J. D. Neelin, Mechanisms of global warming impacts on regional tropical precipitation. J. Climate, **17** (13), 2688-2701 (2004).

[20] K.H. Cook, Generation of the African Easterly Jet and its role in determining West African precipitation. J. Climate, **12**, 1165-1184 (1999).

[21] K. H. Cook and E. K. Vizy, Coupled model simulations of the West African monsoon system: Twentieth and twenty first century simulations, J. Climate **19**, 3681-3703 (2006).

[22] A. Diedhiou, S. Janicot, S. Viltard and P. De Felice, Evidence of tho regimes of easterly waves over West Africa and tropical Atlantic. Geophysical Research Letter **25**, 2805-2808 (1998).

[23] K. A. Emmanuel, A cumulus representation based on the episodic mixing model; the importance of mixing and microphysics in predicting humidity, AMS. Meterol. Monogr, **24**, 185-192 (1993).

[24] F. G. Fogli, E. Manzini, M. Vichi, A. Alessandri, L. Patara, S. Gualdi, E. Scoccimarro, S. Masina, A. Navarra, INGV-CMCC Carbon (ICC): A Carbon Cycle Earth System Model. CMCC Research Paper No. 61. Available at SSRN: http://ssrn.com/abstract=1517282, (2009).

[25] C. K. Folland T. N. Palmer and D. E. Parker, Sahel rainfall and worldwide sea temperatures, Nature **320**, 602-607 (1986).

[26] B. Fontaine, S. Trzaska and S. Janicot, Evolution of the relationship between near global and Atlantic SST modes and the rainy season in West Africa: statistical analyses and sensitivity experiments, Climate Dynamics **14**, 353-368 (1998).

[27] A. Giannini, R. Saravanan and P. Chang, Oceanic forcing of Sahel rainfall on inter-annual to interdecadal time scales, Science **302**, 1027-1030 (2003).

[28] A. Giannini, R. Saravanan and P. Chang, Dynamics of the boreal summer African monsoon in the NSIPP1 atmospheric model, Climate Dynamics **25**, 517-535 (2005)

[29] A. E. Gill, Some simple solutions for heat-induced tropical circulation, Q. J. Roy. Meterol. Soc. **106**, 447-462 (1980).

[30] I. M. Held, T. L. Delworth, J. Lu, K. L. Findell, T. R. Knutson, Simulation of Sahel drought in the 20th and 21st centuries. Proc. Natl. Acd. Sci. USA **102**, 17,891-17,896 (2005).

[31] F. Hourdin, I. Musat, F. Guichard, P. M. Ruti, F. Favot, M. A. Filiberti, M. Pham, J. Y. Grandpeix, J. Polcher, P. Marquet, A. Boone, J. P. Lafore, J. L. Redelsperger, A. Dell'Aquila, T. L. Doval, A. K. Traore and H. Gallee, AMMA-Model Intercomparison project, Amer. Meteorol. Soc. BAMS2791.1 (2010).

[32] M. Hulme, M. Kelly, Exploring the links between desertification and climate change. Environment, **5**, 5-11, 39-45 (1993).

[33] M. Joly, A. Voldoire, H. Douville, P. Terray, J.-F. Royer, African monsoon teleconnections with tropical SSTs: Validation and evolution in a set of IPCC4 simulations, Climate Dyn., **29**, 1-20, doi:10.1007/s00382-006-0215-8 (2007).

[34] S. Janicot, V. Moron and B. Fontaine, Sahel droughts and ENSO dynamics, Geophys Res Letter **23**, 515-518 (1996).

[35] S. Janicot, S. Trzaska, I Poccard, Summer Sahel-ENSO Teleconnection and decadal time scale SST variations, Climate Dynamics **18**, 303-320 (2001)

[36] A. D. Jones, M. Woodage, C. Johnson, Indirect sulfate aerosol forcing in a climate model with an interactive sulfur cycle. J. Geophys. Res., **106** (D17), 20 293-20 310 (2001)

[37] E. Kalnay, M. Kanamitsu, R. Kistler, W. Collins, D. Deaven, L. Gandin, M. Iredell, S. Saha, G. White, J. Woollen, Y. Zhu, A. Leetmaa, B. Reynolds, M. Chelliah, W. Ebisuzaki, W. Higgins, J. Janowiak, K. C. Mo, C. Ropelewski, J. Wang, R. Jenne, and D. Joseph. The NCEP/NCAR 40-Year Reanalysis Project. Bulletin of the American Meteorological Society, March, 1996

[38] H. M. Kawase, Y. Yamada, T. Takemura, T. Yokohata, T. Nozawa, Physical mechanism of long-term drying trend over tropical North Africa. Geophys. Res. Lett. **37**, L09706 (2010)

[39] R. D. Koster, P. A. Dirmeyer, Z. Guo, G. Bonan, E. Chan, P. Cox, C. T. Gordon, S, Kanae, E. Kowalczyk, D. Lawrence, P. Liu, C. H. Lu, S. Maleyshev, B. McAvaney, K. Mitchell, D. Mocko, T. Oki, K. Oleson, A. Pitman, Y. C. Sud, C. M. Taylor, D. Verseghy, R. Vasic, Y. Xue and T. Yamada. Regions of strong coupling between soil moisture and precipitation, Science **305**, 1138-1140 (2004).

[40] F. Kucharski, N. Zeng, E. Kalnay, A further assessment of vegetation feedback on decadal Sahel rainfall variability. Climate Dyn. DOI:10.1007/s00382-012-1397-x, 2012 ,

[41] J. P. Lafore, C. Flamant, V. Giraud, F. Guichard, P. Knippertz, J. F. Mahfouf, P. Mascart and E. Williams, Introduction to the AMMA Special issue on Advances in understanding atmospheric processes over West Africa through the AMMA field campaign, Quarterly Journal of the Royal Meteorological Society **136**, 2-7 (2010).

[42] P. J. Lamb, Case studies of tropical Atlantic surface circulation patterns during recent sub-Saharan weather conditions: 1967 and 1968, Mon Weather Rev **106**, 482-491 (1978a).

[43] P. J. Lamb, Large-scale tropical Atlantic suce circulation patterns associated with sub-Saharan weather anomalies, Tellus **30**, 240-251 (1978b).

[44] C. Lavaysse, C. Flamant, S. Janicot, D. J. Parker, J. P. Lafore, B. Sultan, J. Pelon, Seasonal Evolution of the West African Heat Low: a Climatological perspective, Climate Dynamics **33**, 313-330 (2009).

[45] R. S. Lindzen, A. Y. Hou, Hadley circulation for zonally averaged heating centered off the Equator, J. Atmos. Sci **45**, 2416-2427 (1988).

[46] G. Madec, P. Delecluse, I. Imbard, C. Levy, OPA 8.1 Ocean General Circulation Model reference manual. Note du Pôle de modélisation No. 11, Inst. Pierre-Simon Laplace (IPSL), France, 91 pp (1999)

[47] E. Manzini, M. A. Giorgetta, M. Esch, L. Kornblueh, E. Roeckner, The influence of sea surface temperatures on the Northern winter stratosphere: Ensemble simulations with the MAECHAM5 model. Journal of Clim., **19**, 3863-3881, (2006).

[48] T. Matsuno, Quasi-geostrophic motions in the equatorial area, J. Meterol. Soc. Jpn. **44**, 25-43 (1966).

[49] T. Mitchell, T. R. Carter, P. D. Jones, M. Hulme, M. New, A comprehensive set of high-resolution grids of monthly climate for Europe and the globle: the observed record (1901-2000) and 16 scenarios (2001-2100). Working Paper 55, 2004.

[50] A. D. Moura, J. Shukla, On the dynamics of droughts in northest-Brazil-Observations, theory, and numerical experiments with a general circulation model. J. Atmos. Sci. **38**, 2653-2675 (1981).

[51] J. D. Neelin, C. Chou, H. Su, Tropical drought regions in global warming and El Nino teleconnections, Geophys. Research Letters **24**, 2275 (2003)

[52] R. E. Newell and J. W. Kidson, African mean wind changes between sahelian wet and dry periods, Journal of Climatology, Volume 4, Issue 1, pages 27-33, 1984

[53] S. E. Nicholson, The West African Sahel: A Review of recent studies on the rainfall regime and its interannual variability. ISRN Meteorology, vol. 2013, Article ID 453521, 32 pages, 2013. doi: 10.1155/2013/453521

[54] S. E. Nicholson and J. P. Grist, A conceptual model for understanding rainfall variability in the West African Sahel on interannual and interdecadal timescales. International Journal of Climatology **21**, (2001).

[55] T. E. Nordeng, Extended versions of the convective parameterization scheme at ECMWF and their impact on the mean and transient activity of the model in the tropics. European Centre for Medium-Range Weather Forecasts Tech. Memo. 206, 41 pp. (1994)

[56] G.R. North, T.L. Bell, R.F. Cahalan, and F.J. Moeng, Sampling errors in the estimation of empirical orthogonal functions, Mon. Wea. Rev., **110**, 699706, 1982.

[57] J. Otterman, Baring high-albedo soils by overgrazing: Hypothesized desertification mechanism. Science **186**, 531-533 (1974).

[58] H. Paeth, J. Feichter, Greenhouse-gas versus aerosol forcing and African climate response. Clim. Dynamics **26**, 35-54 (2006).

[59] T. N. Palmer, Influence of the Atlantic, Pacific and Indian Oceans on Sahel rainfall, Nature **322**, 251-253 (1986).

[60] The GLACE team, Regions of strong coupling between soil moisture and precipitation, Science **305**, 1138 (2004).

[61] N. A. Rayner, D. E. Parker, E. B. Horton, C. K. Folland, L. V. Alexander, D. P. Rowell, E. C. Kent, A. Kaplan, Global analyses of sea surface temperature, sea ice, and night marine air temperature since the late nineteenth century, J. Geosphys. Res. **108**(D14), 4407 (2003)

[62] B. Rodriguez-Fonseca, S. Janicot, E. Mohino, T. Losada, J. Bader, C. Caminade, F. Chauvin, B. Fontaine, J. Garcia-Serrano, S. Gervois, M. Joly, I. Polo, P. Ruti, P. Roucou, A. Voldoire, Interannual and decadal SST-forced responses of the Wesr African monsoon, Atmos. Sci. Letter **12**, 67-747 (2011).

[63] L. D. Rotstayn and U. Lohmann, Tropical rainfall trends and the indirect aerosol effect, J. Climate, **15**, 2103-2116 (2002)

[64] D.P. Rowell, C. K. Folland, K. Maskell and M. N. Neil, Variability of summer rainfall pver tropical North Africa (1906-1992): observations and modelling, Quaterly Journal of Royal Meteorological Society **121**, 669-704 (1995).

[65] D. P. Rowell, Teleconnections between the tropical Pacific and the Sahel, Quaterly Journal of the Royal Meteorological Society **127**, 1683-1706 (2001)

[66] A. J. Simmons, S. M. Uppala, D.P. Dee, S. Kobayashi, ERA-Interim: New ECMWF reanalysis products from 1989 onwards, ECMWF Newsletter **110**, 25?35, 2007a.

[67] A. J. Simmons, S. M. Uppala, D.P. Dee, Update on ERA-Interim, ECMWF Newsletter **110**, 5, 2007b.

[68] V. Ramaswamy and Coauthors, Radiative forcing of climate change. Climate Change 2001: The scientific basis, J. T. Houghton et al., Eds., Cambridge University Press, 349-416, 2001.

[69] Roeckner, E., and Coauthors, The atmospheric general circulation model ECHAM5. Part I: Model description. Max Planck Institute for Meteorology Rep. 349, 127 pp. (2003) [Available from MPI for Meteorology, Bundesstr. 53, 20146 Hamburg, Germany.]

[70] E. Roeckner, R. Brokopf, M. Esch, M. Giorgetta, S. Hagemann, L. Kornblueh, E. Manzini, U. Schlese, U. Schulzweida, Sensitivity of Simulated Climate to Horizontal and Vertical Resolution in the ECHAM5 Atmosphere Model, J. Climate, **19**, 3771?3791, doi: http://dx.doi.org/10.1175/JCLI3824.1, (2006)

[71] D. P. Rowell, The impact of the Mediterranean SSTs on the Sahelian rainfall season, J. Climate **16**, 849-862 (1988).

[72] S. J. Smith, H. Pitcher, T. M. L. Wigley, Global and regional anthropogenic sulfur dioxide emissions. Global Planet change, **29**, 99-119 (2001).

[73] S. D. Solomon, M. Qin, M. Manning, K. B. Averyt, M. M. B. Tignor, H. L. Miller Jr. and Z. Chen, Climate change 2007: The scientific Basis, Eds., 2007. Cambridge University Press, **996** pp, (2007).

[74] K. R. Sperber, J. M. Slingo, and H. Annamalai, Predictability and the Relationship between Subseasonal and Interannual Variability during the Asian Summer Monsoon, Quart. J. Roy. Meteor. Soc., **126**, 2545-2574, 2000.

[75] M. Tiedtke, A comprehensive Mass Flux Scheme for Cumulus Parameterization in Large-Scale Models, Mon. Wea. Rev. **117**, 1779-1800 (1989).

[76] R. Timmermann, H. Goosse, G. Madec, T. Fichefet, C. Etheb, V. Dulière, On the representation of high latitude processes in the ORCA-LIM global coupled sea ice ocean model. Ocean Modell, **8** 175-201, (2005).

[77] C. D. Thorncroft, M. Blackburn, Maintenance of the African Easterly Jet, Q.J.R. Meteorological Society **125**, 763-786 (1999).

[78] S. A. Twomey, The influence of pollution on the shortwave albedo of clouds, J. Atmos. Sci., **34**, 1149-1152 (1977).

[79] S. M. Uppala, D. P. Dee, S. Kobayashi, P. Berrisford, A. J. Simmons, Towards a climate data assimilation system: Status update of ERA-Interim ECMWF Newsletter, **115**: 12?18, 2008.

[80] M. N. Ward, Diagnosis and short-lead time prediction of summer rainfall in tropical North Africa at interannual and multidecadal timescales, J. Climate **11**, 3167-3191 (1998).

[81] S. Valcke, R. Budich, M. Carter, E. Guilyardi, M.-A. Foujols, M. Lautenschlager, R. Redler, and L. Steenman-Clark, Nils Wedi, The PRISM Software Framework and the OASIS Coupler, in A.J. Hollies and A.P. Kariko (eds.), The Australian Community Climate Earth System Simulator (ACCESS) - Changes and Opportunities, BMRC Research Report, 132 - 140, Bur. Met. Australia, (2006).

[82] H. Von Storch, F. W. Zwiers, Statistical Analysis in Climate Research, Cambridge University Press, 1999.

[83] J. M. Wallace, C. Smith, C. S. Bretherton, Singular Value Decomposition of Wintertime Sea Surface Temperature and 500-mb Height Anomalies. J. Climate, **5**, 561?576 (1992).

[84] D. S. Wilks Resampling hypothesis tests for autocorrelated fields, J. Climate **10** 65?82 (1997).

[85] K. D. Williams, A. Jones, D. L. Roberts, C. A. Senior, M. J. Woodage, The response of the climate system to the indirect effects of anthropogenic sulfate aerosol. Climate Dyn. **17**, 845-856 (2001).